Influence of Gas Species on Thermophoretic Velocity of PMMA Particle

(PMMA 粒子の熱泳動速度に気体種が及ぼす影響)

Mohd Azahari Bin Razali

A dissertation submitted in partial fulfilment

of the requirements for the degree of

Doctor of Engineering

in

Energy and Environmental Science

Graduate School of Engineering

Nagaoka University of Technology

Nagaoka, Niigata, JAPAN

September, 2013

Influence of Gas Species on

Thermophoretic Velocity of PMMA Particle

(PMMA 粒子の熱泳動速度に気体種が及ぼす影響)

Approved by:

Assoc. Prof. Dr. Masataro Suzuki,
Advisor
Human and Environmental System
Engineering Division
Nagaoka University of Technology

Prof. Dr. Kazuo Aoki
Human and Environmental System
Engineering Division
Nagaoka University of Technology

Prof. Dr. Satoshi Kadowaki
Department of System Safety
Nagaoka University of Technology

Assoc. Prof. Dr. Noboru Yamada
Human and Environmental System
Engineering Division
Nagaoka University of Technology

Assoc. Prof. Dr. Wataru Yamazaki
Top Runner Incubation Center for
Academia-Industry Fusion
Nagaoka University of Technology

Dedication

This work is dedicated to my wonderful parents, Razali Bin Lazim and Rahemah Binti Abdul Rahim.

I also dedicate this work to my beloved wife, Nurmazeha Binti Mail, who have provided never-ending support and encouragement from day one.

Abstract

In the temperature field, a small particle will move towards the lower temperature side. This phenomenon is called thermophoresis, which influences the movement of soot particles in exhaust gas from combustors. In recent years, our group has developed a device for conducting experiments repeatedly under a microgravity environment in a very short period time, i.e. 0.3 s, by means of the free-fall method, to accumulate data of the thermophoretic velocity.

Considering the environment of soot, it is indispensable to understand quantitatively the phenomenon for a gas mixture. However, before analyzing the phenomenon for the gas mixture, it would be desirable also to know the characteristics of the phenomenon for each gas component, since the combustion gas mixture contains many gas species. In the present work, the investigations have been carried out to examine the influence of gas species on thermophoretic velocity of particle.

As the first step, the characteristics of the thermophoresis for several pure gases, i.e., argon, nitrogen, and carbon dioxide are experimentally examined. Particles adopted are PMMA spheres of 2.91 μm in mean diameter. The temperature gradient is set at 10 K/mm, and the pressure is set at several conditions in the range from 20 kPa to 100 kPa. Obtained experimental results are compared with theoretical predictions; a notable discrepancy is found for carbon dioxide, while the results for other two gases are

consistent with predictions. Some attempts are made to fix the discrepancy: first by modifying constants and second by modifying two empirical coefficients in the theory.

In the next step, an attempt is made to investigate dependence of thermophoretic parameters on gas properties. Atmospheric gases chosen are pure gases of argon, nitrogen, carbon dioxide, methane, and nitrous oxide. The residue values for all combinations of the coefficients are calculated from the obtained experimental results; several combinations of the coefficients are possible to fit the prediction with the experimental results. The tangential momentum accommodation coefficient is estimated by assuming the thermal accommodation coefficient to be unity. Physical relationships between the coefficient and gas properties are investigated.

In the final step, the thermophoretic velocity is experimentally investigated for several gas mixtures, i.e., argon-nitrogen, argon-carbon dioxide, and nitrogen-carbon dioxide. The temperature gradient and the pressure are 60 K/mm and 70 kPa, respectively. The tangential momentum accommodation coefficient is estimated from experimental result by assuming the thermal accommodation coefficient at unity, and it is compared with predictions calculated from values of composing pure gases by means of some methods given in references; among those methods, the intermolecular-interaction-based method is found to be the best for all mixture conditions.

Acknowledgement

In the name of **Allah**, Most Gracious and Most Merciful

My deep gratitude goes to my advisor Assoc. Prof. Dr. Masataro Suzuki, who gave me the wonderful opportunity to work in this great laboratory. His years of encouragements and guidance, excellent supervision, invaluable scientific insight and wise advice made my thesis work an exciting and enjoyable experience.

I would also like to express gratitude to Prof. Dr. Wataru Masuda for his help in academic and research studies.

Special thanks are extended to all the members of Suzuki Laboratory for their support and friendship.

I also wish to thank the Ministry of High Education, Malaysia and University Tun Hussein Onn Malaysia, Malaysia for sponsoring my study.

On top of all, I owe a particular debt of gratitude and appreciation to my wonderful parents for their long-distance support. My deepest gratitude I must reserve for my beloved wife Nurmazeha Binti Mail and my son Irsyad Zafran Bin Mohd Azahari, whose I am very thankful for patience and understanding. They never uttered any words of discouragement and always inspired me to carry out the thesis work with sincerity.

Thank you,

Mohd Azahari Bin Razali

List of publications in referred journal

1. Mohd Azahari, B.R., Mori, M., Suzuki, M., and Masuda, W. (2012). Effects of gas species on pressure dependence of thermophoretic velocity. *Journal of Aerosol Science, 54*, 77-87.
2. Mohd Azahari, B.R., Mori, M., Suzuki, M., and Masuda, W. (2013). Measurement of thermophoretic parameters of binary gas mixture. *Journal of Aerosol Science, 63*, 60-68.

List of papers presented in conference

1. Mohd Azahari, B.R., Mori, M., Suzuki, M., and Masuda, W. (2011). Pressure dependence of thermophoretic velocity in surrounding gas of nitrogen and carbon dioxide. *Proceedings of the 49th Symposium (Japanese) on Combustion, Yokohama*.
2. Mohd Azahari, B.R., Suzuki, M., and Masuda, W. (2012). Measurement of thermophoretic parameters for combustion-related gas species. *Proceedings of the 50th Symposium (Japanese) on Combustion, Nagoya*.

Influence of Gas Species on

Thermophoretic Velocity of PMMA Particle

Table of Contents

Chapter 1

Introduction

1.1 Background

The improvement in technology produces development in transportation and industrial such that our lives become convenient. However this improvement requires increment in the energy consumption. Since 1970, the world energy consumption growth is about 2.3% per year [1]. It is estimated about 86% of the energy source is produced from fossil fuels such as coal, petroleum, and natural gas. Fossil fuels are of great importance since they can produce significant amount of energy per unit weight. Consumptions of all these three sources have been increased such that the reserves of these sources have been used up quickly. Some developments have been done to produce alternative energy from the non-fossil sources such as nuclear and biomass energies. Some of these developments have reached the practical stage but only 16% of the global final energy consumption comes from these sources. Currently, fossil fuels are still considered as valuable energy sources; which is important to be used efficiently.

Significant amount of heat energy is released due to the combustion of fossil fuels. However, the use of fossil fuels raises the environmental concerns. Burning of fossil fuels produces carbon dioxide, which is one of the greenhouse's gases that enhances radiative forcing, which contributes to global warming. It is important to understand the

combustion phenomenon in a combustion chamber since improvement of the energy efficiency will produce undesirable gas emissions and environmental pollution.

Soot is one of the main pollutants emitted from the combustion devices. It is important to understand the behavior of soot particles in the combustion field for emission control. Dobashi et al. [2] have conducted experiments to examine smoke generation process in a flickering pool fire and have found the residence time of soot particle in the soot production is increased by the flickering motion of the flame. It is noted that the thermophoretic force might increase the residence time in the soot production region. Quantitative understanding of the phenomenon is indispensable for controlling the movement of particles in this system.

There have been some direct measurements on the thermophoretic phenomenon of such an aggregate particle. Zheng and Davis [3] have measured the thermophoretic force acting on an aggregate of polystyrene latex spheres, and found that the force is affected by the number of primary spheres in the aggregate. Suzuki and Dobashi [4] have conducted direct measurements on the thermophoretic velocity of the soot particles, and have revealed that the velocity is dependent not only on the macroscopic size of the soot particle but also on the aggregation condition; experimental results suggest that this phenomenon is dominated by the size of primary spheres when the aggregation is coarse. Thus, prior understanding for an aggregate, well knowledge about the phenomenon for a single sphere is important.

1.2 Existing Theory of Thermophoresis

Thermophoresis is the phenomenon that a small particle in a gas with a temperature gradient moves toward the lower temperature side. This phenomenon is caused by the momentum exchange between the gas molecules and the particle. The primary mechanism of this exchange is the gas molecules collide from the higher temperature side and later transfer negative momentums to the particle with amount that exceed those of positive momentums transferred by the gas molecules colliding from the lower temperature side. As the result of this momentum exchange, both the particle and the surrounding gas move in mutual opposite direction. The flow of the gas is referred to as the superficial slip flow.

There are several theoretical works have been carried out to study the thermophoretic phenomenon of a spherical particle. Theories of this phenomenon are derived by considering the boundary condition on the surface of a single spherical particle suspended in a gas with a temperature gradient. Brock [5] derived a theoretical solution to the thermophoretic force on the particle by applying a slip boundary condition on its surface, which includes effects of the thermal slip, the viscous slip, and the temperature jump. The equation is shown as below:

$$F_T = -\frac{9\pi\mu^2 d}{2\rho T_{F0}} \frac{\left(k + C_T\, Kn\right)}{\left(1 + 2\,C_M\, Kn\right)\left(1 + 2k + 2\,C_T\, Kn\right)} \left|\nabla T\right|, \qquad (1-1)$$

where μ, d, $|\nabla T|$, ρ, T_{F0}, k, Kn, C_M, and C_T are the viscosity, the particle diameter, the temperature gradient, the density of the surrounding gas, the reference temperature, the gas-to-particle thermal conductivity ratio, Knudsen number, constants for slip flow, and temperature jump, respectively. Here, the reference temperature T_{F0} is defined as the supposed gas temperature at the center of the particle in the given temperature field

without the existence of the particle, and Knudsen number *Kn* is the ratio of the mean-free-path *l* to the particle radius. The mean-free-path is calculated from the following equation [6]:

$$l = \frac{\mu}{0.499P}\sqrt{\frac{\pi R T_{F0}}{8}}, \qquad (1-2)$$

where P and R are the pressure and the gas constant, respectively.

Derjaguin and Yalamov [7] derived the thermophoretic velocity from the Brock's theoretical solution by equating the balance between the thermophoretic and the drag forces:

$$F_T + F_D = 0. \qquad (1-3)$$

Here, the drag force F_D is given as follows:

$$F_D = \frac{3\pi\mu d V_T}{C_C}, \qquad (1-4)$$

where V_T and C_C are the thermophoretic velocity and Cunningham's correction factor, respectively. The slip correction factor adopted is $C_C = 1 + A\,Kn$, where $A = 1.257 + 0.4\exp(-1.10/Kn)$ [8]. Thus, the equation of thermophoretic velocity is shown as below:

$$V_T = \frac{3}{2}\frac{\mu C_C}{\rho_g T}\frac{(k + C_T Kn)}{(1 + 2C_M Kn)(1 + 2k + 2C_T Kn)}|\nabla T|. \qquad (1-5)$$

Hoshino et al. [9] have derived an improved theoretical solution of the thermophoretic velocity by applying the boundary condition proposed by Lockerby et al. [10], which includes the thermal stress slip and the higher order isothermal slip. The equation is given as follows:

$$V_T = \frac{3\mu C_c}{2\rho T_{F0}} \frac{\left[\left(k + C_T Kn\right) + \frac{4}{3}\left(C_M C_T Kn^2 + C_M Kn[k-1]\right) \right]}{\left[1 + 3C_M Kn + \frac{9}{2\pi} PrKn^2 \left(1 - \gamma^{-1}\right) \right] \left(1 + 2k + 2C_T Kn\right)} \left|\nabla T\right|, \qquad (1-6)$$

where Pr and γ are Prandtl number and the specific heat ratio, respectively. Detail of the derivation of thermophoretic velocity is shown in ***Appendix A***.

1.3 Previous Experiments of Thermophoresis

Several experiments have been performed to measure the thermophoretic force or the thermophoretic velocity. Fredlund [11] attempted a systematic experiment to examine the effect of the temperature field upon a disk suspended on a balance. The experiments have been performed with various gases: hydrogen, argon, nitrogen, oxygen, and air. It is shown that at the given distance between the plates with different temperatures, the thermophoretic force is a linear function of pressure.

The thermophoretic force and the thermophoretic velocity are measured by several methods: Millikan cell [12 – 15], electrodynamic balance [16, 17], precipitation in a thermoprecipitator [18, 19], jet technique [8, 20, 21], and deflection of a particle suspended by a small wire [22, 23].

Above experimental methods are complex in practical implementation, and as a consequence, involve numerous errors. Among those, errors caused by buoyancy are the largest problem; in a field with a temperature gradient, buoyancy induces natural convection, which influences the movement of particles and disturbs the measurement. The velocity of such natural convection is usually comparable to the thermophoretic velocity and cannot be measured directly. To avoid this problem, some experiments have been conducted under microgravity conditions. Toda et al. [24, 25] performed

experiments in a drop tower facility and demonstrated that the microgravity environment satisfactorily suppresses the disturbance. Prodi et al. [26, 27] also conducted microgravity experiments by means of a drop tower facility and/or parabolic flights. However, their reported data still seem to contain some errors, possibly owing to limited trial numbers of experiments, so that those data are not sufficient enough to make a quantitative comparison with theories [28].

1.4 Motivation of Present Work

Recently, our group has developed a device for conducting experiments repeatedly under a microgravity environment in a very short period of time, i.e. 0.3 s, by means of the free-fall method, to accumulate data of the thermophoretic velocity. It has been confirmed that satisfactory accuracy can be attained if the amount of data is sufficient for statistical treatment [28]. By comparing the obtained experimental results with the existing theory as shown in Eq. (1-5), a notable difference is found for particles with high thermal conductivity [29].

The problem of the difference has been solved by reconsidering the boundary condition to improve the theory as shown in Eq. (1-6). Figure 1.1 shows the comparison between these equations for PMMA, Al_2O_3, and Zn. Results show that the prediction from Eq. (1-6) agrees satisfactorily with the experiments for all types of test particles.

Considering the environment of soot, it is indispensable to understand quantitatively the phenomenon for gas mixtures. Before analyzing the phenomenon for the gas mixture, it would be desirable also to know the characteristics of the phenomenon for each gas component, since the combustion gas mixture contains many gas species.

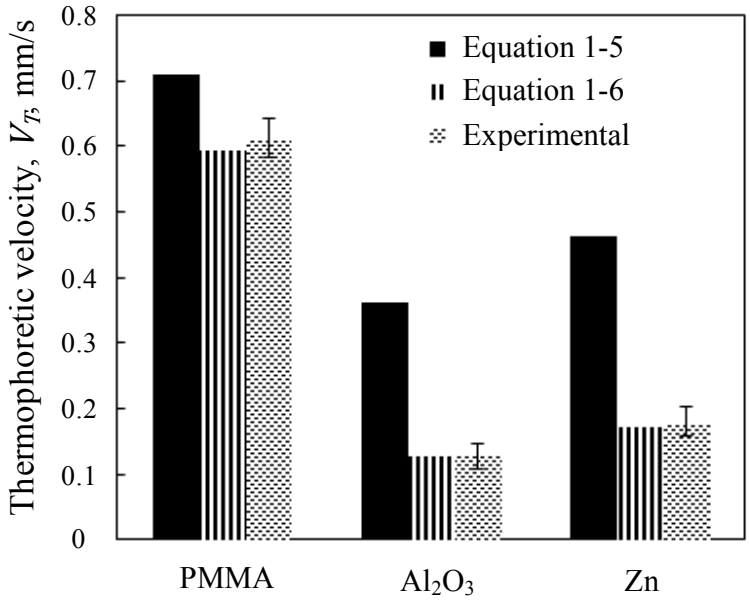

Fig. 1.1 Thermophoretic velocities for different type of particles.

1.5 Scope and Objective of Present Work

The main objective of the present study is to investigate the influence of gas species on the thermophoretic velocity. Systematic investigations have been carried out in order to achieve the objective. For the first step, the characteristics of the thermophoresis for several pure gases, i.e., argon, nitrogen, and carbon dioxide are experimentally examined. Obtained experimental results are compared with theoretical predictions; a notable discrepancy is found for carbon dioxide, while the results for other two gases are consistent with predictions. Some attempts are made to fix the discrepancy: first by modifying constants and second by modifying two empirical coefficients in the theory. In the next step, an attempt is made to investigate dependence of the thermophoretic parameters on gas properties; the thermophoretic parameters for argon and nitrogen are reexamined, and compared with those of carbon dioxide, methane, and nitrous oxide. In

the final step, thermophoretic velocities are experimentally measured for several gas mixtures, i.e., argon-nitrogen, argon-carbon dioxide, and nitrogen-carbon dioxide. The tangential momentum accommodation coefficient is estimated from experimental result by assuming the thermal accommodation coefficient at unity, and it is compared with predictions calculated from values of composing pure gases by means of some methods given in references.

Dissertation Outline

In ***Chapter 1***, brief introduction about the background and previous theoretical and experimental works of thermophoresis phenomenon is described. The motivations, scope and objective of the present study have also been addressed.

Experimental apparatus and particle sample used in the present study have been presented in ***Chapter 2***. In the section of experimental apparatus, information about the configuration of experimental apparatus, the temperature control, and the relay control have been described. Information about the material, the diameter distribution, and the mean diameter of particles are reported in the section of particle sample.

The explanation about the experimental method is given in ***Chapter 3***. Information about methods for measurement of the thermophoretic velocity, measurement of the temperature field, blowing particles, and experimental condition are presented.

Considering the environment of soot, it is indispensable to understand quantitatively the thermophoretic phenomenon for pure gases and gas mixtures. For the first step in this investigation, the characteristics of the thermophoresis for several gas

species have been experimentally examined in ***Chapter 4***. Atmospheric gases chosen are pure gases of argon, nitrogen, and carbon dioxide. Obtained experimental results have been compared with theoretical predictions. Some attempts are made to fix the discrepancy for carbon dioxide.

It would be desirable to know physical relationship between the coefficients and the gas properties since the combustion gas mixture contains many gas species. An attempt is made to investigate dependence of the thermophoretic parameters on gas properties; the thermophoretic parameters are examined for argon and nitrogen, carbon dioxide, methane, and nitrous oxide. The residue values of all combinations of accommodation coefficients are calculated from the obtained experimental results. The tangential momentum accommodation coefficient is estimated by assuming the thermal accommodation coefficient to be unity. Relations between the tangential momentum accommodation coefficient and gas properties have been discussed and presented in ***Chapter 5***.

The obtained experimental results in ***Chapter 5*** show the coefficients are approximately the same for argon and nitrogen, while a significant difference is seen for carbon dioxide, methane and nitrous oxide. A problem arises here for the treatment of the tangential momentum accommodation coefficients for a mixture of pure gases having different values. It should better be confirmed even when the mixture is composed of pure gases that have the same coefficient value. Therefore, further investigation in ***Chapter 6*** has been carried out to determine the tangential momentum accommodation coefficient that is estimated from the experimental results by assuming the thermal accommodation coefficient at unity. The estimated coefficient has been compared with

predictions calculated from values of composing pure gases by means of some methods given in the references to determine the appropriate method for evaluating the mixture's coefficients. Gas mixtures chosen are argon-nitrogen, argon-carbon dioxide, and nitrogen-carbon dioxide.

Finally, the general conclusions of the current study and suggestion for further research have been addressed in ***Chapter 7***.

References:

[1] Statistical Review of World Energy, London, 2009.

[2] Dobashi, R., Kong, Z.W., Toda, A., Takahashi, N., Suzuki, M., and Hirano, T. (1999). Mechanism of smoke generation in a flickering pool flame. *Proceeding of the 6th International Symposium on Fire Safety Science,* 255-264.

[3] Zheng, F., and Davis, E.J. (2001). Thermophoretic force measurements of aggregates of micro-spheres. *Journal of Aerosol Science, 32,* 1421-1435.

[4] Suzuki, S., and Dobashi, R. (2007). Thermophoretic effect on soot particle behavior –influence of particle morphology. *21st ICDERS*, 239.

[5] Brock, J.R. (1962). On the theory of thermal forces acting on aerosol. *Journal of Colloid Science, 17,* 768-780.

[6] Kennard, E.H. (1938). *Kinetic Theory*. McGraw-Hill: New York.

[7] Derjaguin, B.V., and Yalamov, Yu. (1965). Theory of thermophoresis of large aerosol particles. *Journal of Colloid Science, 20,* 555-570.

[8] Talbot, L., Cheng, R.K., Schefer, R.W., and Willis, D.R. (1980). Thermophoresis of particles in a heated boundary layer. *Journal of Fluid Mechanics, 101,* 737-758.

[9] Hoshino, A., Suzuki, M., and Masuda, W. (2010). Influence of particle size distribution on measurement accuracy of thermophoretic velocity. *Proceeding of the 48th Symposium (Japanese) on Combustion,* 464-465.

[10] Lockerby, D.A., Reese, J.M., Emerson, D.R., and Barber, R.W. (2004). Velocity boundary condition at solid walls in rarefied gas calculations. *Physical Review E, 70,* 017303-1-017303-4.

[11] Fredlund, E. (1938). Absolute measurements of radiometric action in gases. *Philosophical Magazine, 26,* 987-1000.

[12] Jacobsen, S., and Brock, J.R. (1965). The thermal force on spherical sodium chloride aerosols. *Journal of Colloid Science, 20,* 544-554.

[13] Rosenblatt, P., and La Mer, V.K. (1946). Motion of a particle in a temperature gradient; thermal repulsion as a radiometer phenomenon. *Physical Review, 70,* 385-395.

[14] Saxton, R.L., and Ranz, W.E. (1952). Thermal force on an aerosol particle in a temperature gradient. *Journal of Applied Physics, 23,* 917-923.

[15] Schadt, C.F., and Cadle, R.D. (1961). Thermal forces on aerosol particles. *Journal of Physical Chemistry, 65,* 1689-1694.

[16] Li, W., and Davis, E.J. (1995). Measurement of the thermophoretic force by electrodynamic levitation: microspheres in air. *Journal of Aerosol Science, 26,* 1063-1083.

[17] Li, W., and Davis, E.J. (1995). The effects of gas and particle properties on thermophoresis. *Journal of Aerosol Science, 26*, 1085-1099.

[18] Keng, E., and Orr, C. (1966). Thermal precipitation and particle conductivity. *Journal of Colloid and Interface Science, 22,* 107-116.

[19] Schadt, C.F., and Cadle, R.D. (1957). Thermal forces on aerosol particles in a thermal precipitator. *Journal of Colloid Science, 12,* 356-362.

[20] Kousaka, Y., Okuyama, K., Nishio, S., and Yoshida, T. (1976). Experimental study of thermophoresis of aerosol particles. *Journal of Chemical Engineering of Japan, 9,* 147-150.

[21] Prodi, F., Santachiara, G., and Prodi, V. (1979). Measurements of thermophoretic velocities of aerosol particles in the transition region. *Journal of Aerosol Science, 10,* 421-425.

[22] Davis, L.A., and Adair, T.W.III. (1975). Thermal force on a sphere. *Journal of Chemical Physics, 62,* 2278-2285.

[23] Tong, N.T. (1975). Experiments on photophoresis and thermophoresis. *Journal of Colloid and Interface Science, 51,* 143-151.

[24] Toda, A., Ohi, Y., Dobashi, R., Hirano, T., and Sakuraya, T. (1996). Accurate measurement of thermophoretic effect in microgravity. *Journal of Chemical Physics, 105,* 7083-7087.

[25] Toda, A., Ohnishi, H., Dobashi, R., Hirano, T., and Sakuraya, T. (1998). Experimental study on the relation between thermophoresis and size of aerosol particles. *International Journal of Heat and Mass Transfer, 41,* 2710-2713.

[26] Prodi, F., Santachiara, G., Travaini, S., Vedernikov, A., Dubois, F., Minetti, C., and Legros, J.C. (2006). Measurements of phoretic velocities of aerosol particles in microgravity conditions. *Atmospheric Research, 82,* 183-189.

[27] Prodi, F., Santachiara, G., Di Matteo, L., Vedernikov, A., Beresnev, S.A., and Chernyak, V.G. (2007). Measurements of thermophoretic velocities of aerosol particles in microgravity conditions in different carrier gases. *Journal of Aerosol Science, 38,* 645-655.

[28] Suzuki, M., Maruko, K., Iwahara, K., and Masuda, W. (2009). Accurate measurement of thermophoretic velocity under high temperature gradient. *6th International Symposium on Scale Modelling (ISSM6),* 1.12.1-1.12.8.

[29] Suzuki, T., Suzuki, M., and Masuda, W. (2009). Effect of water vapor to thermophoresis phenomenon. *Proceeding of the 47th Symposium (Japanese) on Combustion,* 448-449.

Chapter 2

Experimental Apparatus and Particle Sample

2 Experimental Apparatus and Particle Sample

2.1 Experimental Apparatus

2.1.1 Configuration of Experimental Apparatus

Experimental apparatus is divided into three main units: drop tower, drop unit and measuring unit. Table 2.1 shows the specification of equipment used in each unit. Each unit is explained as follows:

2.1.1.1 Drop Tower

Figures 2.1 and 2.2 show the overview and the schematic of the apparatus, which is included a drop tower, a measuring unit, and a damping cushion. The measuring unit is hung at the top of the drop tower by an electric magnet. The unit starts falling when the electric magnet is deactivated. The falling distance is 0.6 m, which corresponds to the duration time of the microgravity condition at 0.3 s. In this research, the drop tower with the height about 2 m is chosen based on consideration of the drop distance, the height of the drop unit, and height of the damping cushion.

The framework of the drop tower is W1 m × L0.7 m × H2 m and is manufactured from angle frames. The base of the tower is fixed to the floor by bolts for

preventing the movement of the tower during experiments. The electric magnet is attached to the center of the upper of the drop tower to hang the drop unit 1 m height from the floor. When the magnet is deactivated, the drop unit falls before it hits the damping cushion. The damping cushion is chosen from the commercial comforter and is placed inside the cardboard box with the size of W0.9 m × L0.6 m × H0.4 m.

Figure 2.3 shows a variation of the gravity level during an experiment. The gravity level is measured by the G-sensor attached on the measuring unit. The duration time of the free-fall is about 0.3 s as seen in the figure. When the electric magnet is deactivated at t = 0, the gravity level in z-axis changes from −1.0 G to +0.4 G once, possibly owing to the vibrational motion of the frame of the unit, and then decays as time passes until the unit reaches the cushion. The range between ±0.1 G in gravity level is regarded as the microgravity condition in this work, the duration time of which is about 0.25 s.

Table 2.1 Specification of equipment.

		Maker	Model	Specification
A	Electric magnet	Toho Electrical	TRM76-24V	Outward appearance: ϕ 76.3 × 100 Maximum load: 700 N Voltage: DC 24 V
B	G-sensor	Slik	G-MEN DR10	Measurement range: – 10～10 G Measurement sensitivity: 0.1 G
C	G-sensor	Slik	G-MEN DR02	Measurement range: – 2～2 G Measurement sensitivity: 0.02 G
D	Laser	Broadband	MGL532-400-1 %	Peak power : 500 mW Wave length : 501~561 nm
E	Electromagnet valve	CKD	S-21	Pressure: – 0.1~0.16 MPa
F	High-speed camera	Katokoken	K-Ⅱ	Frame rate : 200 fps Shutter speed : 1/200 s Pixel count : 640 × 480
G	Micro-lens	Keyence	SLB-50-300P	Optical magnification : × 2 Working distance : 66.9 mm Imaging view : 2.4 × 1.8
H	Ball valve	Swagelok	SS-6P6T	Maximum pressure: 20.6 MPa
I	Needle valve	Swagelok	SS-6L	Maximum pressure: 6.89 MPa
J	Electromagnet valve	CKD	AB31022	Input voltage: AC100 V
K	Pressure gauge	Migishita	S-21	Pressure range: – 0.1~0.16 MPa
L	Pressure gauge	Naganokeiki	DG85-31A-6C11	
M	Seamless cylinder	Swagelok	304L-HDF2	Maximum pressure: 3.44 MPa Volume: 150 cm^3
N	PLC	OMRON		
O	Switching power supply	TDK-Lambda	HK150A-24	Step-down AC100 V to DC24 V

Fig. 2.1 Overview of apparatus.

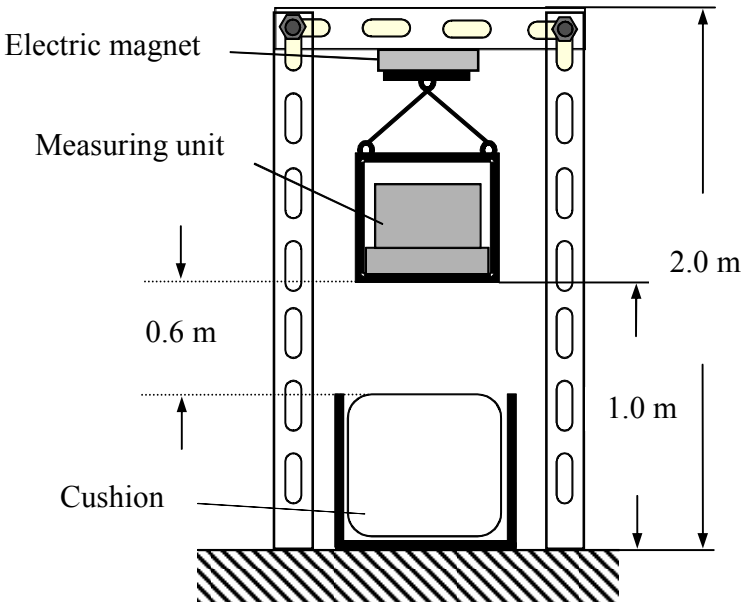

Fig. 2.2 Schematic of apparatus.

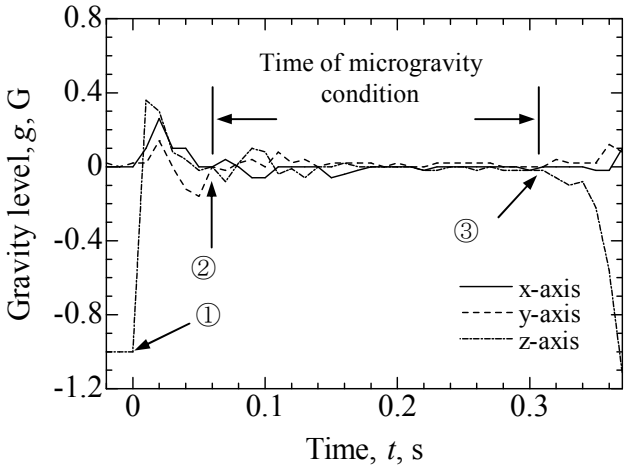

① Electric magnet is deactivated
② Starts of microgravity condition
③ Measuring unit hits the cushion

Fig. 2.3 Gravity level during experiment.
Gravity level is measured by the G-sensor which is attached on the measuring unit.

2.1.1.2 Drop Unit

Figure 2.4 shows the drop unit. The size of the unit is W0.6 m × L0.32 m × H0.3 m, which is constructed from the measurement unit, laser, electromagnetic valve, and steel plate. The angle frame is used to reduce the vibration during the drop. The steel wire and α-gel cushion are assembled to the frame of the unit for reducing the impact at the beginning of the drop. The chain is attached to the steel plate, which is connected to the electric magnet at the drop tower to hang the drop unit. The unit is hanging 1.0 m height from the floor as seen in Fig. 2.2. When the electric magnet is deactivated, the unit drops and hits the cushion.

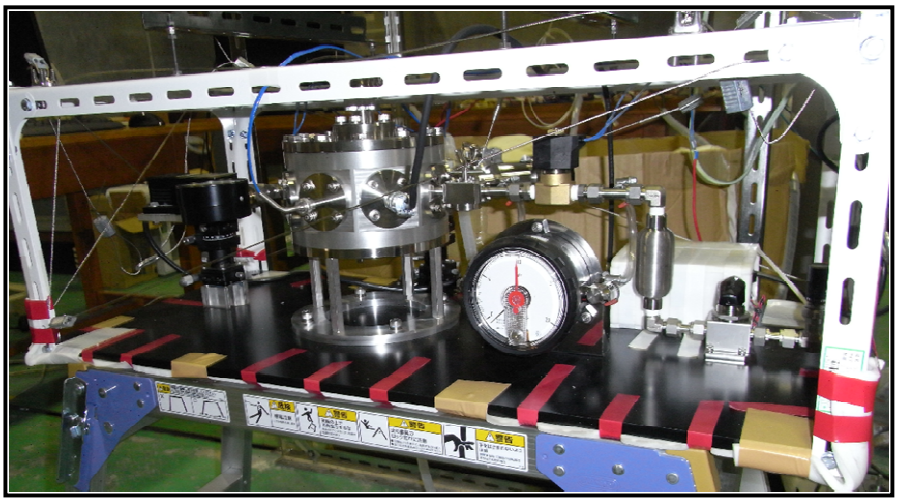

(a) Overview

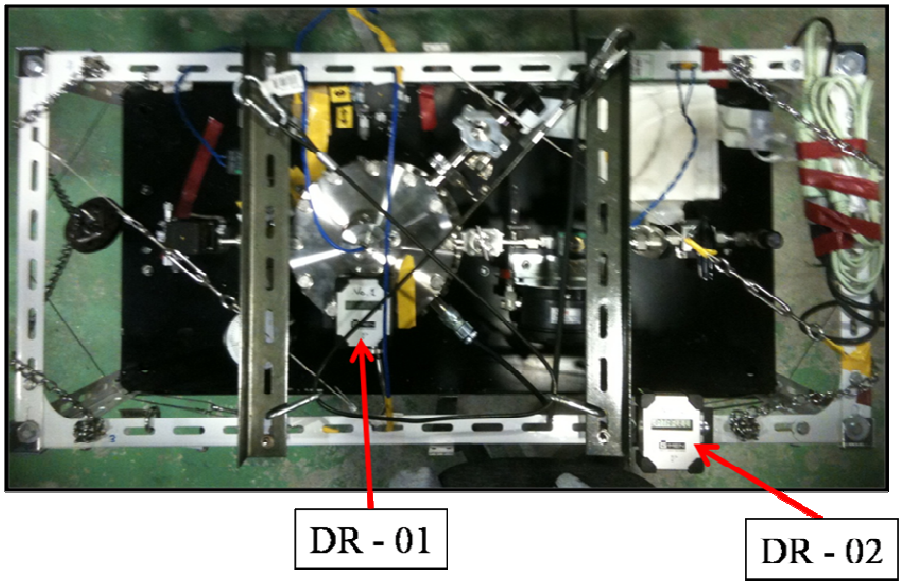

(b) Top view

Fig. 2.4 Drop unit.

2.1.1.3 Measuring Unit

Figure 2.5 shows the schematic of the measuring unit. The unit includes the pressure vessel, the particle reservoir, the laser, and the high-speed camera. This unit is assembled on the aluminum base of the drop unit. Figure 2.6 shows the schematic of the pressure vessel, which is main part of the measuring unit.

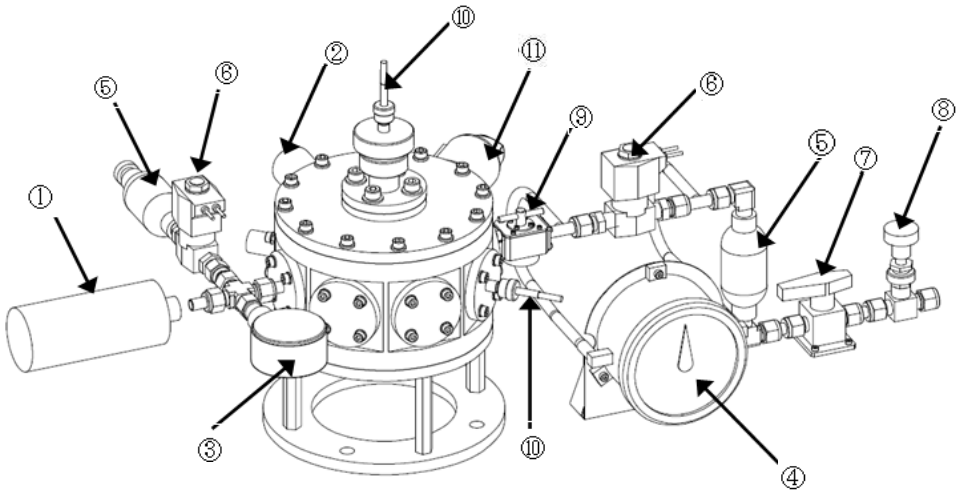

(a) Overview of measurement unit

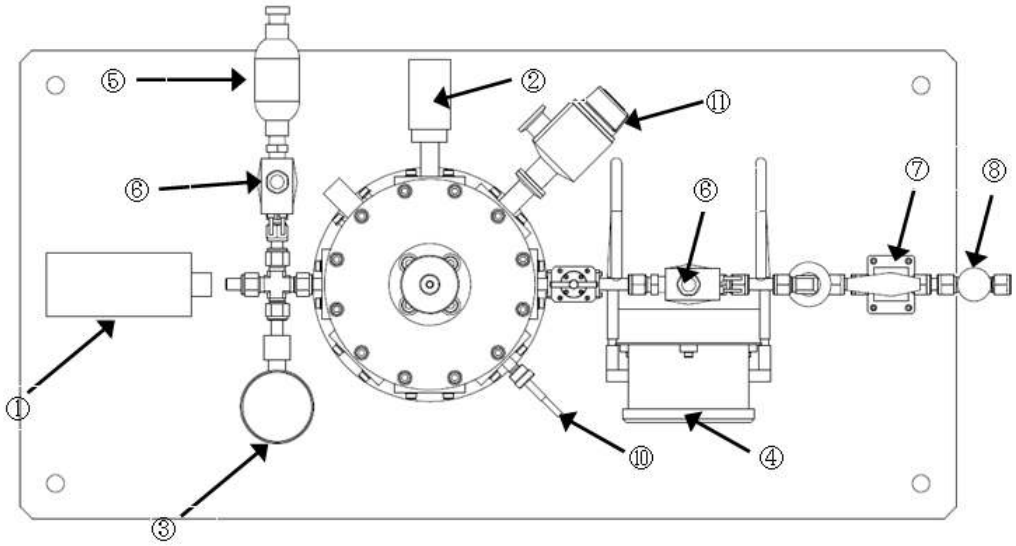

(b) Top view of measurement unit

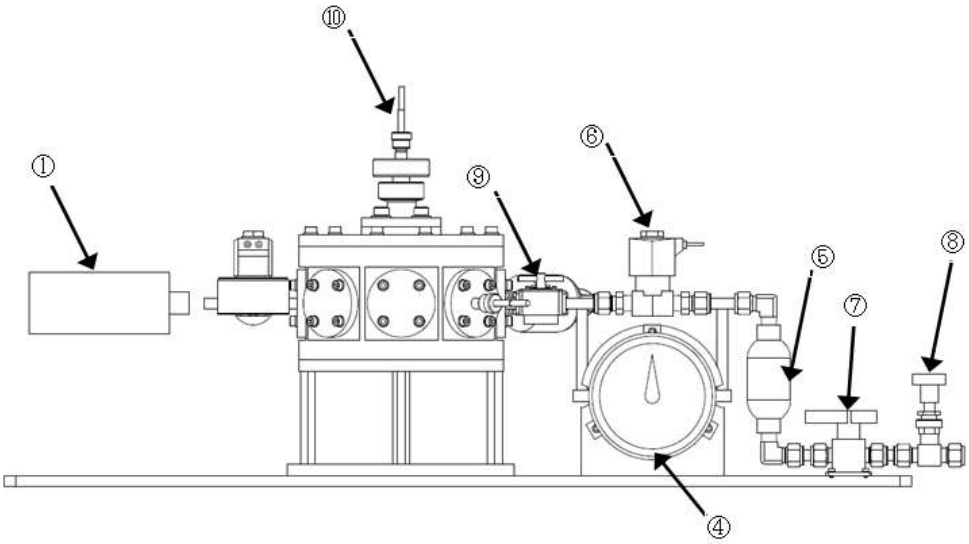

(b) Front view of measurement unit

① Laser ② High speed camera ③ Compound pressure gage
④ Micrometer pressure gauge ⑤ Seamless cylinder
⑥ Electromagnetic valve ⑦ Ball valve
⑧ Needle valve ⑨ Particle reservoir ⑩ Thermocouple
⑪ Vacuum exhaust valve

Fig. 2.5 Schematic of measuring unit.

(a) Pressure vessel

Figure 2.6 shows a cross-section of the pressure vessel. Placed in the vessel is a cylindrical thin chamber of 1.5 mm in height between two opposing aluminum plates of 10 mm × 80 mm × 80 mm. The upper plate, initially at the room temperature, is kept cool by moving it 15 mm away from the bottom plate while the latter is under the process of heating to raise its temperature, which is shown in Fig. 2.6(a). Keeping this arrangement, the vessel is evacuated by a pump. When the bottom plate reaches the appointed temperature, the upper plate is put in place where the distance between the plates is 1.5 mm as seen in Fig. 2.6 (b). Then, the vessel is filled with the test gas. The

temperature of the both plates is measured by two thermocouples, which are connected to the temperature control unit.

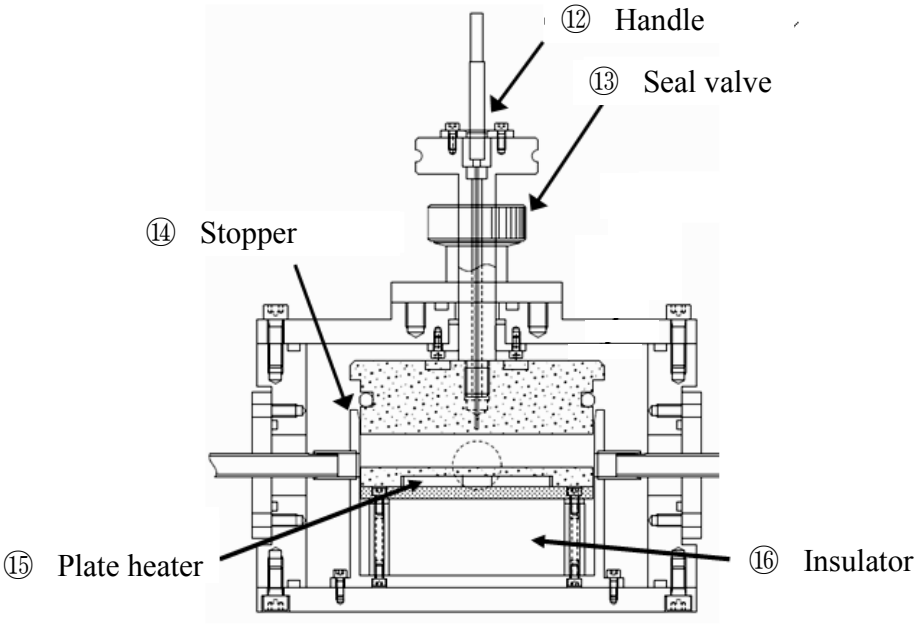

(a) Heating bottom plate

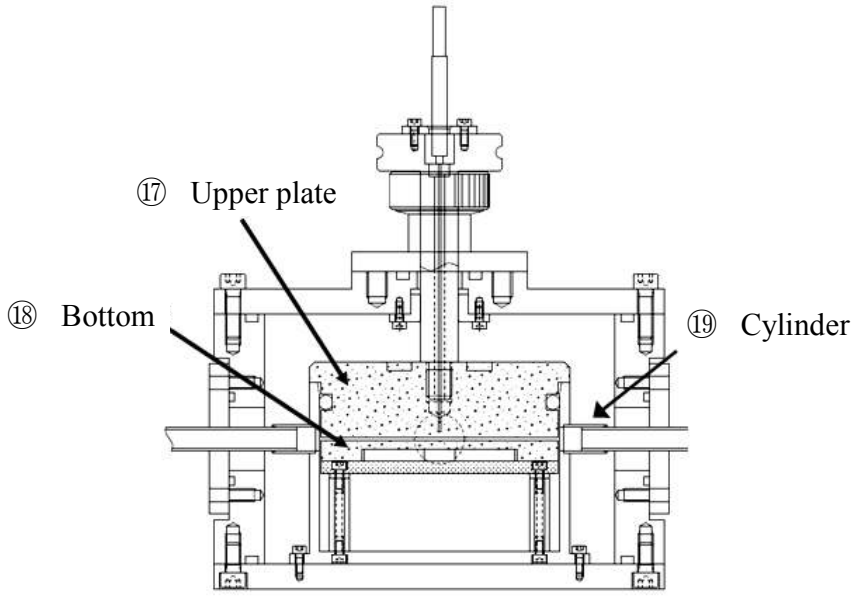

(b) During experiment

Fig. 2.6 Schematic of pressure vessel.

A sidewall of the vessel is attached with the mirror for capturing the image of particles via the high-speed camera. Figure 2.7 shows the coordinate system in the vessel. The origin is fixed at the center of the bottom plate. x, y, and z –axis's represent the horizontal, the vertical, and the optical directions, respectively.

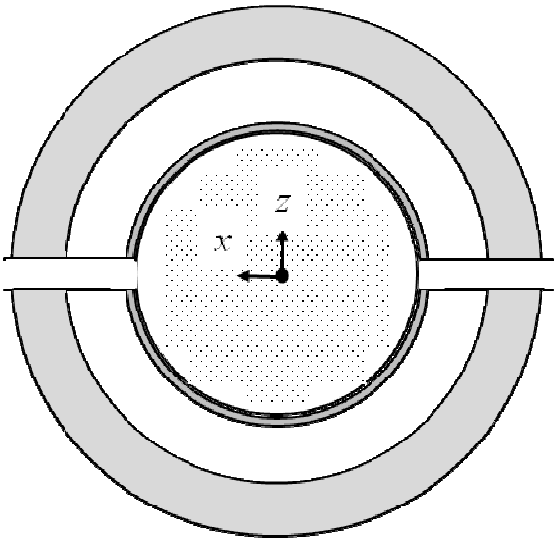

(a) Top view of pressure vessel

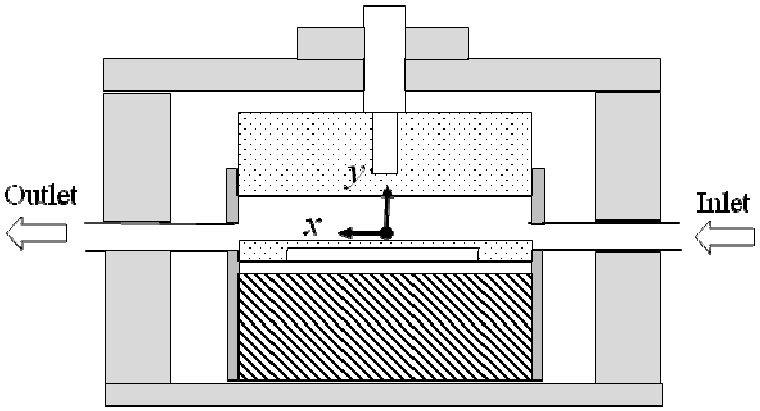

(b) Side view of pressure vessel

Fig. 2.7 Coordinate system in pressure vessel.

(b) Particles blowing

The method for particles blowing is explained by using Fig. 2.5. Both inlet and outlet valves are open when some particles are inserted to the particle reservoir. The pressure vessel is evacuated by the pump before it is refilled with the test gas to the target pressure. The compound pressure gauge is used to show the pressure. Later, the electromagnetic valves are closed and the small amount of the pressure is added to create a different pressure between the right side and the left side of the electromagnetic valve at the inlet. This pressure is indicated by the micrometer pressure gauge. Several preparatory experiments have been conducted to find the appropriate pressure for blowing the particles into the measurement field. The ball and needle valves are closed after setting the pressure. The particle reservoir includes the handle allowing the reservoir to open and close during the experiment. The reservoir is closed when the pressure vessel is evacuated and refilled with the test gas in order to prevent the particles in the reservoir from disappearing. The reservoir is opened after setting the blow pressure.

(c) Imaging unit

Those blown particles are illuminated by the laser beam introduced into the chamber to produce scattering lights, the image of which is recorded by a high-speed camera under the condition of the frame rate at 200 fps and of the shutter speed at 2 ms. The laser used in this research is chosen from the all-solid-state green laser. It is selected based on the high output power stability, ultra compact, good beam profile, and easy for operating. Since the distance between the plates is only 1.5 mm, the micro-lens is attached to the camera to enlarge the image of the measurement field.

2.2 Particle Sample

It is noted that the measurement accuracy of thermophoretic velocity is influenced by variation of the size and the shape of particles. In the present work, particles having a small variation of the size and the shape are chosen in order to increase the measurement accuracy. The thermophoretic velocity is derived from the balance between the thermophoretic force and the drag. The drag is estimated from the Stokes' law. Even the shape of particles influences the drag on the particles, the Stokes' approximation is applicable since Reynolds number is far less than one.

It is necessary to carefully choose the size of particles since the size influences on the Knudsen number, which one of the important parameter in the thermophoresis. The following conditions should be considered during the selection of the particle:

(1) Viscosity drag is verified.

(2) Physical characteristics are known.

(3) Particle size is in μm.

(4) Cohesion between particles is difficult to happen.

(5) Spherical particles.

Sample particles used in this research are PMMA (polymethylmethacrylate) sphere particle from Sekisui Plastics Co., Ltd. The density and the thermal conductivity of the particles are 1200 kg/m^3 and 0.21 W /(m K), respectively. These particles are chosen since the size is quite uniform. Figures 2.8 and 2.9 show the SEM image and the probability density distribution of the particles diameter measured from the images, respectively. The mean diameter of these particles is 2.91 μm as shown in Table 2.2.

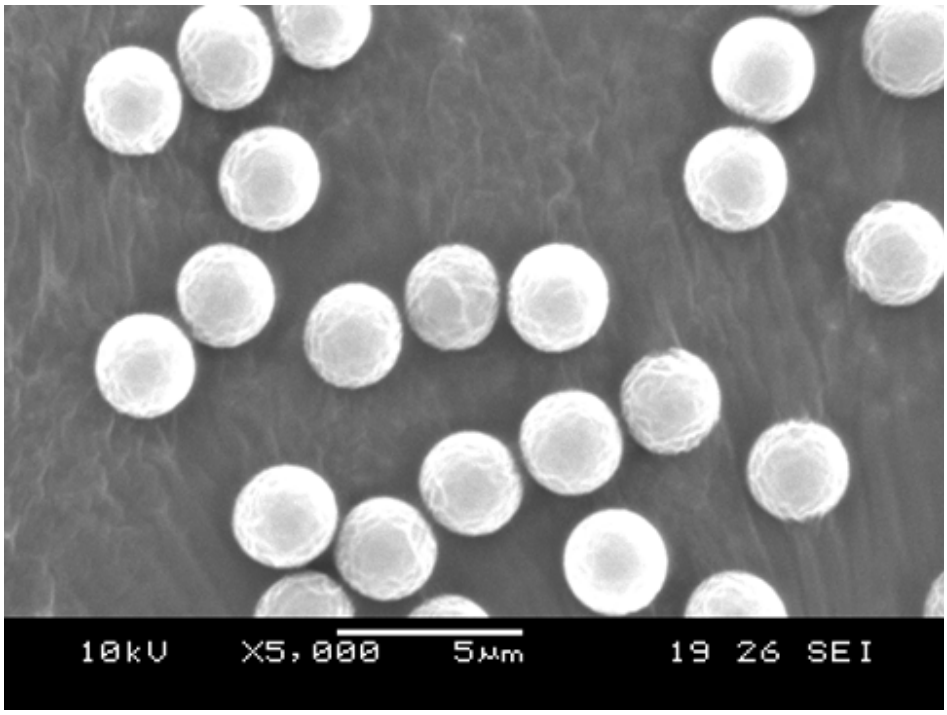

Fig. 2.8 SEM image of PMMA particles.

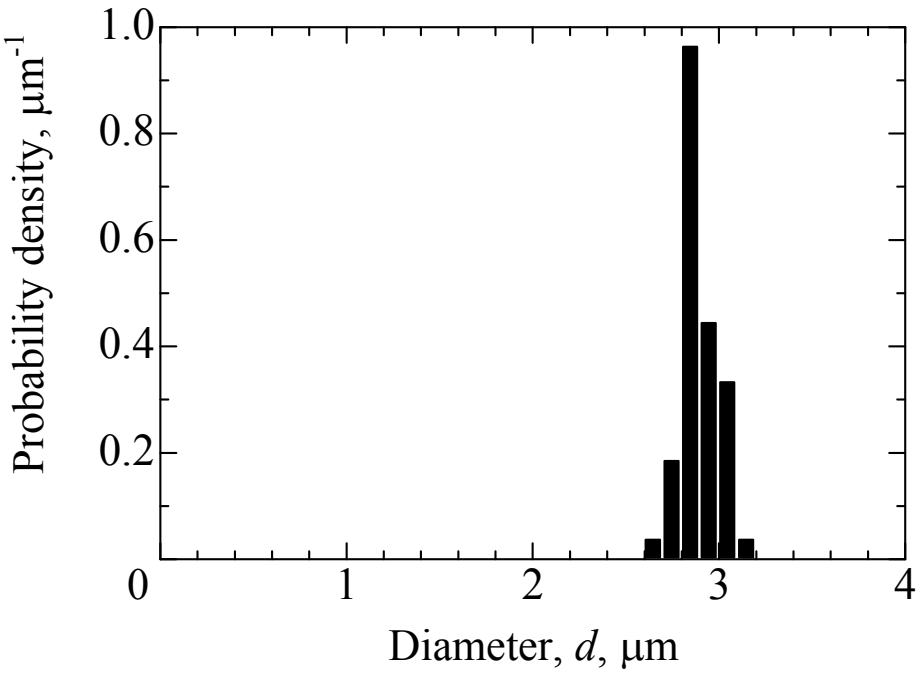

Fig. 2.9 Diameter distribution of particles.

Table 2.2 Diameters of PMMA particles

Mean, μm	Standard deviation, μm	Confidence interval (95%) for the mean, μm
2.91	0.09	0.03

Chapter 3

Experimental Method

3 Experimental Method

Experimental method is divided into four main sections: measurement of the thermophoretic velocity, measurement of the temperature field, method for blowing particles, and experimental condition. Each section is explained as follows:

3.1 Measurement of Thermophoretic Velocity

3.1.1 Reference Temperature

The thermophoresis is a phenomenon due to the momentum exchange from the collision between of gas molecules and the particle. The mean velocity of gas molecules increases as the temperature increases, such that the momentum of gas molecules increases accordingly. The measurement of the thermophoretic velocity should be taken at a fixed temperature since the velocity is dependent on not only the temperature gradient but also the temperature itself.

In this research, two experiments with different conditions are conducted: first is a pure gas and another is a gas mixture. For the former one, the thermophoretic velocity is measured at 313±2 K. Figure 3.1 (a) shows the position of the reference temperature; which is 1.0 mm from the hot surface. For the latter one, the measurement is performed at

338±10 K. The position of the reference temperature is determined at 1.2 mm from the hot surface as shown in Fig. 3.1 (b). It is noted that the position of the reference temperatures are different between these two experiments. The position is related to the measurement area. For the former experiment in carbon dioxide, most of particles drop quickly than the latter condition. The measurement could not be done since there is no particle in the measurement area when the measuring unit is dropped. Thus, the measurement area is changed, such that the position is changed accordingly, in order to easily capture the image of particles during the experiment.

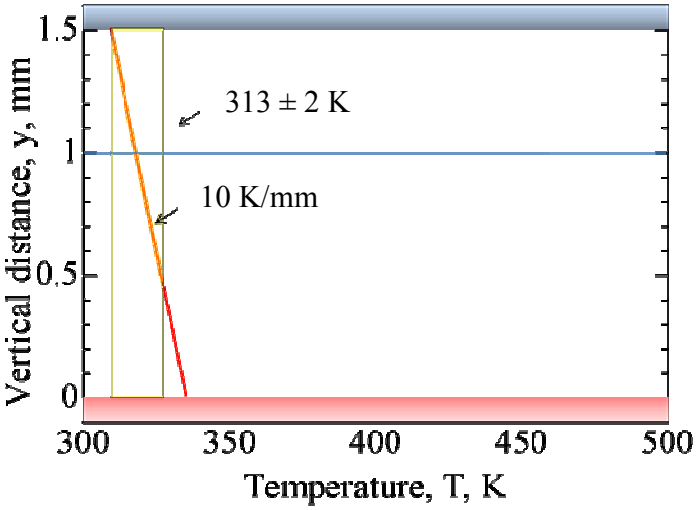

(a) Pure gas

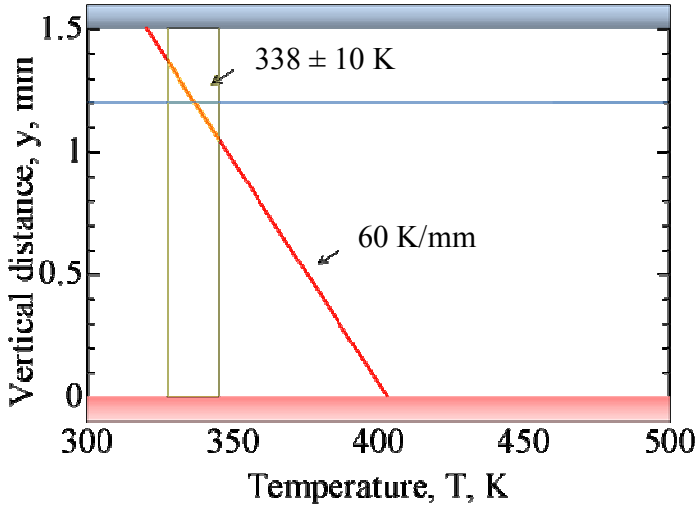

(b) Gas mixture

Fig. 3.1 Determination of temperature gradient and temperature reference for each experiment.

3.1.2 Measurement Software of Thermophoretic Velocity

The movement of particles is captured via a high-speed camera. The image is analyzed by using two-dimensional image measurement software. Table 3.1 shows the specification of the measurement software. This software analyzes the position for each selected particle from the image. The position is measured based on two-dimensional coordinate. The setting of the brightness and the contrast can be adjusted in order to make the image more clearly.

Table 3.1 Specification of measurement software.

Name	Maker	Model	Hardware requirement
A two-dimensional image measurement software	Library company	Move-tr / 2D 7.0	OS : Windows2000/XP/Vista CPU : PentiumⅢ and above Memory : 256 MB and above

The thermophoretic velocity is calculated based on position of each particle provided via the measurement software. Figure 3.2 shows the position for several PMMA particles in surrounding gas of nitrogen. The result shows that the position of particle is proportional to the time. In order to obtain accurate results, the measurement of position should be larger than 10 scenes. The thermophoretic velocity for each particle is estimated by means of the least-squares method.

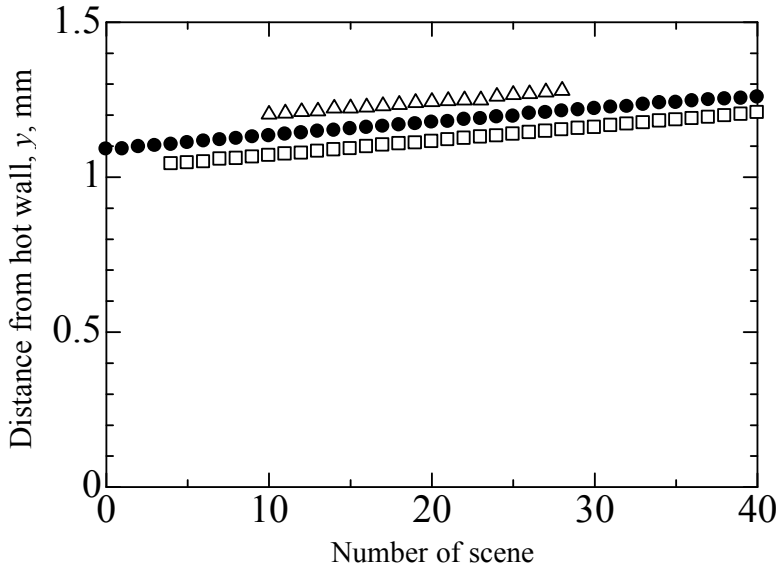

Fig. 3.2 Movement of particles.

Concerning the measurement from the software, there is a possibility that a particle is mistakenly selected. The position of each particle is confirmed from the graph in order to remove this error. Figure 3.3 shows the comparison of the movement between two particles. In the case of the particle noted as 'A', the position is constantly increased by the number of scene. On the other hand, in the case of the particle 'B', the notable change in the position is seen at scene number 24. The thermophoretic velocity is re-estimated after removing such error.

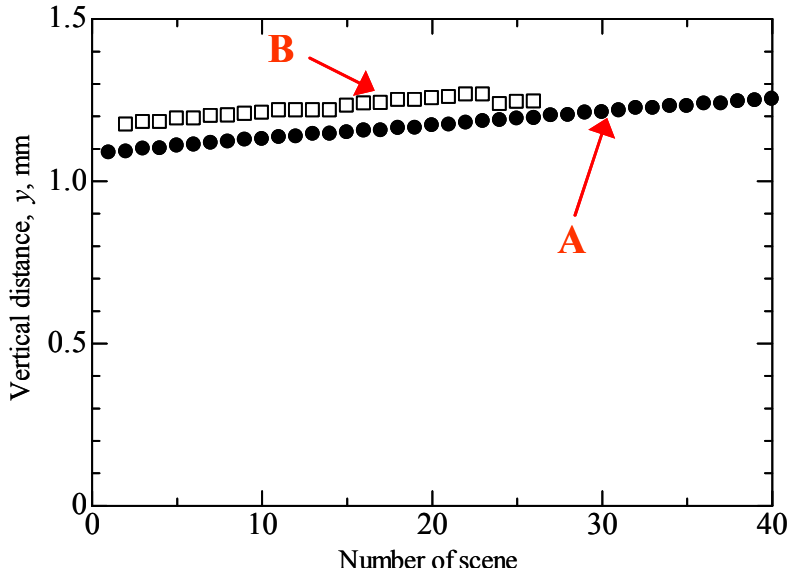

Fig. 3.3 Comparison of movement between particles.

3.1.3 Statistical Analysis of Measured Data

Experiments have been conducted repeatedly to accumulate data of the thermophoretic velocity. The satisfactory accuracy can be attained if the amount of data is sufficient for statistical treatment. Confidence interval is determined for indicating the range of expected mean value of the population.

For samples $X_1, X_2, \ldots, X_n$ from a normally distributed population with mean m and variance σ^2, the probability density of the population is given as follows:

$$P\left\{ \left| \overline{X} - m \right| \le 1.96 \frac{\sigma}{\sqrt{n}} \right\} = 0.95, \tag{3-1}$$

$$\overline{X} - 1.96 \frac{\sigma}{\sqrt{n}} \le m \le \overline{X} + 1.96 \frac{\sigma}{\sqrt{n}}, \tag{3-2}$$

where $\overline{X}$ and $\sigma/\sqrt{n}$ are the sample mean and the standard error, respectively. Equation (3-2) expresses the 95% confidence interval of the mean for thermophoretic velocity. In this work, it is 95% confident that the mean value is in the confidence interval.

3.2 Measurement of Temperature Field

The temperature field is created by using the temperature control unit. The lower plate is heated via a plate heater while the upper plate is kept cold in order to perform the temperature gradient. When the bottom plate reaches its pointed temperature, the upper plate is put in the place where the distance between the plates is 1.5 mm. It should be kept in mind that the target temperature of cold plate should be higher than environmental temperature. The measuring unit is dropped when the temperature of upper plate becomes

the target temperature. Efficiency of the experiment is increased by preparing two upper plates; which are changing after every experiment.

The temperature field during the experiment is monitored by measuring temperatures at two points in the vessel: one is in the upper plate and the other in the bottom one. The temperature field is controlled based on these measured temperatures. Before making experiments, the preparatory measurement for the temperature field is conducted by inserting two more thermocouples suspended in the chamber at different heights. Measuring two points is sufficient because the linearity of the temperature field has already been confirmed by the Mach-Zehnder interferometry. The relation between these temperatures at monitoring points and the actual temperature field in the chamber is examined from this preparatory measurement. When conducting thermophoresis experiments, additional two thermocouples are removed; the temperature field is controlled based on the temperatures at those two monitoring points.

It is noted that the maximum temperature of the plate heater is 300ºC. The experiment should be conducted lower than this temperature. The heater plate is fixed 3 mm under the bottom plate, thus the temperature of bottom plate is considered to be the same as the temperature of the heater plate. Therefore the temperature of the bottom plate is controlled below than the maximum temperature of the heater plate.

Figure 3.4 shows a circuit diagram of temperature controller. Thermocouples I and II indicate the temperature of bottom and upper plates, respectively. Output I responses to the temperature setting from the thermocouple I. The output I is connected to the solid stay relay (SSR), which is used to control the temperature of bottom plate such that the temperature becomes constant when it reaches the target temperature.

Figure 3.5 shows the temperature variation for both plates during the experiment. Blue and red lines represent the temperature for bottom and upper plates, respectively. For example, the temperature of bottom plate is set at 210ºC and the distance between plates is 1.5 mm. It is seen that the temperature of bottom plate becomes constant after the plate reaches its target temperature while the temperature of upper plate increases as time increases.

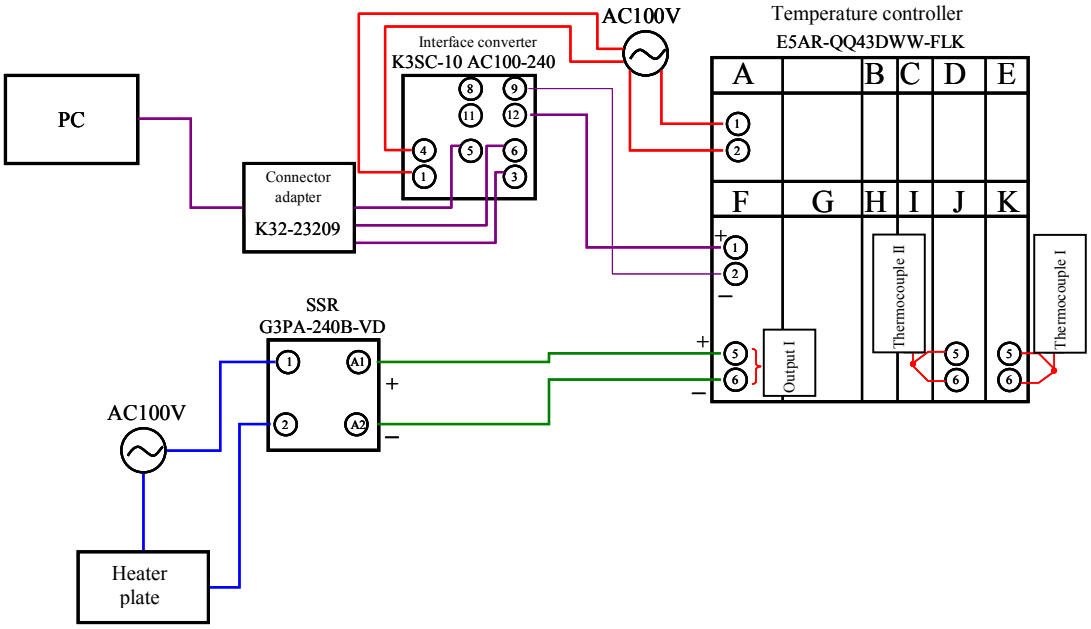

Fig. 3.4 Circuit diagram of temperature controller.

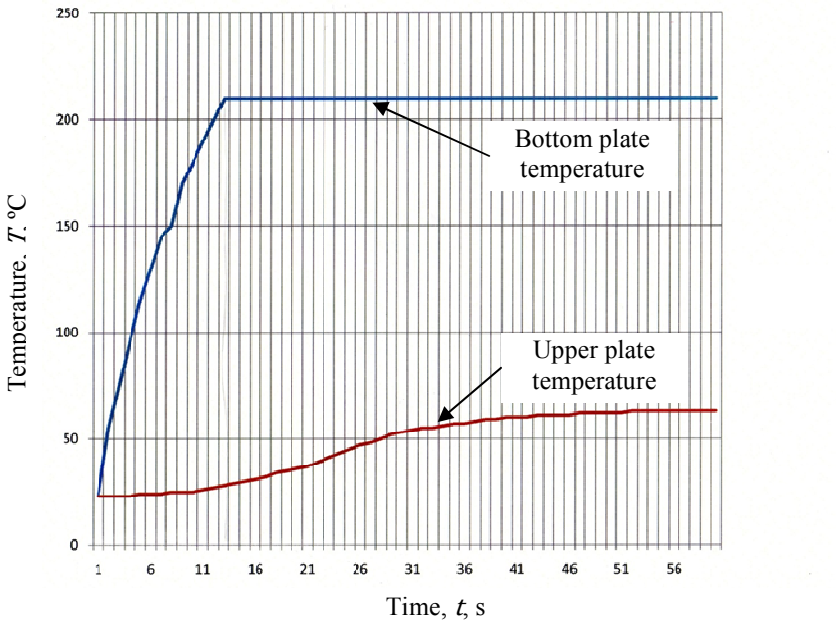

Fig. 3.5 Relation between time and temperature.

3.3 Method for Blowing Particles

The sequence controller is used for controlling each stage during the experiment such as recording the image of measurement field, falling of the drop unit, and blowing particles. Figure 3.6 shows the time chart during the experiment. The chart shows that after the high-speed camera is started, the electromagnet is deactivated to create the microgravity environment and particles movement in the measurement field are recorded. Figure 3.7 shows the ladder chart of programmable logic controller (PLC). Symbols T, B, M, and Q in the chart represent the timer, the button, auxiliary relay, and output relay, respectively. Q1, Q2, and Q3 are the electric magnet for holding the drop unit, the inlet electromagnetic valve, and the outlet electromagnetic valve, respectively.

The electromagnetic valves are open by pushing the button ⑤ on the PLC to evacuate and fill the vessel with the test gas. Both the electromagnetic valves are closed

and the magnet for holding the drop unit is activated by pushing the button ④. When the temperature of the upper plate becomes the target temperature, the button ② is pushed such that both electromagnetic valves at the inlet and the outlet are simultaneously opened for 0.01 s. Some particles are blown into the chamber from a particle reservoir upstream the inlet. The magnet holding the measuring unit is deactivated 0.85 s after the closure of both valves. The disturbances caused by the blow are expected to cease within this period before the drop; since it is larger than both characteristic times for the flow field and the temperature field to reach the steady state; those characteristic times are expressed as $t_f = (\delta/2)^2 / \nu$ and $t_t = (\delta/2)^2 / \alpha$, respectively, where δ, ν, and α are the distance between two plates, the kinematic viscosity, and the thermal diffusivity, respectively. The largest values of those for present conditions are estimated at 0.06 s and 0.05 s, respectively.

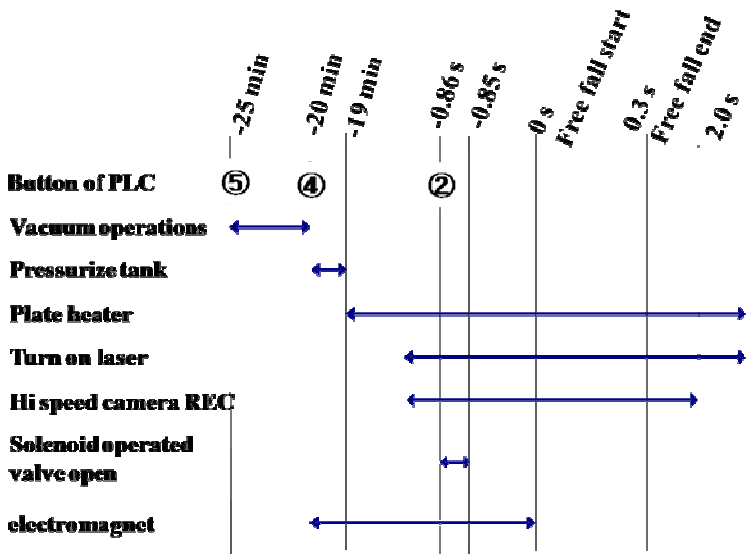

Fig. 3.6 Time chart.

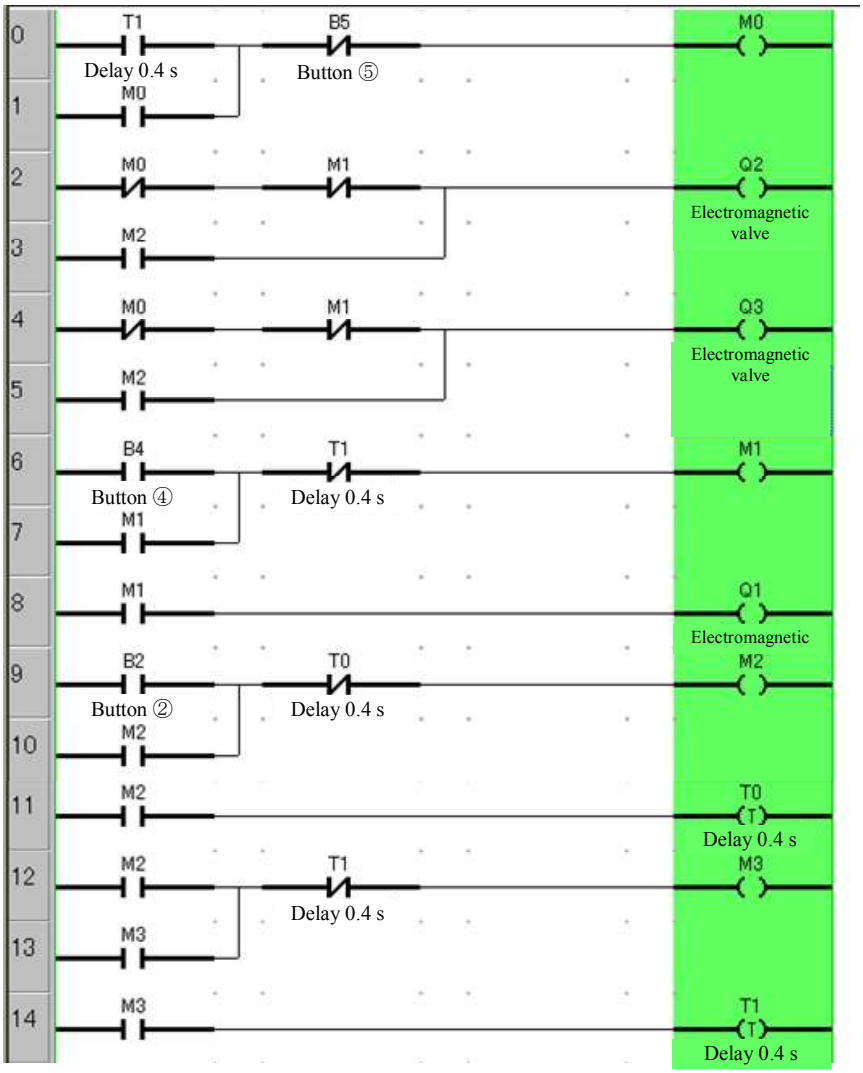

Fig. 3.7 Ladder chart of PLC.

The movement of particles in the microgravity environment has been confirmed by conducting the experiment without temperature gradient. Figures 3.8 and 3.9 show the movement of particles in the vertical and horizontal directions, respectively. It is seen that there is negligible effect of blowing and gravitational since the particles has almost no movement in the horizontal and the vertical directions.

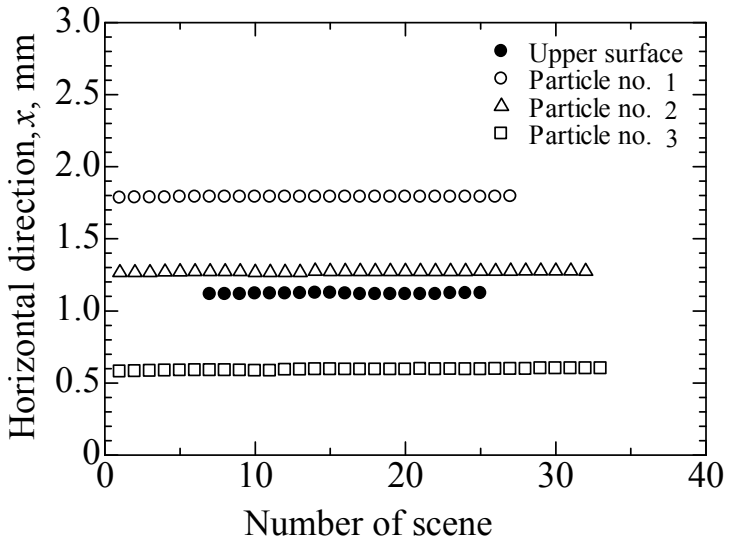

Fig. 3.8 Movement of particles in vertical direction.

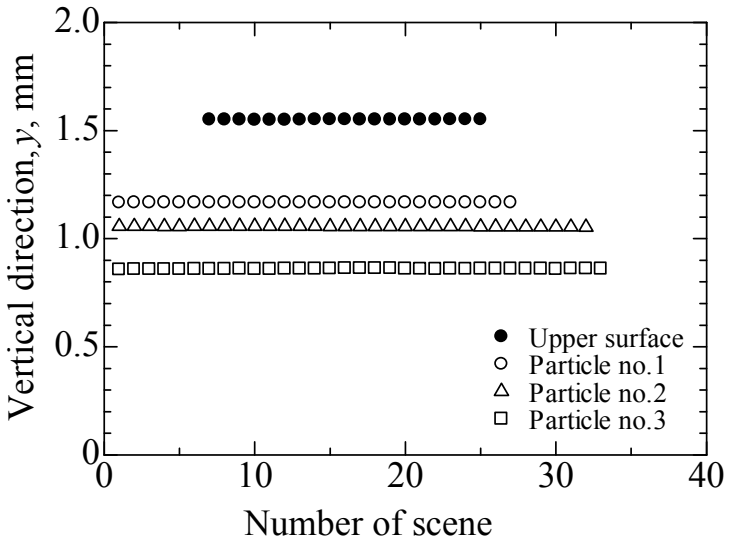

Fig. 3.9 Movement of particles in horizontal direction.

3.4 Experimental Condition

3.4.1 Pure Gases

Experiments are conducted with the test gas of argon, nitrogen or carbon dioxide. The target temperature and the temperature gradient are 313 K and 10 K/mm, respectively. Various pressure conditions are chosen from 20 kPa to 100 kPa. The thermophoretic velocity for each particle is individually measured, and the mean value and its 95% confidence interval for each experimental condition are statistically obtained.

3.4.2 Gas Mixtures

The experimental configuration used in this work is the same as the pure gases except that a gas mixer is introduced. A mixture of two gases is created before it is inserted into the pressure vessel, in which particles are supplied to measure the thermophoretic velocity. The mixer is evacuated by a pump before two gases feed into it. Gas mixtures in various ratios are prepared by adjusting the partial pressure of each gas. The gases used in this work are argon, nitrogen, and carbon dioxide. The pressure, the reference temperature, and the temperature gradient of the surrounding gas are 70 kPa, 338 K, and 60 K/mm, respectively. It is noted that the temperature gradient in this work is increased, and the reference temperature is changed accordingly, from the previous condition such that the thermophoretic velocity increases and the measurement accuracy increases.

Chapter 4

Effect of Gas Species

4.1 Introduction

Thermophoresis is the phenomenon that a small particle in a gas with a temperature gradient moves toward the lower temperature side. This phenomenon is supposed to influence practically on the movement of soot particles in exhaust gas from combustors, especially near cool walls around the hot gas flow, where the temperature gradient can become as large as the order of 10^2 K/mm. For example, the measured size-distribution of particulate matter is influenced by the temperature of the transfer tube connecting the exhaust pipe of a diesel engine to the dilution tunnel ahead of the measuring device [1]. It is described in the ***Chapter 1*** that there have been some direct measurements on the thermophoretic phenomenon of such an aggregate particle. The results of measurements on the thermophoretic velocity of soot particles suggested that the velocity is dependent not only on the macroscopic size of the soot particle but also on the aggregating condition [2, 3]. Suzuki et al. [3] have shown experimental results suggesting that the phenomenon is dominated by the size of primary spheres when the aggregation is coarse. Thus, the understanding of the phenomenon for a single sphere is indispensable before understanding for an aggregate.

The thermophoretic phenomenon of a spherical particle has been studied both theoretically and experimentally. The detail of these works is described in the ***Chapter 1***. Experimental methods in the previous works are complex in practical implementation, and as a consequence, involve numerous errors. Among those, errors caused by buoyancy are the largest problem; in a field with a temperature gradient, buoyancy induces natural convection, which influences the movement of particles and disturbs the measurement. The velocity of such natural convection is usually comparable to the thermophoretic velocity, and cannot be measured directly. Toda et al. [4, 5] and Prodi et al. [6, 7] have conducted some experiments under microgravity conditions in order to avoid this problem. However, their reported data still seem to contain errors, possibly owing to limited trial numbers of experiments, so that those data are not sufficient to make quantitative comparison with theories [8].

Recently, our group has developed a device for conducting experiments repeatedly under a microgravity environment in a very short period time, i.e. 0.3 s, by means of the free-fall method, to accumulate data of the thermophoretic velocity. It has been confirmed that satisfactory accuracy can be attained if the amount of data is sufficient for statistical treatment [8]. By comparing the obtained experimental results with the existing theory [9], a notable difference is found for particles with high thermal conductivity [10]. The problem of the difference has been solved by reconsidering the boundary condition to improve the theory [11]. Hoshino et al. [12] has derived an improved theoretical solution of the thermophoretic velocity by applying the boundary condition proposed by Lockerby et al. [13], which includes the thermal stress slip and the higher order isothermal slip.

Considering the soot environment, it is indispensable to understand quantitatively the phenomenon for a gas mixture. Before analyzing the influence of the composition of the gas mixture, it is indispensable to know the characteristics of the phenomenon for each gas component since the combustion gas mixture contains many gas species.

In this study, the characteristics of the thermophoresis for several gas species, i.e., argon, nitrogen, and carbon dioxide are experimentally examined. The first one is chosen as the reference, and the latter two are chosen as the major components of exhaust gas from combustors.

4.2 Theory for Thermophoretic Velocity

The theory adopted in this work is based on the works by Hoshino et al. [12] and by Chang and Keh [14]. The thermophoretic velocity is calculated from the balance between the thermophoretic and the drag forces, the equation of which is shown as below:

$$V_T = \frac{2\mu C_f}{\rho T_{F0}} \frac{\left[C_S\left(k + C_T Kn\right) + C_H\left(C_M C_T Kn^2 + C_M Kn\left[k-1\right]\right)\right]}{\left[1 + 3C_M Kn + h\right]\left(1 + 2k + 2C_T Kn\right)} \left|\nabla T\right|, \qquad (4-1)$$

where μ, $|\nabla T|$, ρ, T_{F0}, C_f, k, Kn, h, C_M, C_T, C_S, and C_H are the viscosity, the temperature gradient, the density of the surrounding gas, the reference temperature, the slip correction factor of the drag force for rarefied condition, the gas-to-particle thermal conductivity ratio, Knudsen number, the term of higher order isothermal slip, and constants for slip flow, temperature jump, thermal creep, and thermal stress slip, respectively. Here, the reference temperature T_{F0} is defined as the supposed gas temperature at the center of the particle in the given temperature field without the existence of the particle, and Knudsen

number Kn is the ratio of the mean-free-path l to the particle radius. The mean-free-path is calculated from the following equation [15]:

$$l = \frac{\mu}{0.499P}\sqrt{\frac{\pi R T_{F0}}{8}}, \qquad (4-2)$$

where P and R are the pressure and the gas constant, respectively. The slip correction factor C_f adopted in this work is Cunningham's correction factor $C_{fc} = 1 + A\,Kn$, where $A = 1.257 + 0.4\exp(-1.10/Kn)$ [16]. The term h of higher order isothermal slip is written as below:

$$h = \frac{9}{2\pi} PrKn^2\left(1 - \gamma^{-1}\right), \qquad (4-3)$$

where Pr and γ are Prandtl number and the specific heat ratio, respectively.

Equation (4-1) is basically identical to both of those proposed by Hoshino et al. [12] and Chang and Keh [14]. If constant values $C_S = 0.75$ and $C_H = 1.00$ [13] are applied, the equation becomes just the same as the one given by Hoshino et al. [12]. On the other hand, the equation becomes the same as the one given by Chang and Keh [14] by neglecting the term h, which is usually negligible in the range of $Kn \le 0.1$, and applying Basset's correction [17], $C_{fb} = (1 + 3C_M Kn)/(1 + 2C_M Kn)$, instead of the Cunningham's correction for the slip correction factor C_f. The Basset's correction is applicable in $Kn \le 0.1$ while the Cunningham's one in $Kn < 1$, and both are basically identical in those applicable ranges.

Two constants C_M and C_T are calculated as follows from two empirical coefficients, i.e., the tangential momentum accommodation coefficient α_m and the thermal accommodation coefficient α_t:

$$C_M = \frac{2-\alpha_m}{\alpha_m}, \tag{4-4}$$

$$C_T = \frac{15}{8}\left(\frac{2-\alpha_t}{\alpha_t}\right). \tag{4-5}$$

These accommodation coefficients represent the magnitude of the momentum and energy exchange in the collision between gas molecules and the particle [15, 18], which are defined as below:

$$\alpha_m \equiv \frac{M_i - M_r}{M_i - M_s}, \tag{4-6}$$

$$\alpha_t \equiv \frac{E_i - E_r}{E_i - E_s}, \tag{4-7}$$

where M and E are average tangential components of the momentum and the energy flux normal to the particle surface, respectively, of gas molecules, and subscripts i, r, and s refer to incident molecules, molecules reflecting from the surface, and molecules leaving the surface in equalibrium with the surface, respectively. For example, $\alpha = 1$ corresponds to the situation that incident molecules achieve complete equilibrium with the particle surface before leaving, while $\alpha = 0$ corresponds to the situation of complete specular reflection.

In many cases, values of accommodation coefficients are simply assumed to be unity [10, 11]. There are some experimental measurements, e.g., Thomas and Lord [19] and Douglas [20], who measured accommodation coefficients on steel spheres and gas covered tungsten tube, respectively. Although those experiments report values different from unity under some conditions, yet there are no commonly accepted values.

4.3 Results

Figure 4.1 shows examples of the movement of particles during a free-fall in the surrounding gas of argon at 20 kPa. The measurement of the velocity should be taken at a fixed temperature since the thermophoretic velocity is dependent on not only the temperature gradient but also the temperature itself. The velocity of each particle is measured by tracing its movement while it travels within the range of the temperature between 313±2 K. It is seen from the figure that the velocity of each particle can be considered as constant in the range. The velocity is constant also in other two gases.

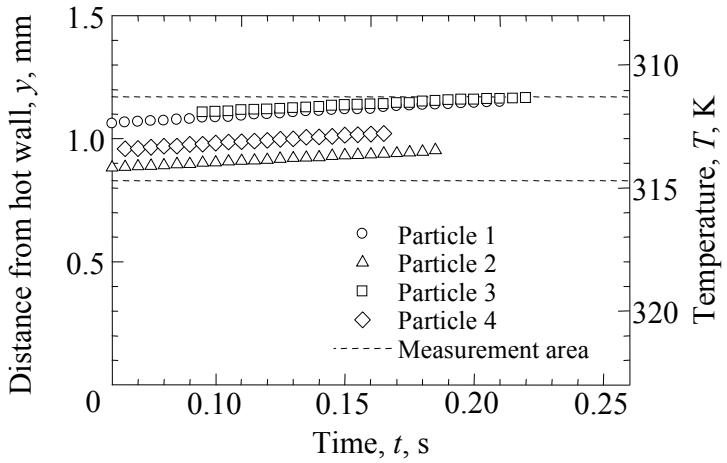

Fig. 4.1 Movement of particles in surrounding gas of argon.

Table 4.1 shows the statistical data for the tested pressure conditions with the argon gas. It is noted that the 95% confidence interval indicates not the range of data scattering but the range of expected mean value of the population. It is seen that the confidence interval is roughly estimated at around 0.01 mm/s to 0.02 mm/s. The ratio of the confidence interval to the mean value is only 3% for the pressure at 20 kPa. As the pressure increases, the velocity decreases, and as a consequence, the ratio tends to increase.

Table 4.1 Statistical data of thermophoretic velocity in surrounding gas of argon.

Pressure, P, kPa	20	40	60	80	100
Sampling number, n, –	39	35	37	33	47
Mean thermophoretic velocity, $\overline{V_T}$, mm/s	0.538	0.183	0.111	0.075	0.066
Standard deviation, σ, mm/s	0.053	0.044	0.026	0.030	0.036
Confidence interval (95%), mm/s	0.017	0.015	0.009	0.011	0.011
Ratio of confidence interval to mean thermophoretic velocity, –	0.03	0.08	0.08	0.15	0.17

Figure 4.2 shows the thermophoretic velocity for each gas. The white rectangle (□), the black circle (●), and the white circle (○) represent experimental values for argon, nitrogen, and carbon dioxide, respectively. Error bars in the figure indicate the 95% confidence interval for the mean. The solid line is the prediction calculated by assuming constants to be identical to those in the previous work [11], namely, C_M, C_T, C_S, and C_H to be 1.000, 1.875, 0.750, and 1.000, respectively.

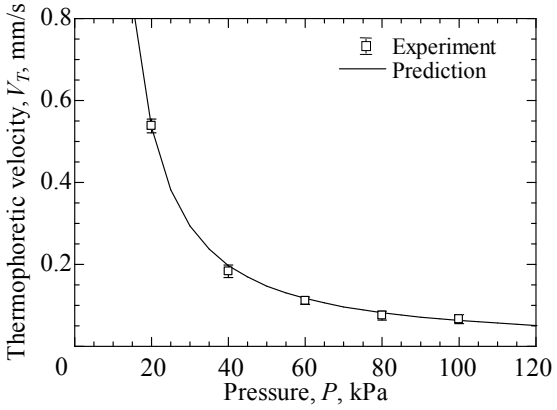

(a) Argon

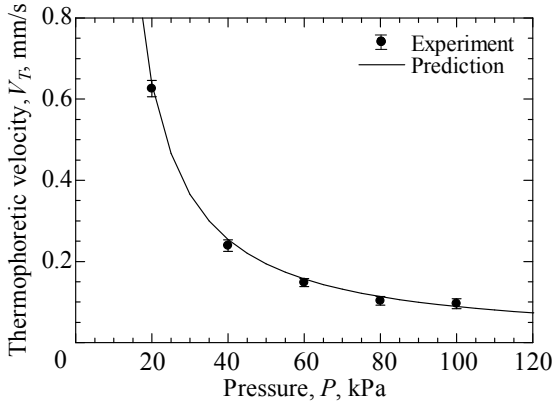

(b) Nitrogen

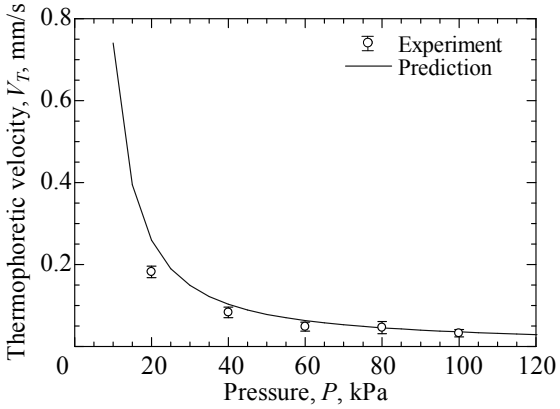

(c) Carbon dioxide

Fig. 4.2 Pressure dependence of thermophoretic velocity in each gas. Error bars represent the confidence interval (95%) for the mean. Predictions are calculated under the assumption of $C_M = 1.000$, $C_T = 1.875$, $C_S = 0.750$, and $C_H = 1.000$.

For argon and nitrogen, predictions are in good agreement with experiments throughout all the tested pressure conditions; the solid line runs through the range of the confidence interval at every tested pressure. On the other hand, for carbon dioxide, discrepancy is seen at low pressure conditions; the prediction is within the range of the confidence interval only when the pressure is at 100 kPa or 80 kPa. As the pressure decreases, discrepancy becomes notable; the experimental value at 20 kPa is 0.182 mm/s, which is 70% of the theory.

4.4 Discussion

It is quite interesting that the discrepancy is seen only for carbon dioxide. Also, previous work [11] has shown satisfactory accordance between the prediction and the experiment for the air. As noted earlier, the theory contains four constants, C_M, C_T, C_S, and C_H, and the former two of these are calculated from accommodation coefficients α_m and α_t. These constants and coefficients have been determined empirically; different researchers have given different proposed values. Attempts should be made for finding suitable values to fit the prediction to these experimental results.

The first attempt is done by applying proposed values from references, which are shown in Table 4.2. The set of values noted as Case 1 is from the paper by Hoshino et al. [11], and those as Case 2 and 3 are both from the paper by Chang and Keh [14]. Figure 4.3 shows predictions together with experimental results. The vertical axis represents the reduced thermophoretic velocity, which is a dimensionless parameter defined as follows:

$$V_{TR} \equiv \frac{V_T T_{F0}}{\upsilon \nabla T}, \qquad (4-8)$$

where υ is the kinematic viscosity of the gas. This parameter is often used when making comparison between different conditions. Lines labeled as Prediction 1, 2, and 3 are those predicted from Eq. (4-1) by applying values of Case 1, 2, and 3, respectively. For both argon and nitrogen, the best fit to experimental results is Prediction 1, and then Prediction 3 follows; the velocity predicted from Case 3 is higher than the experiment at $Kn = 0.25$ for both two gases, whereas that from Case 1 is within the error bar throughout all the measured range of Kn. For carbon dioxide, on the other hand, there is no line predicting satisfactorily the experimental result at $Kn = 0.15$, though Prediction 3 seems to be better than Prediction 1. Prediction 2 can be omitted from the discussion since it obviously disagrees with the experiment for all gases.

Table 4.2 Constants for each case.

	C_M, –	C_T, –	C_S, –	C_H, –	α_m, –	α_t, –	References
Case 1	1.000	1.875	0.750	1.000	(1.000)	(1.000)	[11]
Case 2	1.140	2.180	1.170	1.000	(0.935)	(0.925)	[14]
Case 3	1.140	2.180	1.170	3.000	(0.935)	(0.925)	[14]

[a] Values in bracket are from Eqs. (4-4) and (4-5) (not directly given in the reference).

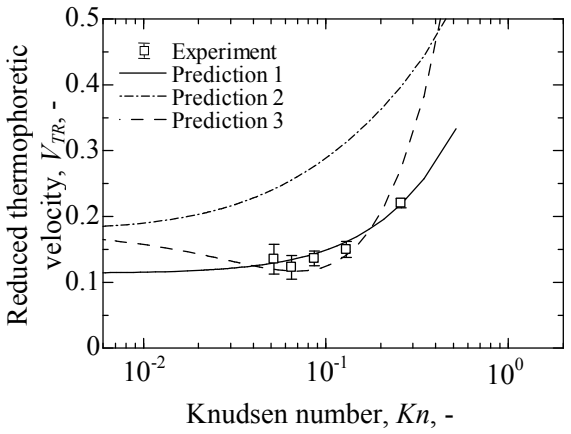

(a) Argon

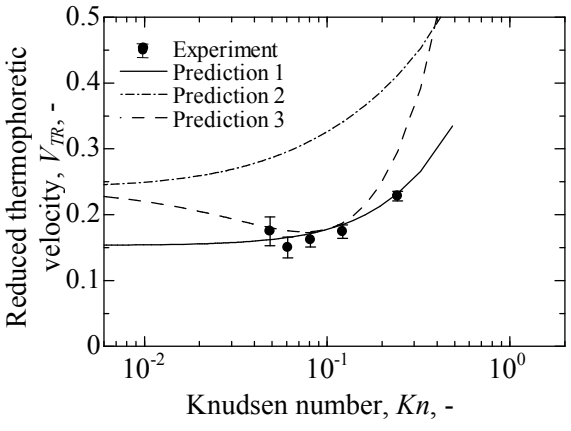

(b) Nitrogen

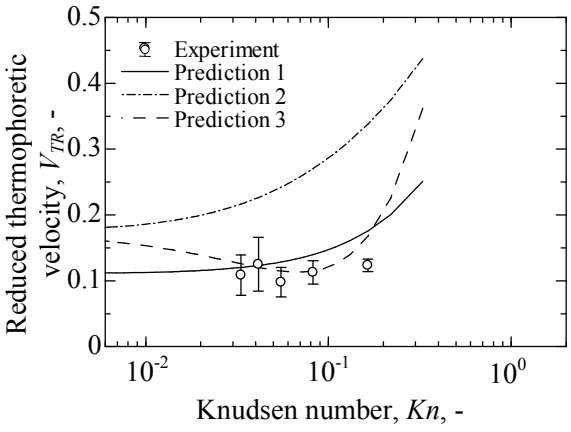

(c) Carbon dioxide

Fig. 4.3 Comparison between predictions and experiment in each gas. Error bars represent the confidence interval (95%) for the mean. Predictions are calculated using constants in Table 4.2.

Provisionally, Case 1 is chosen as the best among three cases; Case 3 is not good enough for high *Kn* for all tested gases in comparison to Case 1. Choosing Case 1 instead of Case 3 is also consistent with the previous work, in which experiments have been conducted in the air under the atmospheric pressure for particles of PMMA, alumina, and Zn [10]; as shown in Table 4.3, significant differences are seen between Case 3 and experimental results for alumina and Zn, whereas agreements are satisfactory for all particles with Case 1. In the theory, only the radius and the thermal conductivity are considered as particle-related parameters. It would be reasonable to assume that coefficients for CO_2 are different from those for other gases; Sharipov [21] has reviewed related papers and summarized accommodation coefficients for various gases, in which CO_2 values are notably different from Ar and N_2.

Table 4.3 Reduced thermophoretic velocity in air under atmospheric pressure.

	$V_{TR,-}$		
Material	Prediction (Case 1)	Prediction (Case 3)	Experiment*
PMMA	0.167	0.210	0.172 ± 0.011
Al_2O_3	0.037	-0.035	0.036±0.008
Zn	0.049	-0.034	0.050±0.010

*From Suzuki et al. [10].

The second attempt is done by changing the accommodation coefficients from Case 1 by means of the least square fit. The residue *R* representing the discrepancy between the experiment and the prediction is defined as follows:

$$R \equiv \sum_{j=1}^{n} \left(V_{ej} - V_{pj} \right)^2, \quad (j = 1,\ldots,n) \qquad (4-9)$$

where V_e, V_p, and n are thermophoretic velocities of the experiment and the prediction, and the number of the tested pressure conditions, respectively, and the subscript j refers to each tested condition. The values for C_S and C_H are unchanged from the Case 1, and those for C_M and C_T are calculated from Eqs. (4-4) and (4-5), respectively, with accommodation coefficients α_m and α_t determined such that the residue R becomes the lowest.

Table 4.4 shows the result of the least square fit for carbon dioxide. The best fit is attained with the coefficients noted as "without limitation" in the table. It should be noted that both values are clearly above unity, which is curious when interpreting the physical meaning of those values. Based on the kinetic theory, both those coefficients should lie between 0 and 1 [9, 15, 18]. The Cercignani-Lampis (CL) model provides a more physical description of the gas-surface interaction [21, 22], which allows α_m to vary between 0 and 2 while α_t remains between 0 and 1. In this CL model, α_m can exceed unity when the surface is rough. Considering this, additional work is done for the fitting by applying the limitation of $0 \leq \alpha_t \leq 1$ and $0 \leq \alpha_m \leq 2$, the result of which is shown as "with limitation" in the table. In this case, R becomes the lowest when both the coefficients are bellow unity even α_m is allowed to exceed it.

Table 4.4 Estimated accommodation coefficients for carbon dioxide.

	α_m, –	α_t, –
without limitation	1.193	1.307
with limitation	0.841	1.000

Figure 4.4 shows the comparison of predictions based on these values. It is seen that both predictions are in good agreement with the experiment within the range of the tested conditions. The difference between these two predictions is notable only under the condition of higher Knudsen number than the current work.

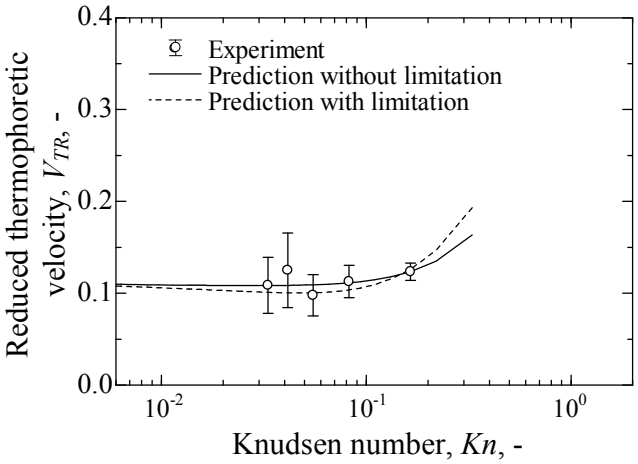

Fig. 4.4 Comparison of predictions for carbon dioxide.
Error bars represent the confidence interval (95%) for the mean. The solid and the broken lines represent predictions calculated with the coefficients from least-square-fit "without limitation" and "with limitation", respectively.

In order to interpret the different coefficients for the carbon dioxide, authors have found two different points of view from literatures so far; one is the molecular weight, and the other the diameter of a molecule. The former is based on the work by Gronych et al. [23], who have conducted experiments to find out that the tangential momentum accommodation coefficient increases as the molecular weight of the gas decreases. This may be related to the influence of gas species. However, applying this effect for the explanation of the present results would not be appropriate; the molecular weight of argon is closer to carbon dioxide rather than nitrogen, while the thermophoretic characteristic of the argon is much closer to the nitrogen rather than the carbon dioxide.

The latter is based on the work by Arya et al. [24], who have conducted a molecular simulation for a wall-slip phenomenon in rarefied gases. According to their result, the tangential momentum accommodation coefficient decreases as the collision diameter of the molecule increases. Among the gases used in this work, carbon dioxide has a notably larger collision diameter; based on the rigid sphere model, the diameter of argon, nitrogen, and carbon dioxide are 3.659 Å, 3.784 Å, and 4.643 Å, respectively [25]. This can explain qualitatively the results in this work if the coefficients "with limitation" are adopted for the carbon dioxide and those at unity are adopted for other two gases. The thermal accommodation coefficient "with limitation" is also consistent with the work by Winkler et al. [26], in which the coefficient α_t is reported to be approximately unity for water vapor, a polyatomic gas having a large collision diameter. The constants and coefficients, however, cannot be determined from the results in this work, since several combinations of those are possible to fit predictions to experimental results.

4.5 Conclusions

In this study, effects of gas species on the thermophoretic velocity are investigated, and following results are obtained:

1. Experimentally-obtained pressure dependence of the thermophoretic velocity for both argon and nitrogen are quantitatively in good agreement with the theory, while notable discrepancy is seen for carbon dioxide, if values for the constants C_M, C_T, C_S, and C_H to be 1.000, 1.875, 0.750, and 1.000 are applied to the theory.
2. Values of those empirical constants proposed in some references were applied to the theory and compared with experiments; none of those has reduced the notable deviation for the carbon dioxide at $Kn = 0.15$.
3. The coefficients are calculated by means of the least square fit. The obtained values can be interpreted qualitatively by considering the effect of the molecular diameter on the tangential momentum accommodation coefficient. The proposed values of C_M, C_T, C_S, and C_H for carbon dioxide are 1.378, 1.875, 0.750, and 1.000, although further discussion will be required for the determination of the values.

References:

[1] Yuasa, Y., Sasaki, H., and Tsukamoto, T. (2011). Particle size distribution of particulate matter exhausted from four stroke marine diesel engine. *Proceeding of the 49th Symposium (Japanese) on Combustion*, 310-311.

[2] Dobashi, R., Kong, Z.W., Toda, A., Takahashi, N., Suzuki, M., and Hirano, T. (2000). Mechanism of smoke generation in a flickering pool flame. *Proceeding of the 6th International Symposium on Fire Safety Science,* 255-264.

[3] Suzuki, S., and Dobashi, R. (2007). Thermophoretic effect on soot particle behavior –influence of particle morphology. *21st ICDERS*, 239.

[4] Toda, A., Ohi, Y., Dobashi, R., Hirano, T., and Sakuraya, T. (1996). Accurate measurement of thermophoretic effect in microgravity. *Journal of Chemical Physics, 105,* 7083-7087.

[5] Toda, A., Ohnishi, H., Dobashi, R., Hirano, T., and Sakuraya, T. (1998). Experimental study on the relation between thermophoresis and size of aerosol particles. *International Journal of Heat and Mass Transfer, 41,* 2710-2713.

[6] Prodi, F., Santachiara, G., Travaini, S., Vedernikov, A., Dubois, F., Minetti, C., and Legros, J.C. (2006). Measurements of phoretic velocities of aerosol particles in microgravity conditions. *Atmospheric Research, 82,* 183-189.

[7] Prodi, F., Santachiara, G., Di Matteo, L., Vedernikov, A., Beresnev, S.A., and Chernyak, V.G. (2007). Measurements of thermophoretic velocities of aerosol particles in microgravity conditions in different carrier gases. *Journal of Aerosol Science, 38,* 645-655.

[8] Suzuki, M., Maruko, K., Iwahara, K., and Masuda, W. (2009). Accurate measurement of thermophoretic velocity under high temperature gradient. *6th International Symposium on Scale Modelling (ISSM6),* 1.12.1-1.12.8.

[9] Brock, J.R. (1962). On the theory of thermal forces acting on aerosol. *Journal of Colloid Science, 17,* 768-780.

[10] Suzuki, T., Suzuki, M., and Masuda, W. (2009). Effect of water vapor to thermophoresis phenomenon. *Proceeding of the 47th Symposium (Japanese) on Combustion,* 448-449.

[11] Hoshino, A., Suzuki, M., and Masuda, W. (2010). Numerical analysis on thermophoretic phenomenon in slip flow regime considering thermal stress effect. *The 21st International Symposium on Transport Phenomena.*

[12] Hoshino, A., Suzuki, M., and Masuda, W. (2010). Influence of particle size distribution on measurement accuracy of thermophoretic velocity. *Proceeding of the 48th Symposium (Japanese) on Combustion,* 464-465.

[13] Lockerby, D.A., Reese, J.M., Emerson, D.R., and Barber, R.W. (2004). Velocity boundary condition at solid walls in rarefied gas calculations. *Physical Review E, 70,* 017303-1-017303-4.

[14] Chang, Y.C., and Keh, H.J. (2012). Effects of thermal stress slip on thermophoresis and photophoresis. *Journal of Aerosol Science, 50,* 1-10.

[15] Kennard, E.H. (1938). *Kinetic Theory*. McGraw-Hill: New York.

[16] Talbot, L., Cheng, R.K., Schefer, R.W., and Willis, D.R. (1980). Thermophoresis of particles in a heated boundary layer. *Journal of Fluid Mechanics, 101,* 737-758.

[17] Basset, A.B. (1961). *A Treatise on Hydrodynamics,* vol. 2. Dover: New York.

[18] Shen, C. (2010). *Rarefied Gas Dynamic: Fundamentals, Simulation, and Micro Flows*. Springer: Germany.

[19] Thomas, L.B., and Lord, R.G. (1974). Comparative measurements of tangential momentum and thermal accommodations on polished and on roughened steel spheres. *International Symposium on Rarefied Gas Dynamics, 8,* 405-412.

[20] Douglas, F.S. (1982). Energy and tangential momentum accommodation coefficients on gas covered tungsten. *Journal of Chemical Physics, 76,* 3814-3818.

[21] Sharipov, F. (2004). Data on the velocity slip and temperature jump coefficients. *Proceeding of Euro SimE,* 243-249.

[22] Sharipov, F. (2003). Application of the Cercignani-Lampis scattering kernel to calculations of rarefied gas flows. III. Poiseuille flow and thermal creep through a long tube. *European Journal of Mechanics B/Fluids, 22,* 145-154.

[23] Gronych, T., Ulman, R., Peksa, L., and Repa, P. (2004). Measurements of the relative momentum accommodation coefficient for different gases with a viscosity vacuum gauge. *Vacuum, 73,* 275-279.

[24] Arya, G., Chang, H.C., and Maginn, E.J. (2003). Molecular simulations of Knudsen wall-slip: Effect of wall morphology. *Molecular Simulation, 29,* 697-709.

[25] Ivchenko, I.N., Loyalka, S.K., and Tompson Jr., R.V. (2007). *Analytical Methods for Problems of Molecular Transport*. Springer: The Netherlands.

[26] Winkler, P.M., Vrtala, A., Wagner, P.E., Kulmala, M., Lehtinen, K.E.J., and Vesala, T. (2004). Mass and thermal accommodation during gas-liquid condensation of water. *Physical Review Letters, 93,* 075701-1-075701-4.

Chapter 5

Dependence on Gas Properties

5.1 Introduction

It is described in ***Chapter 4*** that several experiments have been conducted to investigate the influence of gas species on the thermophoretic velocity. The velocities have been measured for pure gases of argon, nitrogen, and carbon dioxide. The results of pure argon and nitrogen have agreed satisfactorily with the theory [1, 2] without any modification, while carbon dioxide has exhibited a noticeable deviation from the theory. It has been demonstrated in that chapter that this deviation can be corrected by modifying two empirical constants, i.e., the tangential momentum accommodation coefficient and the thermal accommodation coefficient, which both are involved in the theory and usually assumed to be unity [3 – 6].

Considering the environment of soot, one should know the accommodation coefficients of each gas species composing gas mixture. It would be desirable to specify physical relationship between the coefficients and the physical parameters for all gas species since the combustion gas contains many gas species. Some of these species are radical intermediates, e.g., OH, H, O, CH, etc. It is difficult for conducting the experiment using these gases since these gases are highly reactive.

In this study, an attempt is made to investigate dependence of thermophoretic parameters on gas properties; the parameters for argon and nitrogen are reexamined and compared with those of carbon dioxide, methane, and nitrous oxide.

5.2 Calculation of Residue Value

The thermophoretic parameters are determined based on the value of the residue. The residue R representing the discrepancy between the experiment and the prediction, which is defined as follows:

$$R \equiv \frac{\sum_{j=1}^{n} \left(V_{ej} - V_{pj}\right)^2}{n}, \quad (j = 1,...,n) \qquad (5-1)$$

where V_e, V_p, and n are the thermophoretic velocity of the experiment, the prediction, and the number of the measured particles, respectively. The subscript j refers to each particle.

The theory [1, 2] of the thermophoretic velocity is derived from the balance between the thermophoretic force and the drag force, which is given below:

$$V_T = \frac{3\mu C_c}{2\rho T_{F0}} \frac{\left[\left(k + C_T Kn\right) + \frac{4}{3}\left(C_M C_T Kn^2 + C_M Kn\left[k-1\right]\right)\right]}{\left[1 + 3C_M Kn + \frac{9}{2\pi} PrKn^2\left(1 - \gamma^{-1}\right)\right]\left(1 + 2k + 2C_T Kn\right)} \left|\nabla T\right|, \qquad (5-2)$$

where μ, $|\nabla T|$, ρ, T_{F0}, C_c, k, Kn, Pr, γ, C_M, and C_T are the viscosity, the temperature gradient, the density of the gas, the reference temperature, the Cunningham's correction factor, the gas-to-particle thermal conductivity ratio, Knudsen number, Prandtl number, the specific heat ratio, and constants for slip flow and temperature jump, respectively. C_M and C_T constants containing the tangential momentum accommodation coefficient α_m and the thermal accommodation coefficient α_t, respectively, which are written as follows:

$$C_M = \frac{2-\alpha_m}{\alpha_m}, \qquad (5-3)$$

$$C_T = \frac{15}{8}\left(\frac{2-\alpha_t}{\alpha_t}\right). \qquad (5-4)$$

These accommodation coefficients represent the magnitude of the momentum and energy exchange in the collision between gas molecules and particles. Based on the kinetic theory, both coefficients should lie between 0 and 1 [7 – 9]. The Cercignani-Lampis (CL) model provides a more physical description of the gas-surface interaction [10, 11], which allows α_m to vary between 0 and 2 while α_t remains between 0 and 1. In this CL model, α_m can exceed unity when the surface is rough.

In this work, the values of residue R are calculated for all combination of the coefficients.

5.3 Results

Figure 5.1 shows the reduced thermophoretic velocity for each gas species. The dimensionless reduced thermophoretic velocity is calculated as follows:

$$V_{TR} \equiv \frac{V_T T_{F0}}{\upsilon |\nabla T|}, \qquad (5-5)$$

where υ is the kinematic viscosity of the gas. The reduced velocity is often used when making comparison between different conditions. The black and the white symbols represent the obtained results from the previous work (***Chapter 4***) and this work, respectively. Lines represent predictions from different combinations of the coefficients, which will be explained later. Error bars in the figure indicate the 95% confidence interval for the mean. It is noted that the pressure, the reference temperature, and the

temperature gradient of those additional data from this work for argon, nitrogen, and carbon dioxide are 70 kPa, 338 K, and 60 K/mm, respectively. These results are added for increasing the number of experimental data such that the measurement accuracy increases. The residue values for all combination of the coefficients are calculated from the discrepancy between the experiment results and the prediction from Eq. (5-5).

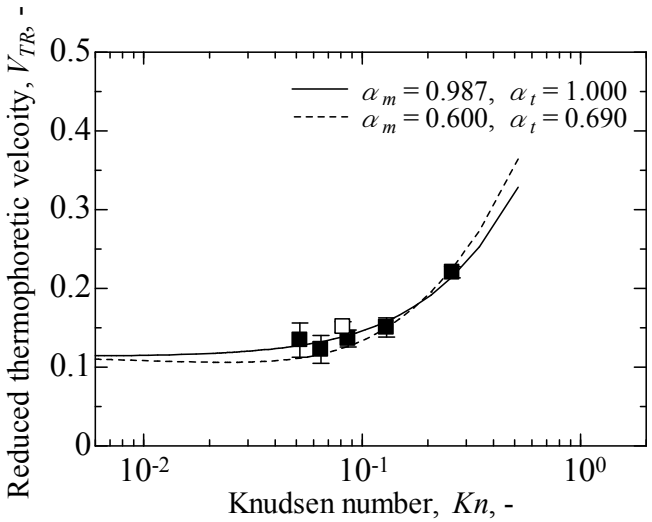

(a) Argon

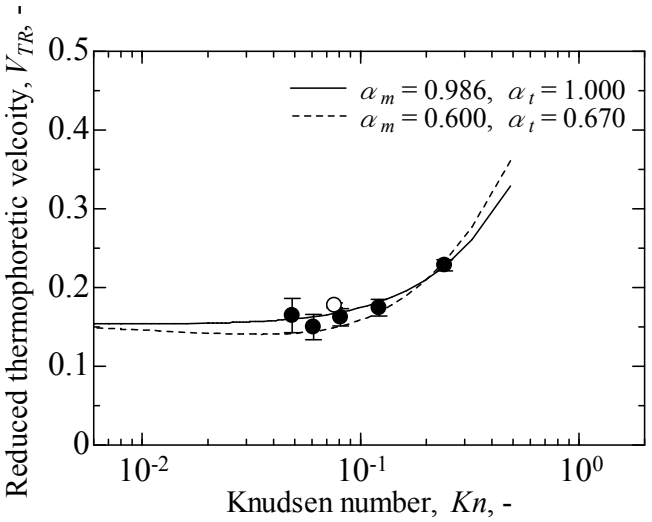

(b) Nitrogen

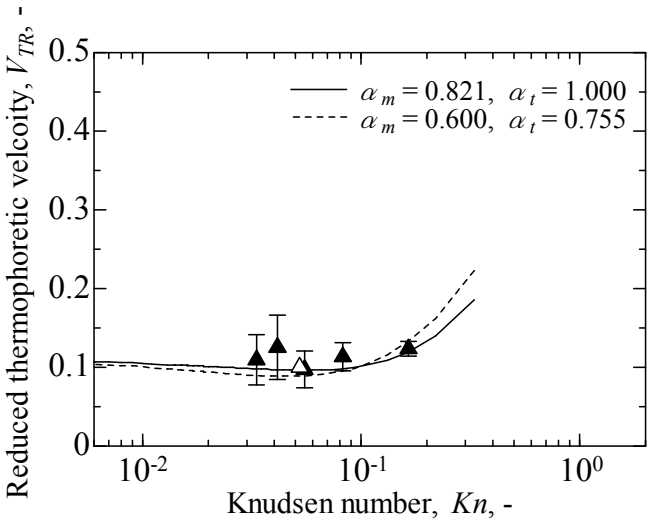

(c) Carbon dioxide

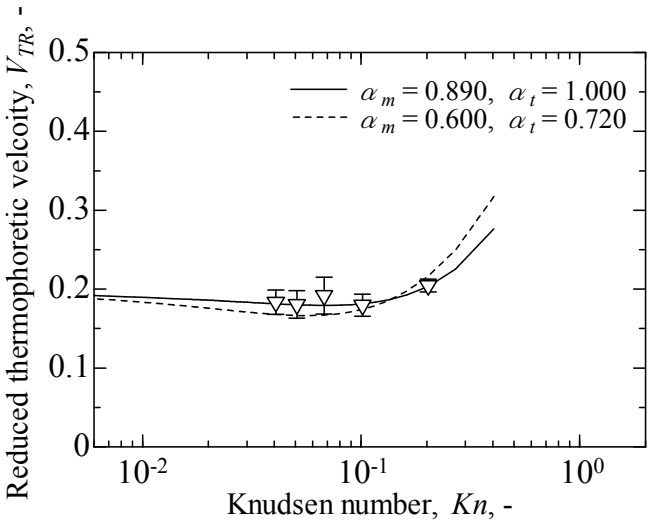

(d) Methane

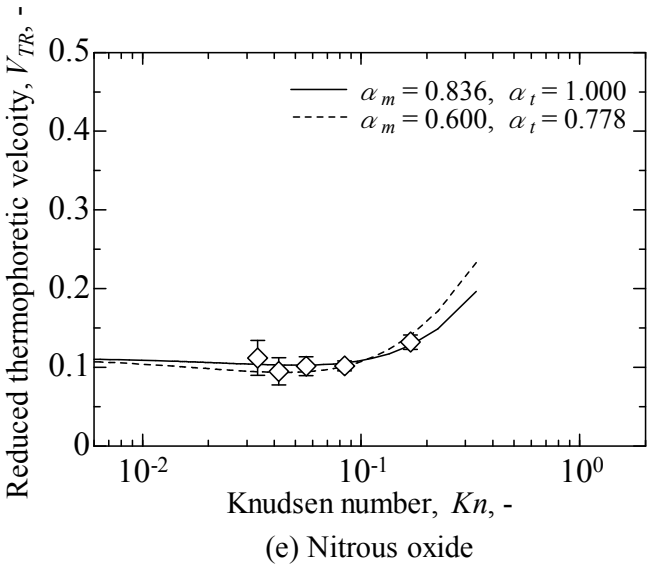

(e) Nitrous oxide

Fig. 5.1 Reduced thermophoretic velocity for each gas species.
Error bars represent the confidence interval (95%) for the mean.

Figure 5.2 shows contours of residues for each gas species. Solid lines represent the contour of the residue. The residue values are calculated within the ranges of $0 \le \alpha_t \le 1$ and $0 \le \alpha_m \le 2$, which are the limitations of both coefficients. It is seen that the contours have positive orientations for all tested gases. The dotted line represents the best approximation of the thermal accommodation coefficient for each tangential momentum accommodation coefficient. The thermal accommodation coefficient is determined such that the residue R becomes the lowest.

There is a problem for estimating the coefficients since the fitting gives several possible combinations. The same problem has been noted also in the ***Chapter 4***. It is impossible to make rigorous calculation of the coefficients owing to the complexity of the equation of thermophoretic velocity or force [12]. Figure 5.3 shows the minimum value of the residue for each tangential momentum accommodation coefficient for argon. It is seen that there are several coefficients exhibit approximately the same values of the

residues. A small increase up to only 4% is noticeable even the coefficient is reduced from 1.000 to 0.600. Comparisons of predictions between different combinations of the coefficients for each gas species are shown in Fig. 5.1. It is seen that for all gases, both predictions are in good agreement with the experiments within the range of the tested conditions.

In order to investigate the dependence of the coefficients on the gas properties, the tangential momentum accommodation coefficient is estimated by assuming the thermal accommodation coefficient to be unity. The assumption of the coefficient is made on the basis of results in the ***Chapter 4***; the thermophoretic velocity can be predicted quantitatively by modifying the tangential momentum accommodation coefficient while the thermal accommodation coefficient is assumed at unity. The assumption is also consistent with the work by Winkler et al. [13], in which the coefficient is reported to be approximately unity for water vapor, a polyatomic gas having a large collision diameter.

The black arrow in Fig. 5.2 represents the estimated tangential momentum accommodation coefficient for each gas. The coefficients are approximately the same for argon and nitrogen, while a significant difference is seen in the coefficient between the other three gases.

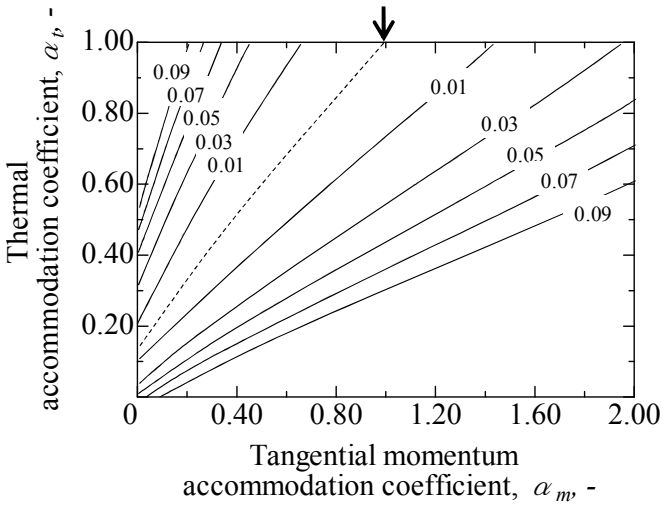

(a) Argon

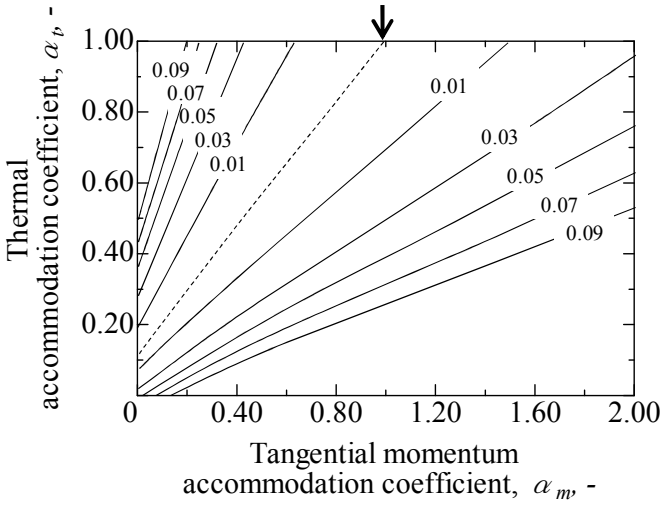

(b) Nitrogen

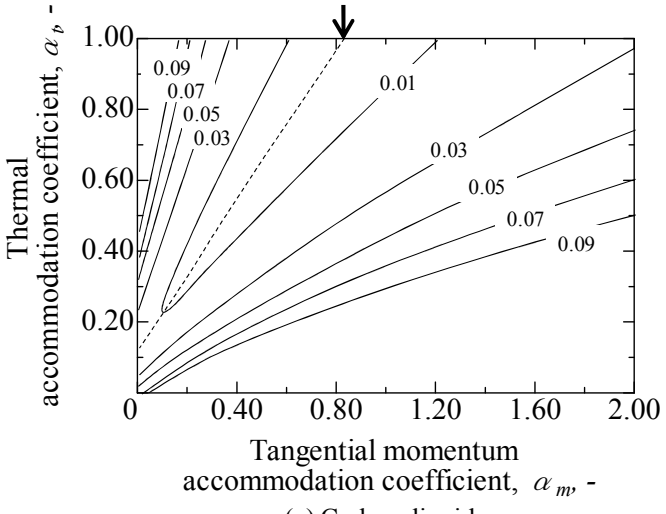

(c) Carbon dioxide

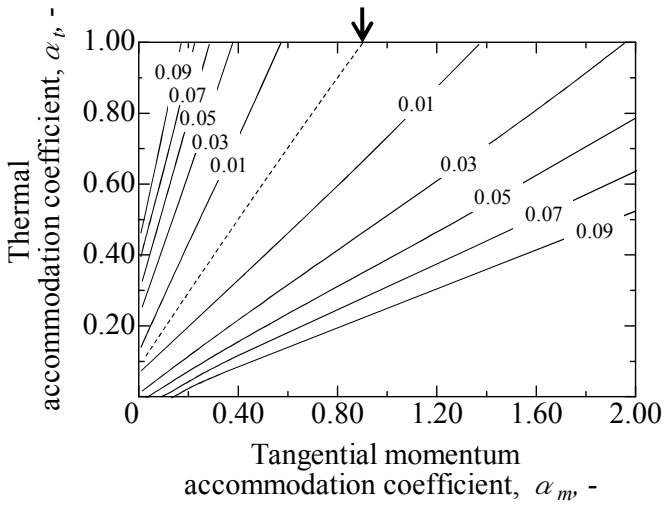

(d) Methane

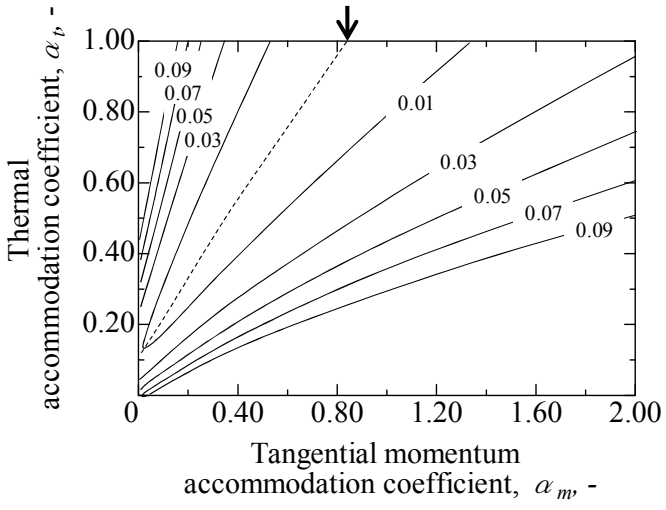

(e) Nitrous oxide

Fig. 5.2 Residue values for all combinations of coefficients for each gas species. The broken line represents best approximation of thermal accommodation coefficient for each tangential momentum accommodation coefficient.

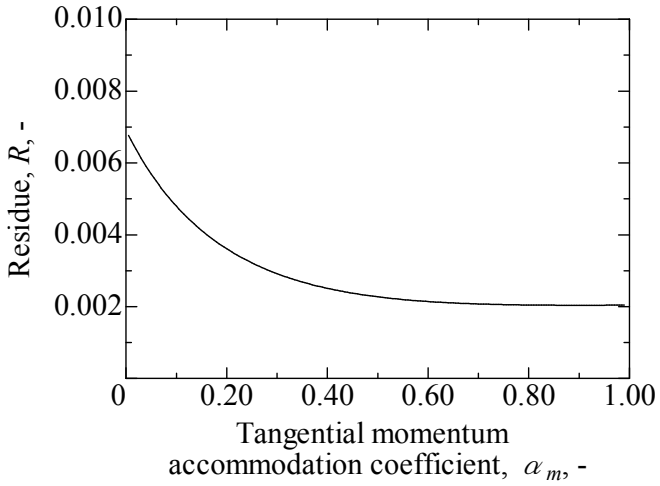

Fig. 5.3 Minimum value of residue of each tangential momentum accommodation coefficient for argon.

5.4 Discussion

It is interesting that the tangential momentum accommodation coefficient differs among the tested gases. The different coefficients between gases can be interpreted by gas properties. Several researches have been done to investigate the dependence of the coefficient on gas properties. Arya et al. [14] have conducted a molecular simulation for a wall-slip phenomenon in rarefied gases flowing through micro- and nano-channels and have found that the coefficient decreases as the collision diameter of the molecule increases. Gronych et al. [15] have performed experiments to determine the coefficient by means of a viscosity vacuum gauge with a vibrating metal ribbon. The measurements show that the coefficient is dependent on the molecular weight; the coefficient of the lighter gas molecule is greater than that of heavier ones. Dadzie and Meolens [16] have proposed a new model of scattering kernels by considering more possible reflection types of molecules at a wall by employing a partial coefficient concept of various modes, i.e.,

translation, rotation, and vibration. The coefficient has been suggested to be influenced by the degree of freedom.

Table 5.1 shows the estimated tangential momentum accommodation coefficient and the gas properties for each gas species. It is seen that carbon dioxide has almost the same properties as nitrous oxide, while differences are found between other three gases.

Table 5.1 Estimated tangential momentum accommodation coefficient and gas properties for each gas species.

Gas	α_m, -	Molecular weight, g/mol	Degree of freedom, -	Molecular diameter, Å
Argon	0.987	39.944	3	3.659
Nitrogen	0.986	28.02	5	3.784
Carbon dioxide	0.821	44.01	5	4.643
Methane	0.890	16.04	6	4.158
Nitrous oxide	0.836	44.02	5	4.662

Figure 5.4 shows the dependence of the tangential momentum accommodation coefficient on the molecular weight of gases. It is suggested that the coefficient decreases as the molecular weight increases [15]. Two disagreements are seen between the results in this work and the hypothesis given in the reference. In cases of methane, nitrogen, and argon, it is seen that the coefficient increases as molecular weight increases. In cases of carbon dioxide and nitrous oxide, the coefficients for both gases are smaller than the coefficient of argon even the molecular weights are approximately the same for those gases.

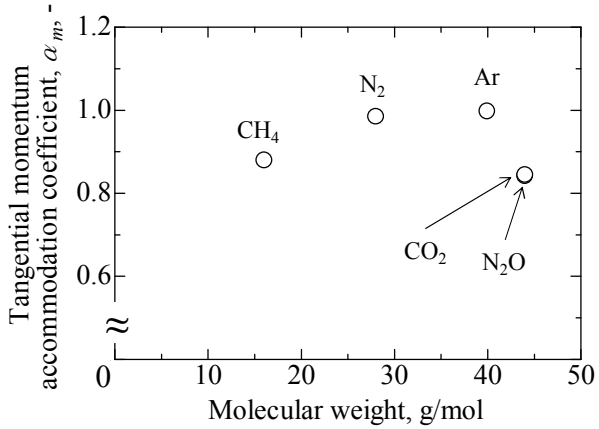

Fig. 5.4 Relation between coefficient and molecular weight.

Figure 5.5 shows the dependence of the coefficient on the degree of freedom of gases. The result is inconsistent with the hypothesis that the coefficient is influenced by the degree of freedom [16]. It is seen that the results cannot be explained by a simple relationship between the coefficient and the degree of freedom. Two curious relationships are found from the results. First, the coefficients for argon and nitrogen are almost identical even both gases have different degree of freedom. Second, the coefficient for nitrogen is significantly greater than the coefficients for carbon dioxide and nitrous oxide, even nitrogen has the same degree of freedom with the other two gases.

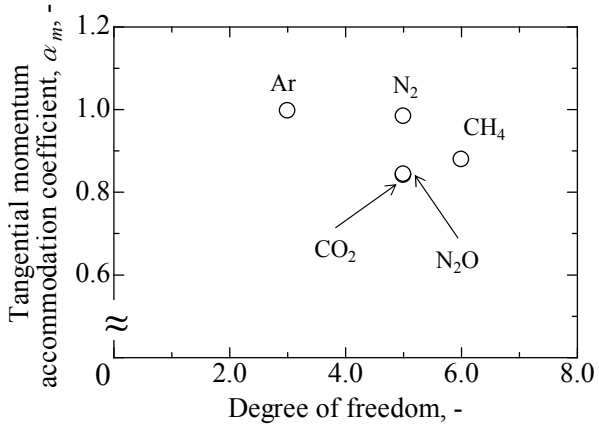

Fig. 5.5 Relation between coefficient and degree of freedom.

Figure 5.6 shows the dependence of the coefficient on the molecular diameter of gas molecule. The results in this work can be explained qualitatively based on the effect of molecular diameter; the coefficient decreases as the diameter increases. These results are consistent with the work done by Arya et al. [14]. The value of coefficient is presumably dependent upon the interaction characteristic between gas molecules and the surface. The results infer that when small gas molecule collides with the surface, it loses the tangential momentum more than a large gas molecule.

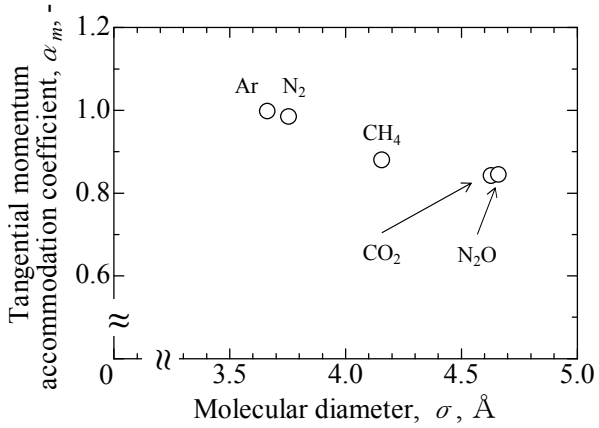

Fig. 5.6 Relation between coefficient and molecular diameter.

There is a possibility that the coefficient is also dependent on the material of the solid; Thomas and Lord [17] have measured coefficients for polished and rough surfaces of steel spheres to find some influence of surface condition of the solid wall. However, this problem can be neglected in the present experiment since all experimental data are obtained from the same kind of particles.

5.5 Conclusions

In this study, the thermophoretic parameters of several gases are estimated from the experimental results, and following results are obtained:

1. The value of the residue R is calculated from the discrepancy between the experiment results and the prediction for all combinations on the coefficients; several combinations of the coefficients are possible to fit the prediction with the experimental results.

2. The tangential momentum accommodation coefficient is estimated by assuming the thermal accommodation coefficient to be unity; the tangential momentum accommodation coefficient are approximately the same for argon and nitrogen, while a significant difference is seen for methane, nitrous oxide, and carbon dioxide.

3. A relation is shown between the tangential momentum accommodation coefficient and the molecular diameter; the coefficient decreases as the diameter increases.

References:

[1] Hoshino, A., Suzuki, M., and Masuda, W. (2010). Influence of particle size distribution on measurement accuracy of thermophoretic velocity. *Proceeding of the 48th Symposium (Japanese) on Combustion,* 464-465.

[2] Chang, Y.C., and Keh, H.J. (2012). Effects of thermal stress slip on thermophoresis and photophoresis. *Journal of Aerosol Science, 50,* 1-10.

[3] Li, W., and Davis, E.J. (1995). Measurement of thermophoretic force by electrodynamics levitation: microspheres in air. *Journal of Aerosol science, 26,* 1063-1083.

[4] Prodi, F., Santachiara, G., Di Matteo, L., Vedernikov, A., Beresnev, S.A., and Chernyak, V.G. (2007). Measurements of thermophoretic velocities of aerosol particles in microgravity conditions in diffirent carrier gases. *Journal of Aerosol Science, 38,* 645-655.

[5] Suzuki, T., Suzuki, M., and Masuda, W. (2009). Effect of water vapor to thermophoresis phenomenon. *Proceeding of the 47th Symposium (Japanese) on Combustion,* 448-449.

[6] Hoshino, A., Suzuki, M., and Masuda, W. (2010). Numerical analysis on thermophoretic phenomenon in slip flow regime considering thermal stress effect. *The 21st International Symposium on Transport Phenomenon,* 464-465.

[7] Brock, J.R. (1962). On the theory of thermal forces acting on aerosol. *Journal of Colloid Science, 17,* 768-780.

[8] Kennard, E.H. (1938). *Kinetic Theory*. McGraw-Hill: New York.

[9] Shen, C. (2010). *Rarefied Gas Dynamic: Fundamentals, Simulation, and Micro Flows*. Springer: Germany.

[10] Sharipov, F. (2003). Application of the Cercignani-Lampis scattering kernel to calculations of rarefied gas flows. III. Poiseuille flow and thermal creep through a long tube. *European Journal of Mechanics B/Fluids, 22,* 145-154.

[11] Sharipov, F. (2004). Data on the velocity slip and temperature jump coefficients. *Proceeding of Euro SimE,* 243-249.

[12] Keng, E., and Orr, C. (1966). Thermal precipitation and particle conductivity. *Journal of Colloid and Interface Science, 22,* 107-116.

[13] Winkler, P.M., Vrtala, A., Wagner, P.E., Kulmala, M., Lehtinen, K.E.J., and Vesala, T. (2004). Mass and thermal accommodation during gas-liquid condensation of water. *Physical Review Letters, 93,* 075701-1-075701-4.

[14] Arya, G., Chang, H.C., and Maginn, E.J. (2003). Molecular simulations of Knudsen wall-slip: Effect of wall morphology. *Molecular Simulation, 29,* 697-709.

[15] Gronych, T., Ulman, R., Peksa, L., and Repa, P. (2004). Measurements of the relative momentum accommodation coefficient for different gases with a viscosity vacuum gauge. *Vacuum, 73,* 275-279.

[16] Dadzie, S.K., and Meolens, J.G. (2004). Anisotropic scattering kernel: generalized and modified Maxwell boundary conditions. *Journal of Mathematical Physics, 45,* 1804-1819.

[17] Thomas, L.B., and Lord, R.G. (1974). Comparative measurements of tangential momentum and thermal accommodations on polished and on roughened steel spheres. *International Symposium on Rarefied Gas Dynamics, 8,* 405-412.

Chapter 6

Effect of Molecular Fraction

6.1 Introduction

As noted earlier, the theory of thermophoretic velocity contains two empirical constants, i.e., the tangential momentum accommodation coefficient and the thermal accommodation coefficient, both which are usually assumed to be unity [1 – 4]. In the ***Chapter 5***, the accommodation coefficients have been estimated for pure gases of argon, nitrogen, carbon dioxide, methane, and nitrous oxide. The results show the coefficients are approximately the same for argon and nitrogen, while significant differences are seen for other three gases.

A problem arises here for the treatment of accommodation coefficients of a mixture of pure gases having different values, e.g., the mixture of nitrogen and carbon dioxide. It should better be confirmed even when the mixture is composed of pure gases having the same coefficient value, e.g. the mixture of argon and nitrogen, since there is no widely-accepted method so far for evaluating the coefficients of the mixture from the values of composing pure gases.

There are some theoretical and experimental researches dealing with one of those coefficients of gas mixtures, although none of those gives explicit discussion for both the coefficients together. Mikami et al. [5] have measured heat-transfer coefficients of a

sphere in hydrogen-nitrogen and helium-nitrogen mixtures by utilizing a thermistor, and have compared those results with an analytical solution based on the Maxwell's model; good agreement has been shown by applying a linearly-dependent relation of the accommodation coefficient to the gas concentration. Wise et al. [6] have conducted experiments to measure the heat transfer with a conductivity cell in a gas mixture of atomic and molecular oxygens. The coefficient for pure atomic oxygen is estimated from extrapolation of experimentally-determined thermal accommodation coefficients of mixtures containing small amount of atomic oxygen. Ivchenko et al. [7, 8] have studied the slip phenomenon in the flow of a gas mixture to develop an analytical solution for planar transport problems. Bentz et al. [9] have performed experiments with a spinning rotor gauge to measure the slip flow constant, which is related to the tangential momentum accommodation coefficient, for helium-argon, helium-nitrogen, and helium-neon mixtures. Bentz et al.'s experimental results exhibit a nonlinear dependence on the mixture concentration; it seems to agree qualitatively well with the prediction from the Ivchenko et al.'s solution, though they have written of it "there are large differences". Further investigation will be needed in order to determine the appropriate method for evaluating mixture's coefficients.

In this study, thermophoretic parameters are experimentally investigated for several gas mixtures, i.e., argon-nitrogen, argon-carbon dioxide, and nitrogen-carbon dioxide. The dependence of the tangential momentum accommodation coefficient on the concentration of the mixture is examined from the measured thermophoretic velocity.

6.2 Factors Affected by Gas Mixing

The problem for a gas mixture is the treatment of two empirical parameters, i.e., tangential momentum- and thermal-accommodation coefficients, which characterize the interaction between the solid surface of the particle and surrounding gas molecules. In the gas mixture, a diffusiophoretic force will be exerted on a particle in addition to the thermophoretic force since the temperature gradient causes a concentration gradient. The thermodiffusiophoretic velocity for a gas mixture is shown as below:

$$V_{TD} = \frac{3\mu C_c}{2\rho T_{F0}} \frac{\left[\left(k + C_T Kn\right) + \frac{4}{3}\left(C_M C_T Kn^2 + C_M Kn\left[k-1\right]\right)\right]}{\left[1 + 3C_M Kn + \frac{9}{2\pi} PrKn^2\left(1-\gamma^{-1}\right)\right]\left(1 + 2k + 2C_T Kn\right)} \left|\nabla T\right| + C_c c' D_{12} \left|\nabla x_1\right|, \quad (6-1)$$

where μ, $|\nabla T|$, ρ, T_{F0}, C_c, k, Kn, Pr, γ, C_M, C_T, c', D_{12}, and $|\nabla x_1|$ are the viscosity, the temperature gradient, the density of the gas, the reference temperature, the Cunningham's correction factor, the gas-to-particle thermal conductivity ratio, Knudsen number, Prandtl number, the specific heat ratio, the constant for slip flow, the constant for temperature jump, the diffusion slip factor, the coefficient of molecular diffusion, and the concentration gradient, respectively. Here, the reference temperature T_{F0} is defined as the supposed gas temperature at the center of the particle in the given temperature field without the existence of the particle. The first term in the right hand side of eq. (6 - 1) is the thermophoretic term, which is the same as in the previous ***Chapters 4*** and ***5***. The second term is the diffusiophoretic term [10], which is detail discussed in ***Appendix B***. The density ρ, the viscosity μ, and the thermal conductivity of gas k_f for a binary gas mixture are calculated as follows [11]:

$$\rho = \frac{P_1}{R_1 \cdot T} + \frac{P_2}{R_2 \cdot T}, \tag{6-2}$$

$$\mu = \sum_{j}^{n} \frac{\mu_j}{1 + \sum_{\substack{j=1 \\ n \neq i}}^{n} \varphi_{jn} \left(x_n / x_j \right)}, \tag{6-3}$$

$$k_f = \sum_{j}^{n} \frac{k_{fj}}{1 + \sum_{\substack{j=1 \\ n \neq i}}^{n} \phi_{jn} \left(x_n / x_j \right)}. \tag{6-4}$$

Here,

$$\varphi_{jn} = \frac{\left(1 + \left(\mu_j / \mu_n \right)^{1/2} \left(M_n / M_j \right)^{1/4} \right)^2}{2\sqrt{2} \left(1 + \left(M_j / M_n \right) \right)^{1/2}}, \tag{6-5}$$

$$\phi_{jn} = \frac{1}{4} \left(1 + \left[\frac{\mu_j}{\mu_n} \left(\frac{M_n}{M_j} \right)^{3/4} \frac{1 + \left(C_j / T \right)}{1 + \left(C_n / T \right)} \right]^{1/2} \right)^2 \left(\frac{1 + \left(C_{jn} / T \right)}{1 + \left(C_j / T \right)} \right), \tag{6-6}$$

$$C_{jn} = \left(C_j \cdot C_n \right)^{0.5} \tag{6-7}$$

where R, C, M, and x are the gas constant, Sutherland constant, the molecular weight and the molar fraction, respectively. Subscripts j and n refer to the number of each gas species and the total number, respectively. Parameters c', D_{12}, and $|\nabla x_1|$ are calculated by complex equations given by Kihara [12] and Ivchenko et al. [8].

Constants C_M and C_T in eq. (6 - 1) are the ones containing the tangential momentum accommodation coefficient α_m and the thermal accommodation coefficient α_t, respectively, which are written as follows:

$$C_M = \frac{2 - \alpha_m}{\alpha_m}, \tag{6-8}$$

$$C_T = \frac{15}{8}\left(\frac{2-\alpha_t}{\alpha_t}\right). \qquad (6-9)$$

In order to apply this same formula to a gas mixture, those coefficients of the mixture should be determined from values of each pure gas components.

In this work, only the tangential momentum accommodation coefficient is derived from experimental results, and the other one, the thermal accommodation coefficient, is assumed to be unity on the basis of results in the ***Chapter 5***, in which all the thermal accommodation coefficients have been estimated at unity for the same pure gases adopted in this work.

There are three different methods for the calculation of the tangential momentum accommodation coefficient of a mixture, which are explained below:

i. Energy-balance-based method

The first one is given by Mikami et al. [5], who derived the tangential momentum accommodation coefficient for a gas mixture from the energy balance as below:

$$\alpha_{m,mix} = \frac{\sum_{j=1}^{2} \frac{x_j \alpha_{m,j}}{\sqrt{M_j}}}{\sum_{j=1}^{2} \frac{x_j}{\sqrt{M_j}}}, \qquad (6-10)$$

where x and M are the molar fraction and the molecular weight, respectively, and subscript j refers to the number of each gas species.

ii. Mass-fraction-based method

The second one is found in the ANSYS FLUENT theory guide [13], in which both the accommodation coefficients of a mixture are calculated simply by taking the mass-fraction weighted average of each gas species as follows:

$$\alpha_{mix} = \sum_{j=1}^{2} y_j \alpha_j , \qquad (6-11)$$

where y_j and α are the mass fraction of each gas species j and each accommodation coefficient, respectively.

iii. Intermolecular-interaction-based method

The last one can be derived from equations given by Ivchenko et al. [7, 8]. The constant C_M for the slip-flow of a gas mixture was derived using the first-order Chapman-Enskog approximation and the Maxwell method as below:

$$C_M = \frac{5}{16}\pi \frac{P\sqrt{x_1 M_1 + x_2 M_2}}{\mu} \frac{(2-\alpha_{1m})x_1 b_1 + (2-\alpha_{2m})x_2 b_2}{\alpha_{1m} x_1 \sqrt{M_1} + \alpha_{2m} x_2 \sqrt{M_2}}, \qquad (6-12)$$

where P and b are the pressure and the transport coefficient [7, 8] of viscosity corresponding to arbitrary models of the intermolecular interaction, respectively, and subscripts 1 and 2 refer to components of the binary gas mixture. Here, it is noted that the literature adopts the following equation instead of eq. (6 - 8):

$$C_M = \frac{5}{16}\pi \frac{(2-\alpha_m)}{\alpha_m}. \qquad (6-13)$$

This equation is basically identical to the eq. (6 - 8): the additional coefficient of $5\pi/16$ to the eq. (6 - 8) makes the resultant value only 2% less. By equating those two eqs. (6 - 12) and (6 - 13), the tangential momentum accommodation coefficient of the mixture can be formulated as a function of the coefficients of two pure gases as follows:

$$\alpha_{m,mix} = 2\left(1 + \frac{P\sqrt{x_1 M_1 + x_2 M_2}}{\mu} \frac{(2-\alpha_{1m})x_1 b_1 + (2-\alpha_{2m})x_2 b_2}{\alpha_{1m} x_1 \sqrt{M_1} + \alpha_{2m} x_2 \sqrt{M_2}}\right)^{-1}. \qquad (6-14)$$

6.3 Results

Figure 6.1 shows measured velocities for argon-nitrogen, argon-carbon dioxide, and nitrogen-carbon dioxide mixtures. Lines represent predictions by above-mentioned methods, which will be explained later. Error bars in the figure indicate the 95% confidence interval for the mean.

Nitrogen exhibits the highest thermophoretic velocity, followed by argon and carbon dioxide; the thermophoretic velocities for pure nitrogen, argon, and carbon dioxide are 0.880 mm/s, 0.673 mm/s, and 0.273 mm/s, respectively. For the mixture of argon-nitrogen, the thermophoretic velocity increases as the concentration of nitrogen increases. For mixtures of argon-carbon dioxide and nitrogen-carbon dioxide, the thermophoretic velocity decreases as the concentration of carbon dioxide increases.

Figure 6.2 shows tangential momentum accommodation coefficients of pure gases of argon, nitrogen, and carbon dioxide. The accommodation coefficient α_m for each experimental datum is calculated from eqs. (6 - 1), (6 - 8), and (6 - 9) by assuming $\alpha_t = 1$, and the mean value and its 95% confidence interval are statistically obtained for each experimental condition. White and black symbols represent values from the previous (***Chapter 4***) and this works, respectively. Solid lines indicate mean values among all pressure conditions. Coefficients from this work seem to be consistent with those from the previous.

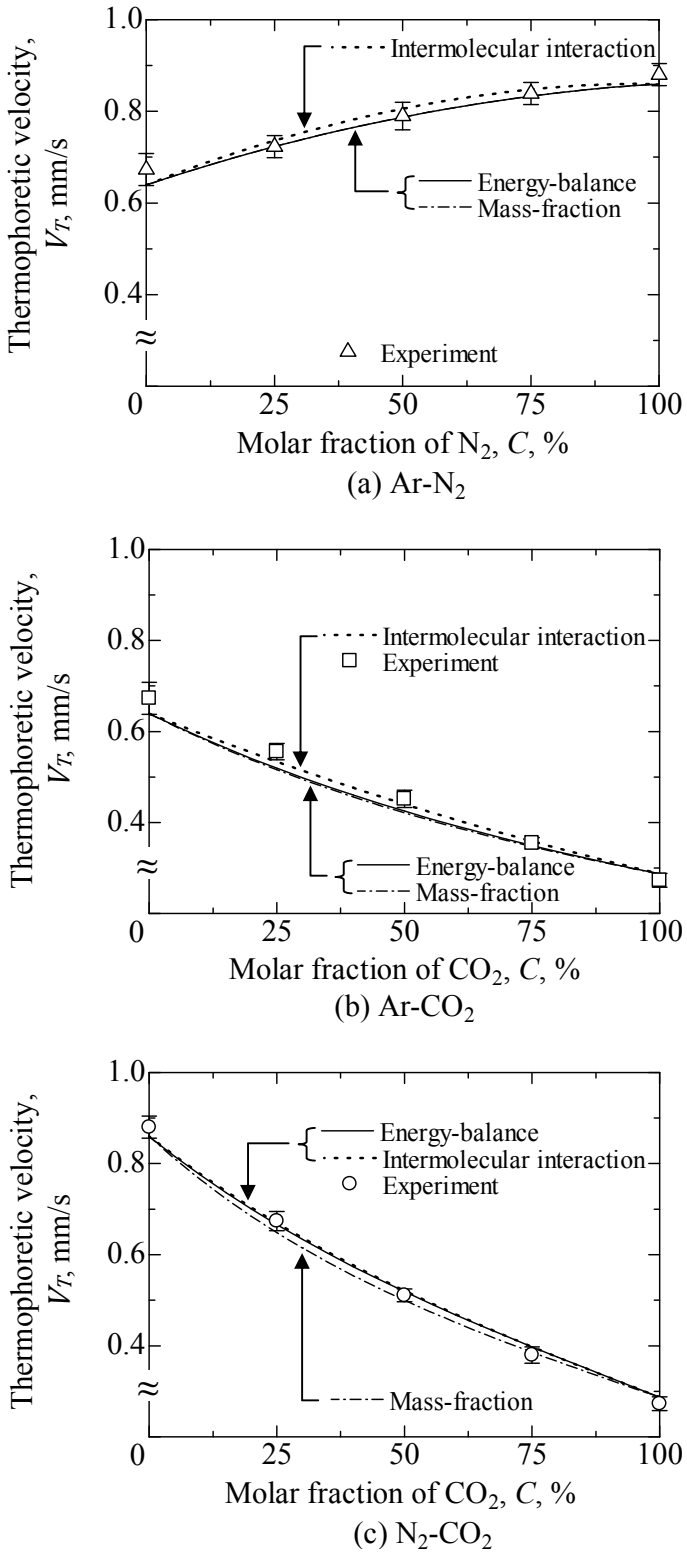

Fig. 6.1 Thermophoretic velocity for each gas mixture.
Error bars represent the confidence interval (95%) for the mean.

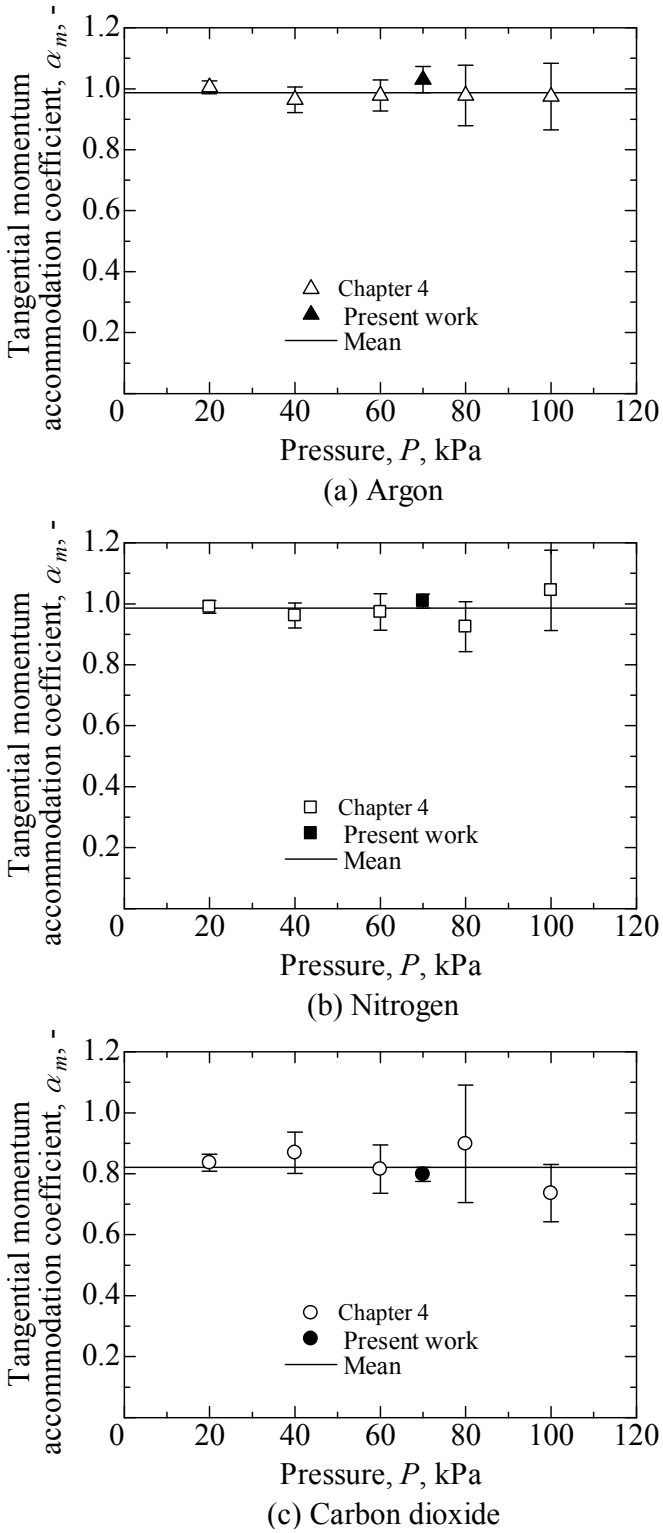

Fig. 6.2 Tangential momentum accommodation coefficient for each pure gas. Error bars represent the confidence interval (95%) for the mean.

Table 6.1 shows mean values of the coefficient from all the pressure conditions. Coefficients for argon and nitrogen are almost the same: 0.987 and 0.986, respectively. That for carbon dioxide exhibits a notably low value at 0.821.

Table 6.1 Tangential momentum accommodation coefficient α_m for each pure gas.

Gas	α_m
Argon	0.987
Nitrogen	0.986
Carbon dioxide	0.821

Table 6.2 shows the tangential momentum accommodation coefficient calculated from experimental results. Error ranges indicate the 95% confidence interval for the mean. For argon-carbon dioxide and nitrogen-carbon dioxide, it is seen that the coefficient is dependent on the gas concentration. For the mixture of argon-nitrogen, the slightly increase up to 1% is noticeable in the mean value. However, it is difficult to make a statistically significant since the mean values are within the error range.

Table 6.2 Estimated tangential momentum accommodation coefficient α_m for each gas mixture.

Ratio	Ar:N_2	Ar:CO_2	N_2:CO_2
1.00:0.00	0.987 ± 0.028	0.987 ± 0.028	0.986 ± 0.026
0.75:0.25	0.989 ± 0.027	0.991 ± 0.025	0.965 ± 0.028
0.50:0.50	0.993 ± 0.031	0.949 ± 0.029	0.905 ± 0.022
0.25:0.75	0.992 ± 0.026	0.877 ± 0.022	0.846 ± 0.033
0.00:1.00	0.986 ± 0.026	0.821 ± 0.031	0.821 ± 0.031

Figure 6.3 shows comparisons of the tangential momentum accommodation coefficient of experiments and predictions from eqs. (6 - 10), (6 - 11), and (6 - 14). In cases of gas mixtures of argon-nitrogen and argon-carbon dioxide, predictions by the energy-balance and the mass-fraction methods are almost identical. On the other hand, in the case of nitrogen-carbon dioxide, predictions by the energy-balance and the intermolecular-interaction methods give close results while the mass-fraction method is distinguishable from others. Although there is slightly difference between methods, all predictions agree satisfactorily with the experimental result for argon-nitrogen. For argon-carbon dioxide, disagreements are seen between the experimental result and predictions by the energy-balance and the mass-fraction methods. For nitrogen-carbon dioxide, slightly disagreement is noticeable between the mass-fraction method and the experimental result at 25% carbon dioxide. The intermolecular-interaction method seems to be the best for all those mixture conditions.

Comparisons of thermophoretic velocities between predictions and experiments for gas mixtures are shown in Fig. 6.1. Although the difference is not so remarkable, the intermolecular-interaction method seems to be the best among compared three methods; the energy-balance and the mass-fraction methods underestimate the velocity for argon-carbon dioxide.

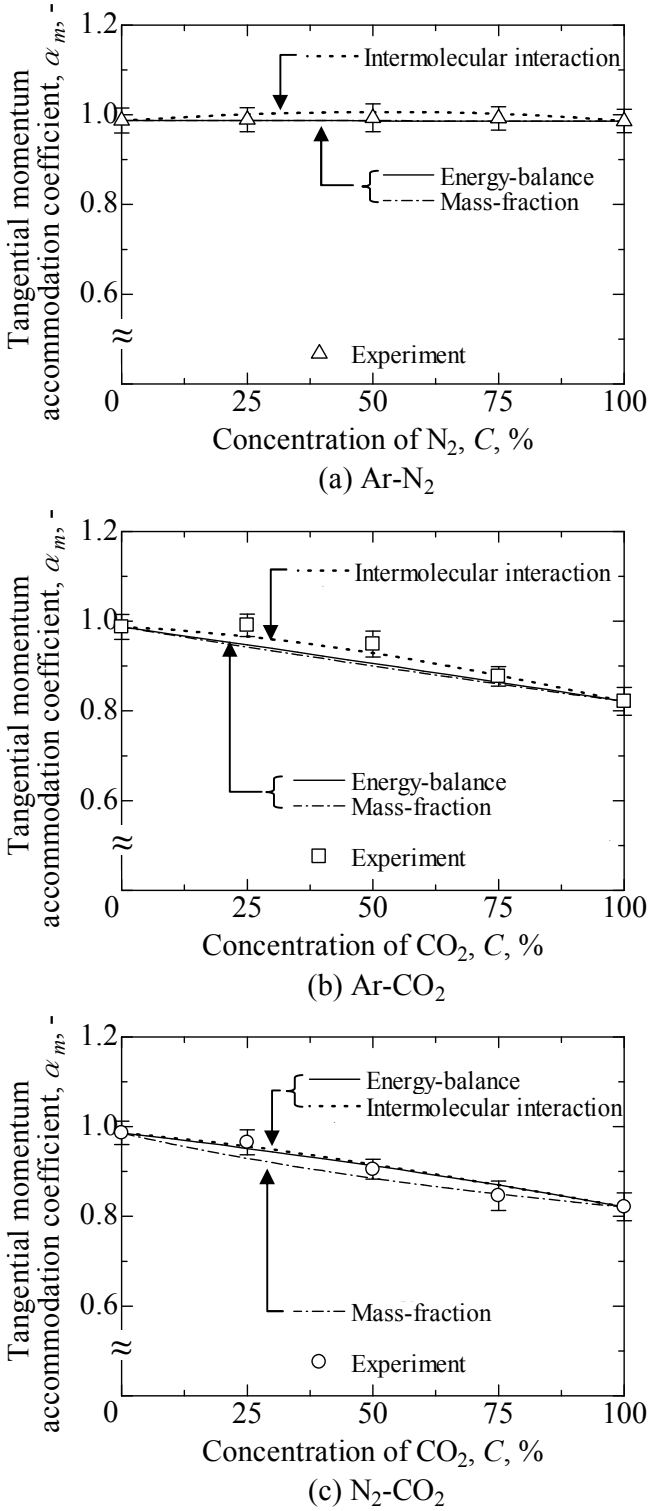

Fig. 6.3 Comparison of tangential momentum accommodation coefficient for each gas mixture.

6.4 Discussion

A problem in the determination of coefficients of a gas mixture is the uncertainty of those values of composing pure gases. Different researchers have proposed different values for a same pure gas. Table 6.3 shows comparisons of coefficients between several references for the concerned pure gases; the values obtained in this work are also shown. These differences in the table infer the possibility that the accommodation coefficient is dependent on the adopted method and/or the material of the solid. The surface condition of the solid wall may also have some influence: Thomas and Lord [14] have measured accommodation coefficients for polished and rough surfaces of steel spheres to find some difference as shown in the table.

This problem should be considered when making quantitative comparison between values from different research works. With regard to the current and its preceding works, all experimental data are obtained from the same method and the same kind of particles. Thus, the comparison given in this work will not be concerned directly by the problem.

Table 6.3 Comparison of coefficients for pure gases.

Tested gas	α_m, –	α_t, –	Solid material	Reference
Argon	0.931	1.102	Steel spheres (polished surface)	[14]
	1.049	1.161	Steel spheres (rough surface)	[14]
	0.916	1.000	Glass	[15]
	1.000	0.900	Paraffin	[3]
	0.987	1.000	PMMA	This work
Nitrogen	1.000	0.680	Tungsten	[16]
	0.911	1.000	Glass	[15]
	1.000	0.900	Paraffin	[3]
	0.986	1.000	PMMA	This work
Carbon dioxide	1.000	0.720	Tungsten	[16]
	1.000	0.450	Glass	[17]
	1.000	0.450	Polystyrene latex (PSL) sphere	[17]
	0.993	1.000	Glass	[15]
	0.821	1.000	PMMA	This work

Another problem is the assumption that the thermal accommodation coefficient is always at unity regardless of the mixing condition. This does not concern when applying energy-balance- and mass-fraction- based methods, since both these methods do not alter the coefficient of the mixture when both the pure gases have the same value at unity. The intermolecular-interaction-based method, on the other hand, may change the value of the thermal accommodation coefficient depending on the concentration as is the case of the

tangential momentum accommodation coefficient. So far, there is no reference that shows the way to calculate the thermal accommodation coefficient on the intermolecular interaction basis. Although there are such vulnerable points in the treatment of coefficients, the current work would be informative for a practical use in predicting the thermophoretic velocity for gas mixtures. Experimental results are satisfactorily predicted when the thermal accommodation coefficient is assumed to be unity and the other coefficient is calculated from pure gas values by means of the intermolecular-interaction-based method.

6.5 Conclusions

In this study, the thermophoretic velocity of gas mixtures are experimentally measured, and following results are obtained:

1. The thermophoretic velocity depends on the concentration of the gas mixture. For an argon-nitrogen mixture, the velocity increases as the concentration of nitrogen increases; for argon-carbon dioxide and nitrogen-carbon dioxide mixtures, the velocity decreases as the concentration of carbon dioxide increases.

2. The tangential momentum accommodation coefficient of a gas mixture is estimated from experimental results to clarify its dependence on the concentration by assuming the thermal accommodation coefficient at unity. The estimated coefficient is compared with predictions from three methods; it is found that the intermolecular-interaction-based method gives the best prediction among those three methods for all mixture conditions.

3. It is shown that the thermophoretic velocity under a binary gas mixture condition is practically predicted from the intermolecular-interaction-based method.

References:

[1] Hoshino, A., Suzuki, M., and Masuda, W. (2010). Numerical analysis on thermophoretic phenomenon in slip flow regime considering thermal stress efeect. *21st International Symposium on Transport Phenomena*.

[2] Li, W., and Davis, E.J. (1995). Measurement of the thermophoretic force by electrodynamic levitation: microspheres in air. *Journal of Aerosol Science, 26,* 1063-1083.

[3] Prodi, F., Santachiara, G., Di Matteo, L., Vedernikov, A., Beresnev, S.A., and Chernyak, V.G. (2007). Measurements of thermophoretic velocities of aerosol particles in microgravity conditions in different carrier gases. *Journal of Aerosol Science, 38,* 645-655.

[4] Suzuki, T., Suzuki, M., and Masuda, W. (2009). Effect of water vapor to thermophoresis phenomenon. *Proceeding of the 47th Symposium (Japanese) on Combustion,* 448-449.

[5] Mikami, H., Endo, Y., and Takashima, Y. (1966). Heat transfer from a sphere to rarefied gas mixtures. *International Journal of Heat and Mass Transfer, 9,* 1435-1448.

[6] Wise, H., Wood, B.J., and Rajapakse, Y. (1966). Heat transfer in reacting gases: thermal conductivity and accommodation coefficient measurements in gas mixture O andO_2. *The Physics of Fluids, 9,* 1321-1327.

[7] Ivchenko, I.N., Loyalka, S.K., and Tompson Jr., R.V. (1997). Slip coefficients for binary gas mixtures. *Journal of Vacuum Science and Technology A, 15,* 2375-2381.

[8] Ivchenko, I.N., Loyalka, S.K., and Tompson Jr., R.V. (2007). *Analytical Methods for Problems of Molecular Transport*. Springer: The Netherlands.

[9] Bentz, J.A., Tompson, R.V., and Loyalka, S.K. (1999). Viscosity and velocity slip coefficients for gas mixtures: Measurements with a spinning rotor gauge. *Journal of Vacuum Science and Technology A, 17,* 235-241.

[10] Waldmann, L. (1959). Uber die kraft eines inhomogenen gases auf kleine suspendierte kugeln. *Zeitschrift Naturforschung Teil A, 14,* 589-599.

[11] Richard, S.B. (1964). Approximate formulas for viscosity and thermal conductivity of gas mixtures. *NASA Technical Note,* TN D-2502.

[12] Kihara, T. (1975). The Chapman-Enskog and Kihara approximations for isotopic thermal diffusion in gases. *Journal of Statistical Physics, 13,* 137-143.

[13] ANSYS Fluent 12.0 theory guide. ANSYS, Inc.,United States, 2009.

[14] Thomas, L.B., and Lord, R.G. (1974). Comparative measurements of tangential momentum and thermal accommodations on polished and on roughened steel spheres. *International Symposium on Rarefied Gas Dynamics, 8,* 405-412.

[15] Sharipov, F. (2004). Data on the velocity slip and temperature jump coefficients. *Proceeding of Euro SimE,* 243-249.

[16] Douglas, F.S. (1982). Energy and tangential momentum accommodation coefficients on gas covered tungsten. *Journal of Chemical Physics, 76,* 3814-3818.

[17] Li, W., and Davis, E.J. (1995). The effects of gas and particle properties on thermophoresis. *Journal of Aerosol Science, 26*, 1085-1099.

Chapter 7

Conclusions and Future Work

7.1 Conclusions

In the present work, influences of gas species on the thermophoretic velocity of PMMA particles are investigated. The main conclusions of this study are summarized follows.

In the present study, effects of gas species on the thermophoretic velocity are investigated. The characteristics of the thermophoresis for argon, nitrogen, and carbon dioxide are experimentally examined. The obtained-experimental results are compared with the theory. It is seen that when values for the constants C_M, C_T, C_S, and C_H to be 1.000, 1.875, 0.750, and 1.000 are applied to the theory, results for both argon and nitrogen are quantitatively in good agreement with the theory, while notable discrepancy is seen for carbon dioxide. The discrepancy for carbon dioxide is corrected by changing values of coefficients, which are calculated by means of the least square fit. It is found the proposed values of C_M, C_T, C_S, and C_H for carbon dioxide are 1.378, 1.875, 0.750, and 1.000.

The attempt is made to investigate dependence of thermophoretic parameters on gas properties. The thermophoretic parameters for argon and nitrogen are reexamined, and compared with those of carbon dioxide, methane, and nitrous oxide. The value of

residue R is calculated for all combinations of coefficients. It is found that several combinations of the coefficients are possible to fit the prediction with the experimental results. The physical relationships between the tangential momentum accommodation coefficient and the gas properties are clarified by assuming the thermal accommodation coefficient to be unity. A relation is shown between the tangential momentum accommodation coefficient and the molecular diameter; the coefficient decreases as the diameter increases.

The thermophoretic velocity is experimentally measured for several gas mixtures, i.e., argon-nitrogen, argon-carbon dioxide, and nitrogen-carbon dioxide. It is found that the thermophoretic velocity depends on the concentration of the gas mixture. In the case of an argon-nitrogen mixture, the velocity increases as the concentration of nitrogen increases. On the other hand, in cases of argon-carbon dioxide and nitrogen-carbon dioxide mixtures, the velocity decreases as the concentration of carbon dioxide increases. The tangential momentum accommodation coefficient of a gas mixture is estimated from experimental results. The dependence of the tangential momentum accommodation on the concentration is clarified by assuming the thermal accommodation coefficient at unity. The comparison is done between the estimated coefficient and predictions from three methods. It is found that the intermolecular-interaction-based method gives the best prediction among those three methods for all mixture conditions. It is shown that the thermophoretic velocity under a binary gas mixture condition is practically predicted from the intermolecular-interaction-based method.

7.2 Recommendations for Future Work

Influences of composition of gas mixture on thermophoretic velocity have been investigated in the present study. However, due to some limitations, other influences could not be examined in this study. Therefore, several suggestions for future works related to the influences on the thermophoresis phenomenon are given as follows:

1. The water vapor is the clue of this work. However, it is excluded owing to technical reasons on conducting experiment. For this purpose, the apparatus need to be modified so that experiments can be conducted in such condition.
2. The influence of thermal conductivity of particle would be an important topic to be explored. Experiments for different type of particles should be considered to investigate this influence.
3. Considering the combustion environment, the thermophoresis phenomenon is supposed to influence on the movement of soot particles. The soot particle is generally an aggregate particle. The understanding of the phenomenon for an aggregate would be interesting topic in the future work.

Appendix A

Thermophoretic Velocity

The thermophoresis is caused by the momentum exchange between gas molecules and the particle. The primary mechanism of this exchange is that gas molecules colliding from the higher temperature side transfer negative momentums to the particles, the overall amount of which exceeds those of positive momentums transferred by gas molecules colliding from the lower temperature side. As the result of this momentum exchange, the particle and the surrounding gas move in mutually opposite directions. The flow of the surrounding gas is referred to as the superficial slip flow.

A-1 Calculation

A-1-1 Assumptions

For determining the governing equations and boundary conditions, the following assumptions are made:

1. A spherical particle is placed into the gas having a constant temperature gradient and fixed in its position.
2. The flow is steady and symmetrical with respect to the z axis, which corresponds to the direction of the temperature gradient.
3. The gas is incompressible.

4. Stoke's approximation is applicable.

A-1-2 Coordinate System

Spherical coordinates are adopted in this calculation. The relation between the spherical coordinates and a Cartesian coordinates is shown in Fig. A-1 and Eq. (A-1).

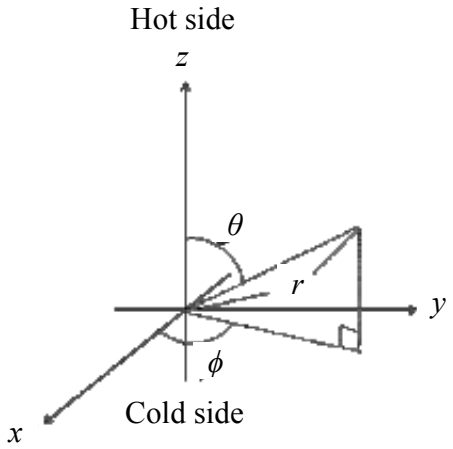

Fig. A-1 Spherical coordinates

$$\begin{aligned} x &= r\sin\theta\cos\phi, \\ y &= r\sin\theta\sin\phi, \\ z &= r\cos\theta. \end{aligned} \qquad (A-1)$$

The center of the spherical particle is located at the origin of the coordinates.

A-1-3 Governing Equations

The incompressible steady Navier-Stokes equation with Stokes' approximation is shown as follows:

$$\mu\nabla^2\vec{V} = \nabla p, \qquad (A-2)$$

where μ, $\vec{V}$, and p are the viscosity, the stream vector, and the pressure, respectively.

Equations of continuity, energy for the gas surrounding the particle, and heat conduction in the spherical particle are shown below:

$$\nabla \cdot \vec{V} = 0, \tag{A-3}$$

$$\nabla^2 T_F = \frac{1}{\alpha}\left(\vec{V} \cdot \nabla\right) T_F, \tag{A-4}$$

$$\nabla^2 T_S = 0, \tag{A-5}$$

where T_F and T_S are temperatures of the gas and the particle, respectively.

A-1-4 Boundary Conditions

The matching condition for the thermal flux at the surface is shown below:

$$k_S \frac{\partial T_S}{\partial r} = k_F \frac{\partial T_F}{\partial r}, \qquad r = a \tag{A-6}$$

where k_S and k_F are thermal conductivities of the particle and the gas, respectively, a is the radius of the particle.

The temperature jump condition at the surface is given as follows:

$$T_F - T_S = C_T l \frac{\partial T_F}{\partial r}, \qquad r = a \tag{A-7}$$

where l is the mean free path and C_T is a constant for the temperature jump.

The superficial slip condition on the surface of the spherical particle is shown as below:

$$V_\theta = C_M l\left[r\frac{\partial}{\partial r}\left(\frac{V_\theta}{r}\right) + \frac{1}{r}\frac{\partial V_r}{\partial \theta} \right] + \frac{3}{4}\frac{\mu}{\rho T_{F0}}\frac{1}{a}\frac{\partial T_F}{\partial \theta} - C_M l \frac{\mu}{\rho T_{F0}}\left(\frac{1}{r}\frac{\partial^2}{\partial r \partial \theta} - \frac{1}{r^2}\frac{\partial}{\partial \theta}\right) T_F$$
$$- \frac{9}{4\pi}\frac{\Pr(\gamma - 1)}{\gamma} l^2 \frac{\partial \omega}{\partial r}, \qquad r = a \tag{A-8}$$

where C_M is the constant for slip flow, V_θ and V_r are θ and r elements of the stream vector, respectively, ρ is the density of the gas, T_{F0} is the reference temperature, ω is the element of vorticity in the ϕ direction, Pr is the Prandtl number, and γ is the ratio of specific heat.

In addition to the superficial slip condition, following boundary conditions are commonly set. Firstly, V_r should be zero at the surface.

$$V_r = 0, \qquad r = a \tag{A-9}$$

The faraway conditions are given as follows:

$$V_r = 0, V_\theta = 0, T_F = |\nabla T| r\cos\theta + T_{F0}, \qquad r \to \infty, \tag{A-10}$$

where $|\nabla T|$ is the temperature gradient given to the domain. The axisymmetric conditions around z axis are shown below:

$$\frac{\partial V_r}{\partial \theta} = 0, V_\theta = 0, \frac{\partial T_F}{\partial \theta} = 0, \frac{\partial T_S}{\partial \theta} = 0, \qquad \theta = 0, \pi. \tag{A-11}$$

A-1-5 Derivation of Thermophoretic Force

The thermophoretic force F_T is derived by integrating the superficial stress as follows:

$$\begin{aligned} F_T &= 2\pi a^2 \int_0^\pi (\tau_{rr}\cos\theta - \tau_{r\theta}\sin\theta - p\cos\theta)\sin\theta d\theta, \\ \tau_{rr} &= 2\mu\frac{\partial V_r}{\partial r}, \\ \tau_{r\theta} &= \mu\left(r\frac{\partial}{\partial r}\left(\frac{V_\theta}{r}\right) + \frac{1}{r}\frac{\partial V_r}{\partial \theta}\right), \end{aligned} \tag{A-12}$$

where τ_{rr} and $\tau_{r\theta}$ are the normal and the tangential components of viscous stress, respectively. The reference point of the pressure is settled at $r = a, \theta = 0$.

A-1-5 Derivation of Thermophoretic Velocity

The thermophoretic velocity is derived from the balance between the thermophoretic force and the drag force. The equation is shown as follows:

$$V_T = \frac{3\mu C_c}{2\rho T_{F0}} \frac{\left[\left(k + C_T Kn\right) + \frac{4}{3}\left(C_M C_T Kn^2 + C_M Kn[k-1]\right)\right]}{\left[1 + 3C_M Kn + \frac{9}{2\pi} PrKn^2\left(1 - \gamma^{-1}\right)\right]\left(1 + 2k + 2C_T Kn\right)} |\nabla T|. \quad (A-13)$$

Here, $C_C = 1 + A\,Kn$, where $A = 1.257 + 0.4\exp\left(-1.10 / Kn\right)$.

Appendix B

Thermodiffusiophoretic Velocity

For a gas mixture in the temperature gradient field, the heavier species in the mixture moves from a hot to cold region while the lighter species moves in the reverse direction. The concentration gradient, called as the Soret effect, is formed in the mixture as a result of a temperature gradient. Thus in the gas mixture, a diffusiophoretic force will be exerted on a particle in addition to the thermophoretic force. This phenomenon is called thermodiffusiophoresis.

The diffusiophoretic force is given as follows:

$$F_{Di} = -6\pi\mu a c' D_{12} \left|\nabla x_1\right|, \qquad \text{(B-1)}$$

where c', D_{12}, and $\left|\nabla x_1\right|$ are the diffusion slip factor, the coefficient of molecular diffusion, and the concentration gradient, respectively.

The diffusion slip factor c_{12} is shown as follows:

$$c' = 0.905\left(\frac{M_1 - M_2}{M_1 + M_2}\right) - 1.05\left(\frac{\sigma_1 - \sigma_2}{\sigma_1 + \sigma_2}\right), \qquad \text{(B-2)}$$

where M is the molecular weight and σ is the molecular diameter, respectively.

The coefficient of molecular diffusion D_{12} is shown below:

$$D_{12} = \frac{1}{2} x_1 x_2 \left(\frac{2kT}{M}\right)^{\frac{1}{2}} d_0,$$

$$d_0 = \frac{3}{2}\left(\frac{2kT}{M}\right)^{\frac{1}{2}} \frac{E}{kT}\left(nx_1x_2\right)^{-1}, \tag{B– 3}$$

$$E = \frac{1}{8}\left(\frac{kT}{M_1M_2\Omega_{12}^{(1,1)}}\right),$$

where x, k, n, and Ω are the molar fraction, the Boltzmann number, the number density, and the Ω-integral, respectively.

The concentration gradient $\left|\nabla x_1\right|$ is given as follows:

$$\left|\nabla x_1\right| = \frac{k_T}{T}\left|\nabla T\right|, \tag{B– 4}$$

where k_T is the thermodiffusion ration calculated below:

$$k_T = \left(\frac{n_1n_2}{n_1+n_2}\right)^2\left(\frac{M_1-M_2}{M_1+M_2}\right)k_T^*,$$

$$k_T^* = \frac{15}{8}\left(\frac{2\Omega_{12}^{(1,1)} - 5\Omega_{12}^{(1,2)}}{\Omega_{12}^{(2,2)}}\right). \tag{B– 5}$$

The thermodiffusiophoretic velocity for the gas mixture is derived by equating the balance between forces acting on a particle:

$$F_T + F_{Di} + F_D = 0,$$

$$V_{TD} = \frac{3\mu C_c}{2\rho T_{F0}} \frac{\left[\left(k + C_T Kn\right) + \frac{4}{3}\left(C_M C_T Kn^2 + C_M Kn\left[k-1\right]\right)\right]}{\left[1 + 3C_M Kn + \frac{9}{2\pi} PrKn^2\left(1-\gamma^{-1}\right)\right]\left(1 + 2k + 2C_T Kn\right)}\left|\nabla T\right| + C_c c' D_{12}\left|\nabla x_1\right|. \tag{B– 6}$$

Journal of Aerosol Science 54 (2012) 77–87

Contents lists available at SciVerse ScienceDirect

Journal of Aerosol Science

journal homepage: www.elsevier.com/locate/jaerosci

Effects of gas species on pressure dependence of thermophoretic velocity

Bin Razali Mohd Azahari [a,b,*], Masayuki Mori [a], Masataro Suzuki [a], Wataru Masuda [a]

[a] Nagaoka University of Technology, 1603-1 Kamitomioka, Nagaoka, Niigata 940-2188, Japan
[b] University Tun Hussein Onn Malaysia, Parit Raja, Batu Pahat, 86400 Johor, Malaysia

ARTICLE INFO

Article history:
Received 24 April 2012
Received in revised form
29 June 2012
Accepted 1 July 2012
Available online 9 July 2012

Keywords:
Microgravity experiment
Thermophoretic velocity
Tangential momentum accommodation coefficient
Thermal accommodation coefficient

ABSTRACT

Microgravity experiments are conducted to measure the thermophoretic velocity, and effects of gas species are investigated. Particles adopted are PMMA spheres of 2.91 μm in mean diameter, and atmospheric gases chosen are pure gases of argon, nitrogen, and carbon dioxide. The temperature gradient is set at 10 K/mm, and the pressure is set at several conditions in the range from 20 kPa to 100 kPa. Terminal velocities of particles suspended in a gas are individually measured during 0.25 s of the microgravity condition, which is achieved by a free-fall. The accuracy of the measurement is attained by accumulating data from repeated trials. Obtained experimental results are compared with theoretical predictions; a notable discrepancy is found for carbon dioxide, while the results for other two gases are consistent with predictions. Some attempts are made to fix the discrepancy: first by modifying constants and second by modifying two empirical coefficients in the theory.

1. Introduction

Thermophoresis is the phenomenon that a small particle in a gas with a temperature gradient moves toward the lower temperature side. This phenomenon is supposed to influence practically on the movement of soot particles in exhaust gas from combustors, especially near cool walls around the hot gas flow, where the temperature gradient can become as large as the order of 10^2 K/mm. For example, the measured size-distribution of particulate matter is influenced by the temperature of the transfer tube connecting the exhaust pipe of a diesel engine to the dilution tunnel ahead of the measuring device (Yuasa et al., 2011). A soot particle is generally an aggregate of fine primary spheres. There have been some direct measurements on the thermophoretic phenomenon of such an aggregate particle. Zheng & Davis (2001) have measured the thermophoretic force acting on an aggregate of polystyrene latex spheres, and found that the force is affected by the number of primary spheres in the aggregate. Dobashi et al. (2000) and Suzuki & Dobashi (2007) have conducted direct measurements on the thermophoretic velocity of soot particles, and have revealed that the velocity is dependent not only on the macroscopic size of the soot particle but also on the aggregating condition; Suzuki & Dobashi (2007) have shown experimental results suggesting that the phenomenon is dominated by the size of primary spheres when the aggregation is coarse. Thus, the understanding of the phenomenon for a single sphere is indispensable before understanding for an aggregate.

* Corresponding author at: Masuda Suzuki Laboratory, 2nd Floor, Mechanical Building, Nagaoka University of Technology, 1603-1 Kamitomioka, Nagaoka, Niigata 940-2188, Japan. Tel.: +81 80 4298 2710.
E-mail addresses: azahari@uthm.edu.my, m-azahari@msl.nagaokaut.ac.jp (B.R. Mohd Azahari).

0021-8502/$ - see front matter © 2012 Elsevier Ltd. All rights reserved.
http://dx.doi.org/10.1016/j.jaerosci.2012.07.002

The thermophoretic phenomenon of a spherical particle has been studied both theoretically and experimentally. Theoretical works have been carried out by considering the boundary condition on the surface of a single spherical particle suspended in a gas with a temperature gradient. Brock (1962) derived a theoretical solution to the thermophoretic force on the particle by applying a slip boundary condition on its surface, which includes effects of the thermal slip, the viscous slip, and the temperature jump. Derjaguin & Yalamov (1965) derived the thermophoretic velocity from the Brock's theoretical solution by equating the balance between the thermophoretic and the drag forces.

Experiments, on the other hand, have been performed by measuring the thermophoretic force or the thermophoretic velocity. Fredlund (1938) attempted a systematic experiment to examine the effect of the temperature field upon a disk suspended on a balance. The thermophoretic force and the thermophoretic velocity are measured by several methods: Millikan cell (Rosenblatt & La Mer, 1946; Saxton & Ranz, 1952; Schadt & Cadle, 1961; Jacobsen & Brock, 1965), electrodynamic balance (Li & Davis, 1995a, 1995b), precipitation in a thermoprecipitator (Schadt & Cadle, 1957; Keng & Orr, 1966), jet technique (Kousaka et al., 1976; Prodi et al., 1979; Talbot et al., 1980), and deflection of a particle suspended by a small wire (Davis & Adair, 1975; Tong, 1975).

Above experimental methods are complex in practical implementation, and as a consequence, involve numerous errors. Among those, errors caused by buoyancy are the largest problem; in a field with a temperature gradient, buoyancy induces natural convection, which influences the movement of particles and disturbs the measurement. The velocity of such natural convection is usually comparable to the thermophoretic velocity, and cannot be measured directly. To avoid this problem, some experiments have been conducted under microgravity conditions. Toda et al. (1996, 1998) performed experiments in a drop tower facility and demonstrated that the microgravity environment satisfactorily suppresses the disturbance. Prodi et al. (2006, 2007) also conducted microgravity experiments by means of a drop tower facility and/or parabolic flights. However, their reported data still seem to contain errors, possibly owing to limited trial numbers of experiments, so that those data are not sufficient to make quantitative comparison with theories (Suzuki et al., 2009a).

Recently, our group has developed a device for conducting experiments repeatedly under a microgravity environment in a very short period time, i.e. 0.3 s, by means of the free-fall method, to accumulate data of the thermophoretic velocity. It has been confirmed that satisfactory accuracy can be attained if the amount of data is sufficient for statistical treatment (Suzuki et al., 2009a). By comparing the obtained experimental results with the existing theory (Brock, 1962), two notable differences are found; one is the substantial difference for particles with high thermal conductivity, and the other the remarkable difference in the dependence of the humidity in the air (Suzuki et al., 2009b). The problem of the former difference has been solved by reconsidering the boundary condition to improve the theory (Hoshino et al., 2010a). Hoshino et al., (2010b) has derived an improved theoretical solution of the thermophoretic velocity by applying the boundary condition proposed by Lockerby et al. (2004), which includes the thermal stress slip and the higher order isothermal slip. However, even this improved theory cannot solve the problem of the latter difference. The deviation of the theory from the experiment infers that the composition of the surrounding gas mixture has some unknown influence on the phenomenon.

Before analyzing the influence of the composition of the gas mixture, it is indispensable to know the characteristics of the phenomenon for each gas component. Thus, in this study, the characteristics of the thermophoresis for several gas species, i.e., argon, nitrogen, and carbon dioxide are experimentally examined. The first one is chosen as the reference, and the latter two are chosen as the major components of exhaust gas from combustors. Water vapor is the clue of starting this work, but it is excluded owing to technical reasons on conducting the experiment.

2. Theory for thermophoretic velocity

The theory adopted in this work is based on the works by Hoshino et al. (2010b) and by Chang & Keh (2012). The thermophoretic velocity is calculated from the balance between the thermophoretic and the drag forces, the equation of which is shown as below

$$V_T = \frac{2\mu C_f}{\rho T_{F0}} \frac{[C_S(k+C_T Kn)+C_H(C_M C_T Kn^2+C_M Kn[k-1])]}{[1+3C_M Kn+h](1+2k+2C_T Kn)} |\nabla T|, \tag{1}$$

where μ, $|\nabla T|$, ρ, T_{F0}, C_f, k, Kn, h, C_M, C_T, C_S, and C_H are the viscosity, the temperature gradient, the density of the surrounding gas, the reference temperature, the slip correction factor of the drag force for rarefied condition, the gas-to-particle thermal conductivity ratio, Knudsen number, the term of higher order isothermal slip, and constants for slip flow, temperature jump, thermal creep, and thermal stress slip, respectively. Here, the reference temperature T_{F0} is defined as the supposed gas temperature at the center of the particle in the given temperature field without the existence of the particle, and Knudsen number Kn is the ratio of the mean-free-path l to the particle radius. The mean-free-path is calculated from the following equation (Kennard, 1938):

$$l = \frac{\mu}{0.499P}\sqrt{\frac{\pi R T_{F0}}{8}}, \tag{2}$$

where P and R are the pressure and the gas constant, respectively. The slip correction factor C_f adopted in this work is Cunningham's correction factor $C_{fc} = 1 + A\,Kn$, where $A = 1.257 + 0.4\exp(-1.10/Kn)$ (Talbot et al., 1980). The term h of

higher order isothermal slip is written as below

$$h = \frac{9}{2\pi}\mathrm{Pr}Kn^2(1-\gamma^{-1}) \tag{3}$$

where Pr and γ are Prandtl number and the specific heat ratio, respectively.

Eq. (1) is basically identical to both of those proposed by Hoshino et al. (2010b) and Chang & Keh (2012). If constant values $C_S=0.75$ and $C_H=1.00$ (Lockerby et al., 2004) are applied, the equation becomes just the same as the one given by Hoshino et al. (2010b). On the other hand, the equation becomes the same as the one given by Chang & Keh (2012) by neglecting the term h, which is usually negligible in the range of $Kn \le 0.1$, and applying Basset's correction (Basset, 1961), $C_{fb} = (1+3C_MKn)/(1+2C_MKn)$, instead of the Cunningham's correction for the slip correction factor C_f. The Basset's correction is applicable in $Kn \le 0.1$ while the Cunningham's one in $Kn < 1$, and both are basically identical in those applicable ranges.

Two constants C_M and C_T are calculated as follows from two empirical coefficients, i.e., the tangential momentum accommodation coefficient α_m and the thermal accommodation coefficient α_t

$$C_M = \frac{2-\alpha_m}{\alpha_m}, \tag{4}$$

$$C_T = \frac{15}{8}\left(\frac{2-\alpha_t}{\alpha_t}\right). \tag{5}$$

These accommodation coefficients represent the magnitude of the momentum and energy exchange in the collision between gas molecules and the particle (Kennard, 1938; Shen, 2010), which are defined as below

$$\alpha_m \equiv \frac{M_i-M_r}{M_i-M_s}, \tag{6}$$

$$\alpha_t \equiv \frac{E_i-E_r}{E_i-E_s}, \tag{7}$$

where M and E are average tangential components of the momentum and the energy flux normal to the particle surface, respectively, of gas molecules, and subscripts i, r, and s refer to incident molecules, molecules reflecting from the surface, and molecules leaving the surface in equalibrium with the surface, respectively. For example, $\alpha=1$ corresponds to the situation that incident molecules achieve complete equilibrium with the particle surface before leaving, while $\alpha=0$ corresponds to the situation of complete specular reflection.

In many cases, values of accommodation coefficients are simply assumed to be unity (Suzuki et al., 2009b; Hoshino et al., 2010a). There are some experimental measurements, e.g., Thomas & Lord (1974) and Douglas (1982), who measured accommodation coefficients on steel spheres and gas covered tungsten tube, respectively. Although those experiments report values different from unity under some conditions, yet there are no commonly accepted values.

3. Experimental

3.1. Apparatus

Fig. 1 shows a schematic of the apparatus, which includes a drop tower, a measuring unit, and a damping cushion. The measuring unit is hung at the top of the drop tower by an electric magnet. The unit starts falling when the electric

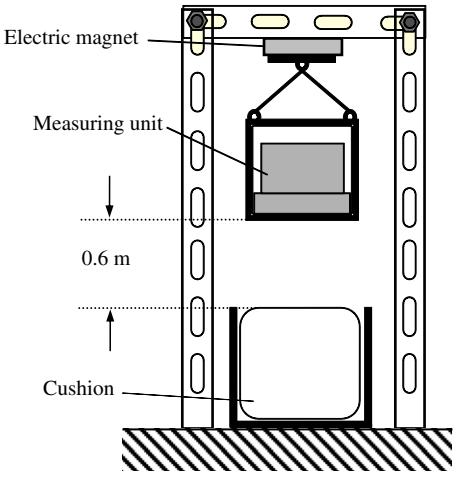

Fig. 1. Schematic of apparatus.

magnet is deactivated. The falling distance is 0.6 m, which corresponds to the duration time of the microgravity condition at 0.3 s.

Fig. 2 shows a variation of the gravity level during an experiment. The gravity level is measured by the G-sensor attached on the measuring unit. The duration time of the free-fall is about 0.3 s as seen in the figure. When the electric magnet is deactivated at $t=0$, the gravity level in z-axis changes from -1.0 G to $+0.4$ G once, possibly owing to the vibrational motion of the frame of the unit, and then decays as time passes until the unit reaches the cushion. The range between ± 0.1 G in gravity level is regarded as the microgravity condition in this work, the duration time of which is about 0.25 s.

Fig. 3 shows a cross-section of the pressure vessel, the main part of the measuring unit. Placed in the vessel is a cylindrical thin chamber of 1.5 mm in height between two opposing aluminum plates. The upper plate, initially at the room temperature, is kept cool by moving it 15 mm away from the bottom plate while the latter is under the process of heating to raise its temperature. Keeping this arrangement, the vessel is evacuated by a pump. When the bottom plate reaches the appointed temperature, the upper plate is put in place where the distance between the plates is 1.5 mm. Then, the vessel is filled with the test gas. When the temperature of the upper plate becomes the target temperature, both electromagnetic valves at the inlet and the outlet are simultaneously opened for 0.01 s such that some particles are blown into the chamber from a particle reservoir upstream the inlet. The magnet holding the measuring unit is deactivated 0.84 s after the closure of both valves. The disturbances caused by the blow are expected to cease within this period before the drop; since it is larger than both characteristic times for the flow field and the temperature field to reach the steady state; those characteristic times are expressed as $t_f=(\delta/2)^2/\nu$ and $t_t=(\delta/2)^2/\alpha$, respectively, where δ, ν, and α are the distance between two plates, the kinematic viscosity, and the thermal diffusivity, respectively (Toda et al., 1996,1998). The largest values of those for present conditions are estimated at 0.06 s and 0.05 s. Those blown particles are illuminated by the laser

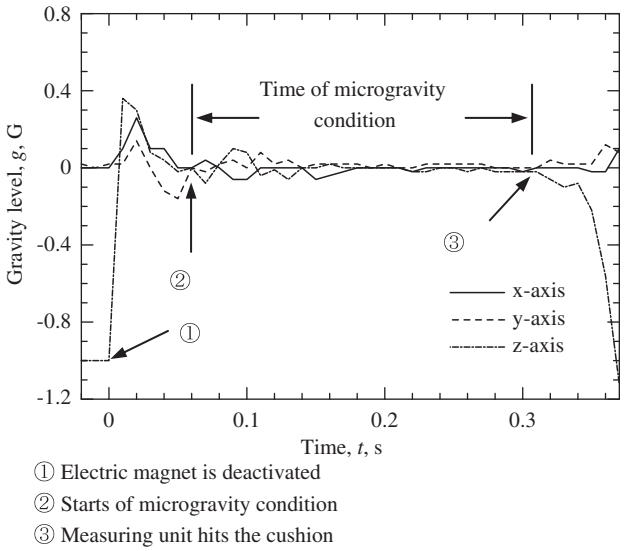

Fig. 2. Gravity level during experiment Gravity level is measured by the G-sensor which is attached on the measuring unit.

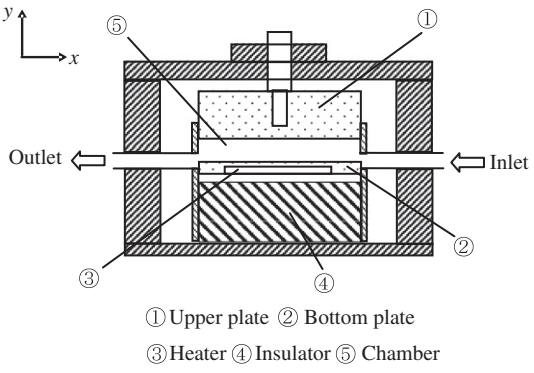

Fig. 3. Schematic of pressure vessel.

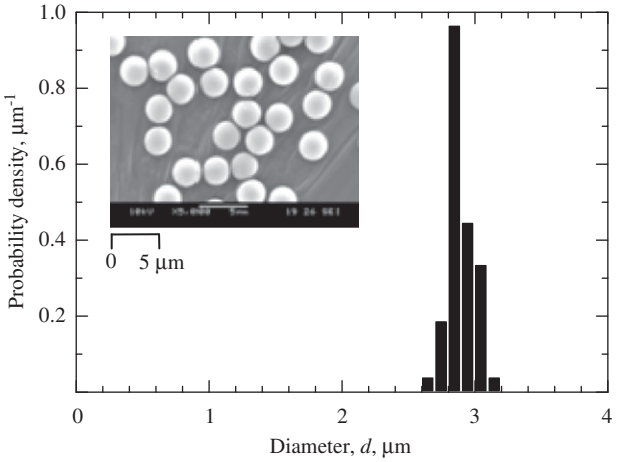

Fig. 4. Diameter distribution of particles.

beam introduced into the chamber to produce scattering lights, the image of which is recorded by a high-speed camera under the condition of the frame rate at 200 fps and of the shutter speed at 2 ms.

3.2. Sample particles and experimental condition

Sample particles used in this work are PMMA sphere particles from Sekisui Plastics Co., Ltd. These are chosen since the size is quite uniform; Fig. 4 shows the probability density distribution of the particle diameter d measured from SEM images. The mean diameter and the standard deviation are 2.91 μm and 0.09 μm, respectively. The thermal conductivity is measured by the manufacturer at 0.21 W/(mK).

Experiments are conducted under the microgravity condition with the test gas of argon, nitrogen or carbon dioxide. The target temperature and the temperature gradient are 313 K and 10 K/mm, respectively. The temperature field during the experiment is monitored by measuring temperatures at two points in the vessel: one is in the top plate and the other in the bottom one. The temperature field is controlled based on these measured temperatures. Before making experiments, the preparatory measurement for the temperature field is conducted by inserting two more thermocouples suspended in the chamber at different heights. Measuring two points is sufficient because the linearity of the temperature field has already been confirmed by the Mach–Zehnder interferometry (Toda et al., 1996,1998). The relation between these temperatures at monitoring points and the actual temperature field in the chamber is examined from this preparatory measurement. When conducting thermophoresis experiments, additional two thermocouples are removed; the temperature field is controlled based on the temperatures at those two monitoring points.

Various pressure conditions are chosen from 20 kPa to 100 kPa. The thermophoretic velocity for each particle is individually measured, and the mean value and the 95% confidence interval for each experimental condition are statistically obtained.

4. Results

Fig. 5 shows examples of the movement of particles during a free-fall in the surrounding gas of argon at 20 kPa. The measurement of the velocity should be taken at a fixed temperature since the thermophoretic velocity is dependent on not only the temperature gradient but also the temperature itself. The velocity of each particle is measured by tracing its movement while it travels within the range of the temperature between 313 ± 2 K. It is seen from the figure that the velocity of each particle can be considered as constant in the range. The velocity is constant also in other two gases.

Table 1 shows the statistical data for the tested pressure conditions with the argon gas. It is noted that the 95% confidence interval indicates not the range of data scattering but the range of expected mean value of the population. It is seen that the confidence interval is roughly estimated at around 0.01 mm/s to 0.02 mm/s. The ratio of the confidence interval to the mean value is only 3% for the pressure at 20 kPa. As the pressure increases, the velocity decreases, and as a consequence, the ratio tends to increase.

Fig. 6 shows the thermophoretic velocity for each gas. The white rectangle (□), the black circle (●), and the white circle (○) represent experimental values for argon, nitrogen, and carbon dioxide, respectively. Error bars in the figure indicate the 95% confidence interval. The solid line is the prediction calculated by assuming constants to be identical to those in the previous work (Hoshino et al., 2010a), namely, C_M, C_T, C_S, and C_H to be 1.000, 1.875, 0.750, and 1.000, respectively.

For argon and nitrogen, predictions are in good agreement with experiments throughout all the tested pressure conditions; the solid line runs through the range of the confidence interval at every tested pressure. On the other hand, for carbon dioxide, discrepancy is seen at low pressure conditions; the prediction is within the range of the confidence interval

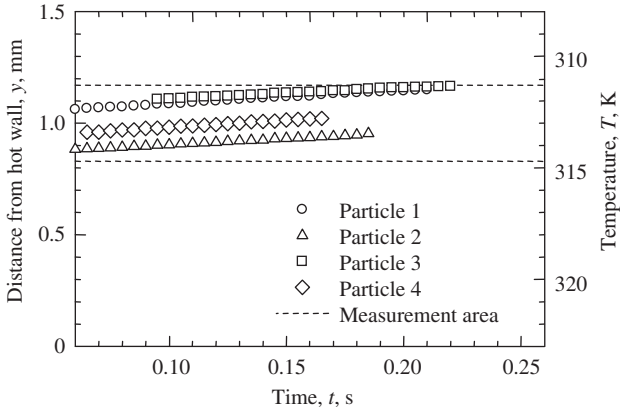

Fig. 5. Movement of particles in surrounding gas of argon.

Table 1
Statistical data of thermophoretic velocity in surrounding gas of argon.

Pressure, P, kPa	20	40	60	80	100
Sampling number, n, –	39	35	37	33	47
Mean thermophoretic velocity, $\overline{V_T}$, mm/s	0.538	0.183	0.111	0.075	0.066
Standard deviation, σ, mm/s	0.053	0.044	0.026	0.030	0.036
Confidence interval (95%), mm/s	0.017	0.015	0.009	0.011	0.011
Ratio of confidence interval to mean thermophoretic velocity, –	0.03	0.08	0.08	0.15	0.17

only when the pressure is at 100 kPa or 80 kPa. As the pressure decreases, discrepancy becomes notable; the experimental value at 20 kPa is 0.182 mm/s, which is 70% of the theory.

5. Discussion

It is quite interesting that the discrepancy is seen only for carbon dioxide. Also, previous work (Hoshino et al., 2010a) has shown satisfactory accordance between the prediction and the experiment for the air. As noted earlier, the theory contains four constants, C_M, C_T, C_S, and C_H, and the former two of these are calculated from accommodation coefficients α_m and α_t. These constants and coefficients have been determined empirically; different researchers have given different proposed values. Attempts should be made for finding suitable values to fit the prediction to these experimental results.

The first attempt is done by applying proposed values from references, which are shown in Table 2. The set of values noted as Case 1 is from the paper by Hoshino et al. (2010a), and those as Case 2 and 3 are both from the paper by Chang & Keh (2012). Fig. 7 shows predictions together with experimental results. The vertical axis represents the reduced thermophoretic velocity, which is a dimensionless parameter defined as follows:

$$V_{TR} \equiv \frac{V_T T_{F0}}{\upsilon \nabla T}, \tag{8}$$

where υ is the kinematic viscosity of the gas. This parameter is often used when making comparison between different conditions. Lines labeled as Prediction 1, 2, and 3 are those predicted from Eq. (1) by applying values of Case 1, 2, and 3, respectively. For both argon and nitrogen, the best fit to experimental results is Prediction 1, and then Prediction 3 follows; the velocity predicted from Case 3 is higher than the experiment at $Kn=0.25$ for both two gases, whereas that from Case 1 is within the error bar throughout all the measured range of Kn. For carbon dioxide, on the other hand, there is no line predicting satisfactorily the experimental result at $Kn=0.15$, though Prediction 3 seems to be better than Prediction 1. Prediction 2 can be omitted from the discussion since it obviously disagrees with the experiment for all gases.

Provisionally, Case 1 is chosen as the best among three cases; Case 3 is not good enough for high Kn for all tested gases in comparison to Case 1. Choosing Case 1 instead of Case 3 is also consistent with the previous work, in which experiments have been conducted in the air under the atmospheric pressure for particles of PMMA, alumina, and Zn (Suzuki et al., 2009b); as shown in Table 3, significant differences are seen between Case 3 and experimental results for alumina and Zn, whereas agreements are satisfactory for all particles with Case 1. In the theory, only the radius and the thermal conductivity are considered as particle-related parameters. It would be reasonable to assume that coefficients for CO_2 are different from those for other gases; Sharipov (2004) has reviewed related papers and summarized accommodation coefficients for various gases, in which CO_2 values are notably different from Ar and N_2.

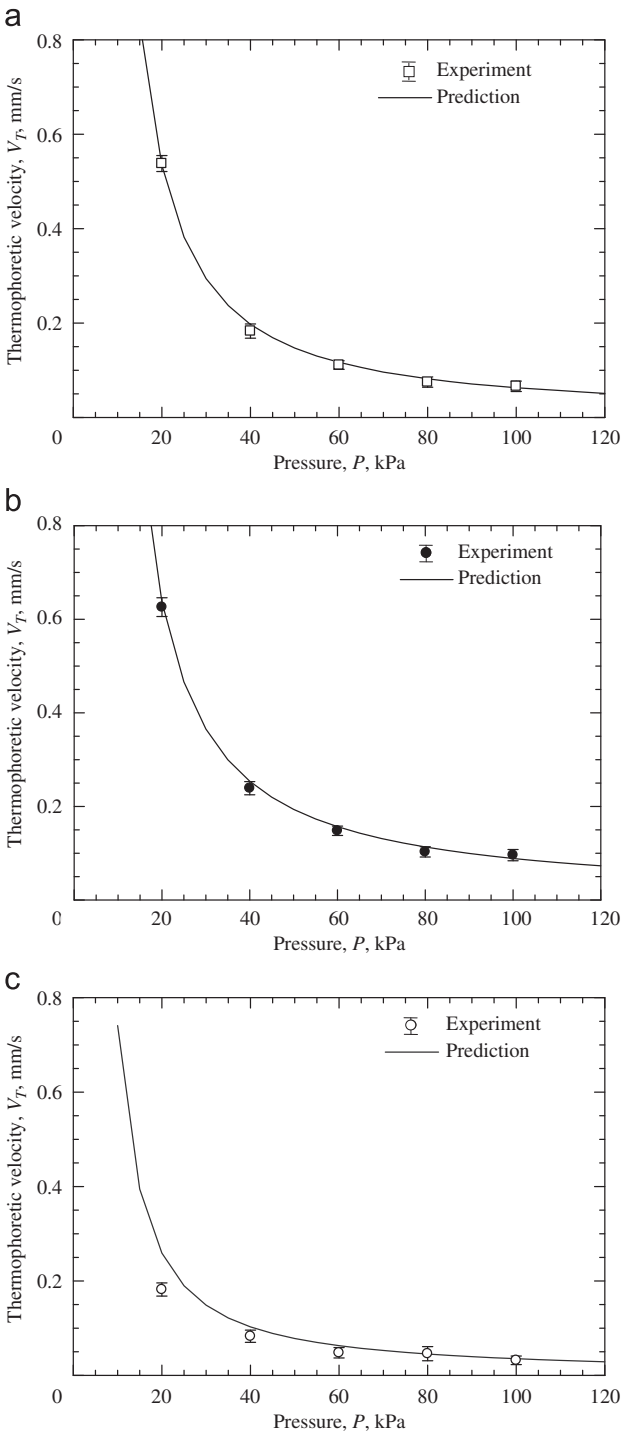

Fig. 6. Pressure dependence of thermophoretic velocity in each gas. Error bars represent the confidence interval (95%). Predictions are calculated under the assumption of C_M=1.000, C_T=1.875, C_S=0.750, and C_H=1.000: (a) argon, (b) nitrogen and (c) carbon dioxide.

Table 2
Constants for each case.

	C_M, –	C_T, –	C_S, –	C_H, –	α_m, –	α_t, –	References
Case 1	1.000	1.875	0.750	1.000	(1.000)[a]	(1.000)[a]	Hoshino et al. (2010a)
Case 2	1.140	2.180	1.170	1.000	(0.935)[a]	(0.925)[a]	Chang & Keh (2012)
Case 3	1.140	2.180	1.170	3.000	(0.935)[a]	(0.925)[a]	Chang & Keh (2012)

[a]Values in bracket are from Eqs. (4) and (5) (not directly given in the reference).

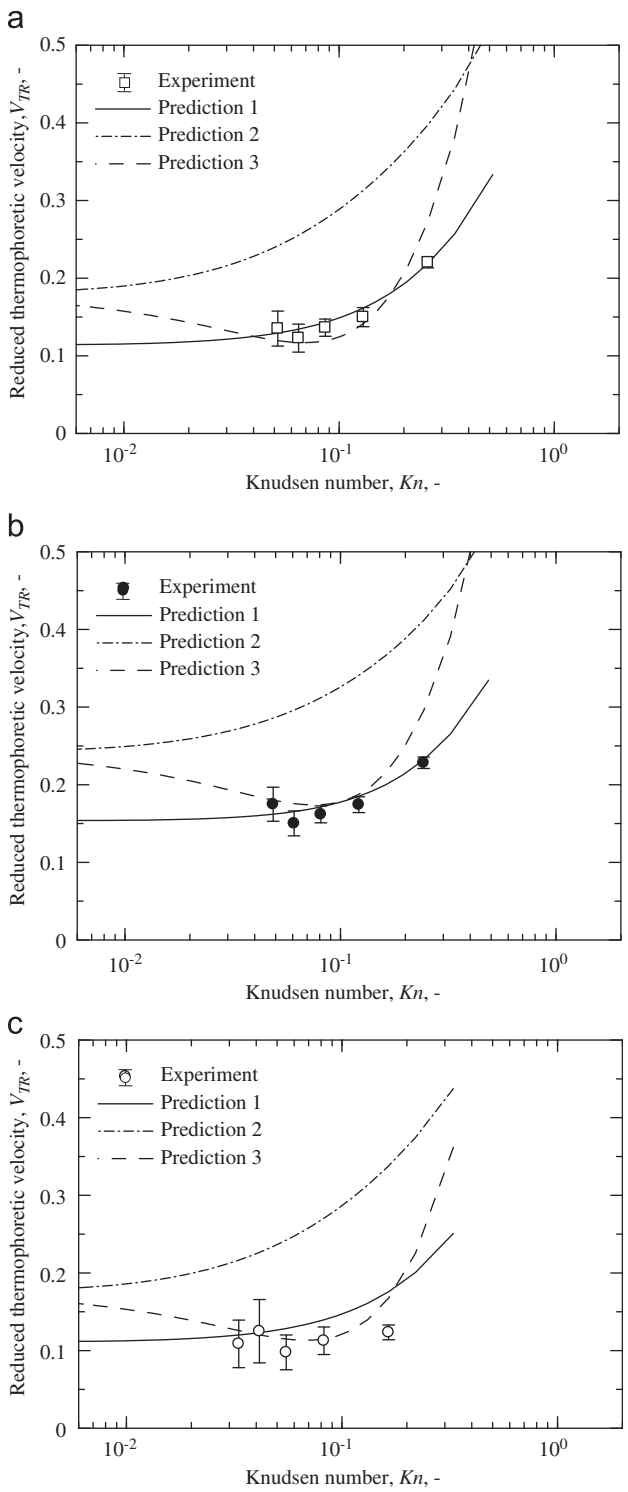

Fig. 7. Comparison between predictions and experiment in each gas Error bars represent the confidence interval (95%). Predictions are calculated using constants in Table 2: (a) argon, (b) nitrogen and (c) carbon dioxide.

The second attempt is done by changing the accommodation coefficients from Case 1 by means of the least square fit. The residue R representing the discrepancy between the experiment and the prediction is defined as follows:

$$R \equiv \sum_{j=1}^{n} (V_{ej} - V_{pj})^2, \ (j = 1,\ldots,n) \tag{9}$$

Table 3
Reduced thermophoretic velocity in air under atmospheric pressure.

Material	V_{TR}, –		Experiment[a]
	Prediction (Case 1)	Prediction (Case 3)	
PMMA	0.167	0.210	0.172 ± 0.011
Al_2O_3	0.037	−0.035	0.036 ± 0.008
Zn	0.049	−0.034	0.050 ± 0.010

[a] From Suzuki et al. (2009b).

Table 4
Estimated accommodation coefficients for carbon dioxide.

	α_m, –	α_t, –
Without limitation	1.193	1.307
With limitation	0.841	1.000

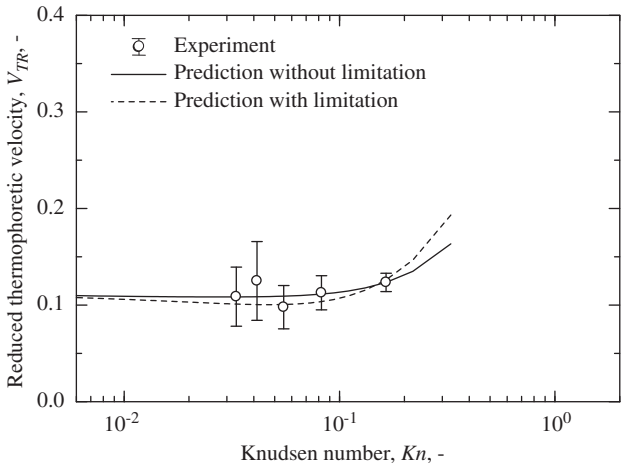

Fig. 8. Comparison of predictions for carbon dioxide Error bars represent the confidence interval (95%). The solid and the broken lines represent predictions calculated with the coefficients from least-square-fit "without limitation" and "with limitation", respectively.

where V_e, V_p, and n are thermophoretic velocities of the experiment and the prediction, and the number of the tested pressure conditions, respectively, and the subscript j refers to each tested condition. The values for C_S and C_H are unchanged from the Case 1, and those for C_M and C_T are calculated from Eqs. (4) and (5), respectively, with accommodation coefficients α_m and α_t determined such that the residue R becomes the lowest.

Table 4 shows the result of the least square fit for carbon dioxide. The best fit is attained with the coefficients noted as "without limitation" in the table. It should be noted that both values are clearly above unity, which is curious when interpreting the physical meaning of those values. Based on the kinetic theory, both those coefficients should lie between 0 and 1 (Brock, 1962; Kennard, 1938; Shen, 2010). The Cercignani-Lampis (CL) model provides a more physical description of the gas-surface interaction (Sharipov, 2003, 2004), which allows α_m to vary between 0 and 2 while α_t remains between 0 and 1. In this CL model, α_m can exceed unity when the surface is rough. Considering this, additional work is done for the fitting by applying the limitation of $0 \leq \alpha_t \leq 1$ and $0 \leq \alpha_m \leq 2$, the result of which is shown as "with limitation" in the table. In this case, R becomes the lowest when both the coefficients are bellow unity even α_m is allowed to exceed it.

Fig. 8 shows the comparison of predictions based on these values. It is seen that both predictions are in good agreement with the experiment within the range of the tested conditions. The difference between these two predictions is notable only under the condition of higher Knudsen number than the current work.

In order to interpret the different coefficients for the carbon dioxide, authors have found two different points of view from literatures so far; one is the molecular weight, and the other the diameter of a molecule. The former is based on the work by Gronych et al. (2004), who have conducted experiments to find out that the tangential momentum accommodation coefficient increases as the molecular weight of the gas decreases. This may be related to the influence of gas species. However, applying

this effect for the explanation of the present results would not be appropriate; the molecular weight of argon is closer to carbon dioxide rather than nitrogen, while the thermophoretic characteristic of the argon is much closer to the nitrogen rather than the carbon dioxide.

The latter is based on the work by Arya et al., (2003), who have conducted a molecular simulation for a wall-slip phenomenon in rarefied gases. According to their result, the tangential momentum accommodation coefficient decreases as the collision diameter of the molecule increases. Among the gases used in this work, carbon dioxide has a notably larger collision diameter; based on the rigid sphere model, the diameter of argon, nitrogen, and carbon dioxide are 3.659 Å, 3.784 Å, and 4.643 Å, respectively (Ivchenko et al., 2007). This can explain qualitatively the results in this work if the coefficients "with limitation" are adopted for the carbon dioxide and those at unity are adopted for other two gases. The thermal accommodation coefficient "with limitation" is also consistent with the work by Winkler et al. (2004), in which the coefficient α_t is reported to be approximately unity for water vapor, a polyatomic gas having a large collision diameter. The constants and coefficients, however, cannot be determined from the results in this work, since several combinations of those are possible to fit predictions to experimental results.

6. Conclusions

In this study, effects of gas species on the thermophoretic velocity are investigated, and following results are obtained:

1. Experimentally-obtained pressure dependence of the thermophoretic velocity for both argon and nitrogen are quantitatively in good agreement with the theory, while notable discrepancy is seen for carbon dioxide, if values for the constants C_M, C_T, C_S, and C_H to be 1.000, 1.875, 0.750, and 1.000 are applied to the theory.
2. Values of those empirical constants proposed in some references were applied to the theory and compared with experiments; none of those has reduced the notable deviation for the carbon dioxide at $Kn=0.15$.
3. The coefficients are calculated by means of the least square fit. The obtained values can be interpreted qualitatively by considering the effect of the molecular diameter on the tangential momentum accommodation coefficient. The proposed values of C_M, C_T, C_S, and C_H for carbon dioxide are 1.378, 1.875, 0.750, and 1.000, although further discussion will be required for the determination of the values.

Acknowledgement

A part of this work was supported by JSPS KAKENHI 24560225.

References

Arya, G., Chang, H.C., & Maginn, E.J. (2003). Molecular simulations of Knudsen wall-slip: effect of wall morphology. *Molecular Simulation*, *29*, 697–709.
Basset, A.B. (1961). *A Treatise on Hydrodynamics*, 2.
Brock, J.R. (1962). On the theory of thermal forces acting on aerosol. *Journal of Colloid Science*, *17*, 768–780.
Chang, Y.C., & Keh, H.J. (2012). Effects of thermal stress slip on thermophoresis and photophoresis. *Journal of Aerosol Science*, *50*, 1–10.
Davis, L.A., & Adair, T.W.I.I.I. (1975). Thermal force on a sphere. *Journal of Chemical Physics*, *62*, 2278–2285.
Derjaguin, B.V., & Yalamov, Yu. (1965). Theory of thermophoresis of large aerosol particles. *Journal of Colloid Science*, *20*, 555–570.
Dobashi, R., Kong, Z.W., Toda, A., Takahashi, N., Suzuki, M. & Hirano, T. (2000). Mechanism of smoke generation in a flickering pool flame. *Proceeding of the 6th International Symposium on Fire Safety Science*, 255–264.
Douglas, F.S. (1982). Energy and tangential momentum accommodation coefficients on gas covered tungsten. *Journal of Chemical Physics*, *76*, 3814–3818.
Fredlund, E. (1938). Absolute measurements of radiometric action in gases. *Philosophical Magazine*, *26*, 987–1000.
Gronych, T., Ulman, R., Peksa, L., & Repa, P. (2004). Measurements of the relative momentum accommodation coefficient for different gases with a viscosity vacuum gauge. *Vacuum*, *73*, 275–279.
Hoshino, A., Suzuki, M. & Masuda, W. (2010a). Numerical analysis on thermophoretic phenomenon in slip flow regime considering thermal stress effect. *The 21st International Symposium on Transport Phenomena*.
Hoshino, A., Suzuki, M., & Masuda, W., (2010b). Influence of particle size distribution on measurement accuracy of thermophoretic velocity. In: *Proceeding of the 48th Symposium (Japanese) on Combustion*, pp. 464–465.
Ivchenko, I.N., Loyalka, S.K., & Tompson, R.V., Jr. (2007). *Analytical Methods for Problems of Molecular Transport*. Springer: The Netherlands.
Jacobsen, S., & Brock, J.R. (1965). The thermal force on spherical sodium chloride aerosols. *Journal of Colloid Science*, *20*, 544–554.
Keng, E., & Orr, C. (1966). Thermal precipitation and particle conductivity. *Journal of Colloid and Interface Science*, *22*, 107–116.
Kennard, E.H. (1938). *Kinetic Theory*. McGraw-Hill: New York.
Kousaka, Y., Okuyama, K., Nishio, S., & Yoshida, T. (1976). Experimental study of thermophoresis of aerosol particles. *Journal of Chemical Engineering of Japan*, *9*, 147–150.
Li, W., & Davis, E.J. (1995a). Measurement of the thermophoretic force by electrodynamic levitation: microspheres in air. *Journal of Aerosol Science*, *26*, 1063–1083.
Li, W., & Davis, E.J. (1995b). The effects of gas and particle properties on thermophoresis. *Journal of Aerosol Science*, *26*, 1085–1099.
Lockerby, D.A., Reese, J.M., Emerson, D.R., & Barber, R.W. (2004). Velocity boundary condition at solid walls in rarefied gas calculations. *Physical Review E*, *70*, 017303–1-017303-4.
Prodi, F., Santachiara, G., Di Matteo, L., Vedernikov, A., Beresnev, S.A., & Chernyak, V.G. (2007). Measurements of thermophoretic velocities of aerosol particles in microgravity conditions in different carrier gases. *Journal of Aerosol Science*, *38*, 645–655.
Prodi, F., Santachiara, G., & Prodi, V. (1979). Measurements of thermophoretic velocities of aerosol particles in the transition region. *Journal of Aerosol Science*, *10*, 421–425.

Prodi, F., Santachiara, G., Travaini, S., Vedernikov, A., Dubois, F., Minetti, C., & Legros, J.C. (2006). Measurements of phoretic velocities of aerosol particles in microgravity conditions. *Atmospheric Research*, *82*, 183–189.
Rosenblatt, P., & La Mer, V.K. (1946). Motion of a particle in a temperature gradient; thermal repulsion as a radiometer phenomenon. *Physical Review*, *70*, 385–395.
Saxton, R.L., & Ranz, W.E. (1952). Thermal force on an aerosol particle in a temperature gradient. *Journal of Applied Physics*, *23*, 917–923.
Schadt, C.F., & Cadle, R.D. (1957). Thermal forces on aerosol particles in a thermal precipitator. *Journal of Colloid Science*, *12*, 356–362.
Schadt, C.F., & Cadle, R.D. (1961). Thermal forces on aerosol particles. *Journal of Physical Chemistry*, *65*, 1689–1694.
Sharipov, F. (2003). Application of the Cercignani-Lampis scattering kernel to calculations of rarefied gas flows. III. Poiseuille flow and thermal creep through a long tube. *European Journal of Mechanics B/Fluids*, *22*, 145–154.
Sharipov, F. (2004). Data on the velocity slip and temperature jump coefficients. *Proceeding of Euro SimE*, 243-249.
Shen, C. (2010). *Rarefied Gas Dynamic: Fundamentals, Simulation, and Micro Flows*. Springer: Germany.
Suzuki, M., Maruko, K., Iwahara, K. & Masuda, W. (2009a). Accurate measurement of thermophoretic velocity under high temperature gradient. 6th *International Symposium on Scale Modelling (ISSM6)*, 1.12.1–1.12.8.
Suzuki, S. & Dobashi, R. (2007). Thermophoretic effect on soot particle behavior influence of particle morphology. 21st ICDERS, 239.
Suzuki, T., Suzuki, M. & Masuda, W. (2009b). Effect of water vapor to thermophoresis phenomenon. *Proceeding of the 47th Symposium (Japanese) on Combustion*, 448–449.
Talbot, L., Cheng, R.K., Schefer, R.W., & Willis, D.R. (1980). Thermophoresis of particles in a heated boundary layer. *Journal of Fluid Mechanics*, *101*, 737–758.
Thomas, L.B., & Lord, R.G. (1974). Comparative measurements of tangential momentum and thermal accommodations on polished and on roughened steel spheres. *International Symposium on Rarefied Gas Dynamics*, *8*, 405–412.
Toda, A., Ohi, Y., Dobashi, R., Hirano, T., & Sakuraya, T. (1996). Accurate measurement of thermophoretic effect in microgravity. *Journal of Chemical Physics*, *105*, 7083–7087.
Toda, A., Ohnishi, H., Dobashi, R., Hirano, T., & Sakuraya, T. (1998). Experimental study on the relation between thermophoresis and size of aerosol particles. *International Journal of Heat and Mass Transfer*, *41*, 2710–2713.
Tong, N.T. (1975). Experiments on photophoresis and thermophoresis. *Journal of Colloid and Interface Science*, *51*, 143–151.
Winkler, P.M., Vrtala, A., Wagner, P.E., Kulmala, M., Lehtinen, K.E.J., & Vesala, T. (2004). Mass and thermal accommodation during gas-liquid condensation of water. *Physical Review Letters*, *93*, 075701–1-075701-4.
Yuasa, Y., Sasaki, H. & Tsukamoto, T. (2011). Particle size distribution of particulate matter exhausted from four stroke marine diesel engine. *Proceeding of the 49th Symposium (Japanese) on Combustion*, 310–311.
Zheng, F., & Davis, E.J. (2001). Thermophoretic force measurements of aggregates of micro-spheres. *Journal of Aerosol Science*, *32*, 1421–1435.

Journal of Aerosol Science 63 (2013) 60–68

Contents lists available at SciVerse ScienceDirect

Journal of Aerosol Science

journal homepage: www.elsevier.com/locate/jaerosci

Measurement of thermophoretic parameters for binary gas mixtures

Bin Razali Mohd Azahari [a,b,*], Masayuki Mori [a], Masataro Suzuki [a], Wataru Masuda [a]

[a] Nagaoka University of Technology, 1603-1 Kamitomioka, Nagaoka, Niigata, 940-2188, Japan
[b] University Tun Hussein Onn Malaysia, Parit Raja, Batu Pahat, 86400, Johor, Malaysia

ARTICLE INFO

Article history:
Received 8 March 2013
Received in revised form
3 May 2013
Accepted 9 May 2013
Available online 16 May 2013

Keywords:
Thermophoretic velocity
Tangential momentum accommodation coefficient
Energy-balance-based method
Mass-fraction-based method
Intermolecular-interaction-based method

ABSTRACT

The thermophoretic velocity of a particle in a gas mixture is measured by means of a microgravity experiment. Adopted particles are PMMA spheres of 2.91 μm in mean diameter, and gas mixtures chosen are argon–nitrogen, argon–carbon dioxide, and nitrogen–carbon dioxide. The temperature gradient and the pressure are 60 K/mm and 70 kPa, respectively. Terminal velocities of particles suspended in a gas are individually measured. The tangential momentum accommodation coefficient is estimated from experimental result by assuming the thermal accommodation coefficient at unity, and it is compared with predictions calculated from values of composing pure gases by means of some methods given in references; among those methods, the intermolecular-interaction-based method is found to be the best for all mixture conditions.

1. Introduction

A small particle suspended in a quiescent gas with a temperature gradient will move towards the lower temperature side. This phenomenon, called thermophoresis, influences the soot formation process in combustion fields (Dobashi et al., 2000). The phenomenon is also applied in a thermopositor used for collecting submicron size particles in a manufacturing process of optical fibers (Morse et al., 1985). Quantitative understanding of the phenomenon is indispensable for controlling the movement of particles in those systems.

Recent experiments by means of the free-fall method, which suppresses the buoyancy-induced disturbance to attain satisfactory accuracy (Toda et al., 1996, 1998; Suzuki et al., 2009a), have exhibited a remarkable difference from the theory when the air contains moisture (Suzuki et al., 2009b). This deviation infers the existence of unknown influence of gas species and/or gas mixing on the phenomenon that has not been taken into consideration in the theory (Hoshino et al., 2010b; Chang & Keh, 2012), which gives reasonable prediction in the case of dry air.

Influence of gas species on the thermophoretic phenomenon has been investigated in the previous work (Mohd Azahari et al., 2012); the thermophoretic velocity has been measured for pure gases of argon, nitrogen, and carbon dioxide. Satisfactory agreement with the theory is seen in cases of argon and nitrogen, while a noticeable deviation from the theory

* Correspondence to: Masuda Suzuki Laboratory, 2nd Floor, Mechanical Building, Nagaoka University of Technology, 1603-1 Kamitomioka, Nagaoka, Niigata, 940-2188, Japan. Tel.: +81 80 4298 2710.
E-mail addresses: azahari@uthm.edu.my, m-azahari@msl.nagaokaut.ac.jp (B.R. Mohd Azahari).

0021-8502/$ - see front matter © 2013 Elsevier Ltd. All rights reserved.
http://dx.doi.org/10.1016/j.jaerosci.2013.05.003

is seen in the case of carbon dioxide. It has been demonstrated in the paper that this deviation can be corrected by modifying two empirical constants, i.e., the tangential momentum accommodation coefficient and the thermal accommodation coefficient, both which are involved in the theory and usually assumed to be unity (Li & Davis, 1995a; Prodi et al., 2007; Suzuki et al., 2009b; Hoshino et al., 2010a).

A problem arises here for the treatment of accommodation coefficients of a mixture of pure gases having different values, e.g., the mixture of nitrogen and carbon dioxide. It should better be confirmed even when the mixture is composed of pure gases having the same coefficient value, e.g. the mixture of argon and nitrogen, since there is no widely-accepted method so far for evaluating the coefficients of the mixture from the values of composing pure gases.

There are some theoretical and experimental researches dealing with one of those coefficients of gas mixtures, although none of those gives explicit discussion for both the coefficients together. Mikami et al. (1966) have measured heat-transfer coefficients of a sphere in hydrogen–nitrogen and helium–nitrogen mixtures by utilizing a thermistor, and have compared those results with an analytical solution based on the Maxwell's model; good agreement has been shown by applying a linearly-dependent relation of the accommodation coefficient to the gas concentration. Wise et al. (1966) have conducted experiments to measure the heat transfer with a conductivity cell in a gas mixture of atomic and molecular oxygens. The coefficient for pure atomic oxygen is estimated from extrapolation of experimentally-determined thermal accommodation coefficients of mixtures containing small amount of atomic oxygen. Ivchenko et al. (1997, 2007) have studied the slip phenomenon in the flow of a gas mixture to develop an analytical solution for planar transport problems. Bentz et al. (1999) have performed experiments with a spinning rotor gauge to measure the slip flow constant, which is related to the tangential momentum accommodation coefficient, for helium–argon, helium–nitrogen, and helium–neon mixtures. Bentz et al.'s experimental results exhibit a nonlinear dependence on the mixture concentration; it seems to agree qualitatively well with the prediction from the Ivchenko et al.'s solution, though they have written of it “there are large differences”. Further investigation will be needed in order to determine the appropriate method for evaluating mixture's coefficients.

In this study, thermophoretic parameters are experimentally investigated for several gas mixtures, i.e., argon–nitrogen, argon–carbon dioxide, and nitrogen–carbon dioxide. The dependence of the tangential momentum accommodation coefficient on the concentration of the mixture is examined from the measured thermophoretic velocity.

2. Factors affected by gas mixing

The problem for a gas mixture is the treatment of two empirical parameters, i.e., tangential momentum- and thermal-accommodation coefficients, which characterize the interaction between the solid surface of the particle and surrounding gas molecules. In the gas mixture, a diffusiophoretic force will be exerted on a particle in addition to the thermophoretic force since the temperature gradient causes a concentration gradient. The thermodiffusiophoretic velocity for a gas mixture is shown as below

$$V_{TD}=\frac{3\mu C_c}{2\rho T_{F0}}\frac{[(k+C_TKn)+(4/3)(C_MC_TKn^2+C_MKn[k-1])]}{[1+3C_MKn+(9/2\pi)\mathrm{Pr}Kn^2(1-\gamma^{-1})](1+2k+2C_TKn)}|\nabla T|+C_cc'D_{12}|\nabla x_1|, \tag{1}$$

where μ, $|\nabla T|$, ρ, T_{F0}, C_c, k, Kn, Pr, γ, C_M, C_T, c', D_{12}, and $|\nabla x_1|$ are the viscosity, the temperature gradient, the density of the gas, the reference temperature, the Cunningham's correction factor, the gas-to-particle thermal conductivity ratio, Knudsen number, Prandtl number, the specific heat ratio, the constant for slip flow, the constant for temperature jump, the diffusion slip factor, the coefficient of molecular diffusion, and the concentration gradient, respectively. Here, the reference temperature T_{F0} is defined as the supposed gas temperature at the center of the particle in the given temperature field without the existence of the particle. The first term in the right hand side of Eq. (1) is the thermophoretic term, which is the same as in the previous work (Mohd Azahari et al., 2012). The second term is the diffusiophoretic term (Waldmann, 1959). The density ρ, the viscosity μ, and the thermal conductivity of gas k_f for a binary gas mixture are calculated as follows (Richard, 1964)

$$\rho=\frac{P_1}{R_1T}+\frac{P_2}{R_2T}, \tag{2}$$

$$\mu=\sum_j^n\frac{\mu_j}{1+\sum_{\substack{j=1\\ n\neq i}}^n\varphi_{jn}(x_n/x_j)}, \tag{3}$$

$$k_f=\sum_j^n\frac{k_{fj}}{1+\sum_{\substack{j=1\\ n\neq i}}^n\phi_{jn}(x_n/x_j)}. \tag{4}$$

here,

$$\varphi_{jn} = \frac{(1+(\mu_j/\mu_n)^{1/2}(M_n/M_j)^{1/4})^2}{2\sqrt{2}(1+(M_j/M_n))^{1/2}}, \tag{5}$$

$$\phi_{jn} = \frac{1}{4}\left(1+\left[\frac{\mu_j}{\mu_n}\left(\frac{M_n}{M_j}\right)^{3/4}\frac{1+(C_j/T)}{1+(C_n/T)}\right]^{1/2}\right)^2\left(\frac{1+(C_{jn}/T)}{1+(C_j/T)}\right), \tag{6}$$

$$C_{jn} = (C_j C_n)^{0.5}, \tag{7}$$

where R and C are the gas constant and Sutherland constant, respectively. Subscripts j and n refer to the number of each gas species and the total number, respectively. Parameters c', D_{12}, and $|\nabla x_1|$ are calculated by complex equations given by Kihara (1975) and Ivchenko et al. (2007).

Constants C_M and C_T in Eq. (1) are the ones containing the tangential momentum accommodation coefficient α_m and the thermal accommodation coefficient α_t, respectively, which are written as follows:

$$C_M = \frac{2-\alpha_m}{\alpha_m}, \tag{8}$$

$$C_T = \frac{15}{8}\left(\frac{2-\alpha_t}{\alpha_t}\right). \tag{9}$$

In order to apply this same formula to a gas mixture, those coefficients of the mixture should be determined from values of each pure gas components.

In this work, only the tangential momentum accommodation coefficient is derived from experimental results, and the other one, the thermal accommodation coefficient, is assumed to be unity on the basis of results in the previous work (Mohd Azahari et al., 2012), in which all the thermal accommodation coefficients have been estimated at unity for the same pure gases adopted in this work.

The authors have found three different methods for the calculation of the tangential momentum accommodation coefficient of a mixture, which are explained below

i. Energy-balance-based method
The first one is given by Mikami et al. (1966), who derived the tangential momentum accommodation coefficient for a gas mixture from the energy balance as below

$$\alpha_{m,mix} = \frac{\sum_{j=1}^{2} x_j \alpha_{m,j}/\sqrt{M_j}}{\sum_{j=1}^{2} x_j/\sqrt{M_j}}, \tag{10}$$

where x and M are the molar fraction and the molecular weight, respectively, and subscript j refers to the number of each gas species.

ii. Mass-fraction-based method
The second one is found in the ANSYS FLUENT theory guide (2009), in which both the accommodation coefficients of a mixture are calculated simply by taking the mass-fraction weighted average of each gas species as follows:

$$\alpha_{mix} = \sum_{j=1}^{2} y_j \alpha_j, \tag{11}$$

where y_j and α are the mass fraction of each gas species j and each accommodation coefficient.

iii. Intermolecular-interaction-based method
The last one can be derived from equations given by Ivchenko et al. (2007). The constant C_M for the slip-flow of a gas mixture was derived using the first-order Chapman–Enskog approximation and the Maxwell method as below

$$C_M = \frac{5}{16}\pi\frac{P\sqrt{x_1M_1+x_2M_2}}{\mu}\frac{(2-\alpha_{1m})x_1b_1+(2-\alpha_{2m})x_2b_2}{\alpha_{1m}x_1\sqrt{M_1}+\alpha_{2m}x_2\sqrt{M_2}}, \tag{12}$$

where P and b are the pressure and the transport coefficient (Ivchenko et al., 2007) of viscosity corresponding to arbitrary models of the intermolecular interaction, respectively, and subscripts 1 and 2 refer to components of the binary gas mixture. Here, it is noted that the literature adopts the following equation instead of Eq. (8):

$$C_M = \frac{5}{16}\pi\frac{(2-\alpha_m)}{\alpha_m}. \tag{13}$$

This equation is basically identical to the Eq. (8): the additional coefficient of $5\pi/16$ to the Eq. (8) makes the resultant value only 2% less. By equating Eqs. (12) and (13), the tangential momentum accommodation coefficient of the mixture

can be formulated as a function of the coefficients of two pure gases as follows:

$$\alpha_{m,mix} = 2\left(1 + \frac{P\sqrt{x_1 M_1 + x_2 M_2}}{\mu}\frac{(2-\alpha_{1m})x_1 b_1 + (2-\alpha_{2m})x_2 b_2}{\alpha_{1m}x_1\sqrt{M_1} + \alpha_{2m}x_2\sqrt{M_2}}\right)^{-1}. \quad (14)$$

3. Experimental

The experimental configuration used in this work is the same as the previous (Mohd Azahari et al., 2012) except that a gas mixer is introduced. A mixture of two gases is created before it is supplied into the pressure vessel, in which particles are supplied to measure the thermophoretic velocity. The mixer is evacuated by a pump before two gases feed into it. Gas mixtures in various ratios are prepared by adjusting the partial pressure of each gas. The gases used in this work are argon, nitrogen, and carbon dioxide.

Sample particles used in this work are the same spherical PMMA particles used in the previous. As it is shown in Table 1, those particles are quite uniform in size. The mean diameter and the thermal conductivity of these particles are 2.91 μm and 0.21 W/ (m K), respectively. The pressure, the reference temperature, and the temperature gradient of the surrounding gas are 70 kPa, 338 K, and 60 K/mm, respectively. The measurement is performed by means of the free-fall method. Drop experiments are conducted repeatedly to accumulate enough amounts of data. Details are described in the previous paper (Mohd Azahari et al., 2012). It is noted that the temperature gradient in the present work is increased, and the reference temperature is changed accordingly, from the previous condition such that the thermophoretic velocity increases and the measurement accuracy increases.

The tangential momentum accommodation coefficient α_m for each experimental datum is calculated from Eqs. (1), (8), and (9) by assuming $\alpha_t = 1$, and the mean value and its 95% confidence interval are statistically obtained for each experimental condition. It is noted that those data for pure gases include experimental results from the previous work (Mohd Azahari et al., 2012). The experimentally-obtained coefficient α_m of a gas mixture is compared with the ones calculated from values of pure gases by Eqs. (10), (11), and (14).

4. Results

Fig. 1 shows measured velocities for argon–nitrogen, argon–carbon dioxide, and nitrogen–carbon dioxide mixtures. Lines represent predictions by above-mentioned methods, which will be explained later. Error bars in the figure indicate the 95% confidence interval for the mean.

Nitrogen exhibits the highest thermophoretic velocity, followed by argon and carbon dioxide; the thermophoretic velocities for pure nitrogen, argon, and carbon dioxide are 0.880 mm/s, 0.673 mm/s, and 0.273 mm/s, respectively. For the mixture of argon–nitrogen, the thermophoretic velocity increases as the concentration of nitrogen increases. For mixtures of argon–carbon dioxide and nitrogen–carbon dioxide, the thermophoretic velocity decreases as the concentration of carbon dioxide increases.

Fig. 2 shows tangential momentum accommodation coefficients of pure gases of argon, nitrogen, and carbon dioxide. White and black symbols represent values from the previous (Mohd Azahari et al., 2012) and this works, respectively. Solid lines indicate mean values among all pressure conditions. Coefficients from this work seem to be consistent with those from the previous.

Table 2 shows mean values of the coefficient from all the pressure conditions. Coefficients for argon and nitrogen are almost the same: 0.987 and 0.986, respectively. That for carbon dioxide exhibits a notably low value at 0.821.

Table 3 shows the tangential momentum accommodation coefficient calculated from experimental results. Error ranges indicate the 95% confidence interval for the mean. For argon–carbon dioxide and nitrogen–carbon dioxide, it is seen that the coefficient is dependent on the gas concentration. For the mixture of argon–nitrogen, the slightly increase up to 1% is noticeable in the mean value. However, it is difficult to make a statistically significant since the mean values are within the error range.

Fig. 3 shows comparisons of the tangential momentum accommodation coefficient of experiments and predictions from Eqs. (10), (11), and (14). In cases of gas mixtures of argon–nitrogen and argon–carbon dioxide, predictions by the energy-balance and the

Table 1
Diameter of PMMA particles.

Mean (μm)	Standard deviation (μm)	Confidence interval (95.0%) for the mean (μm)
2.91	0.09	0.03

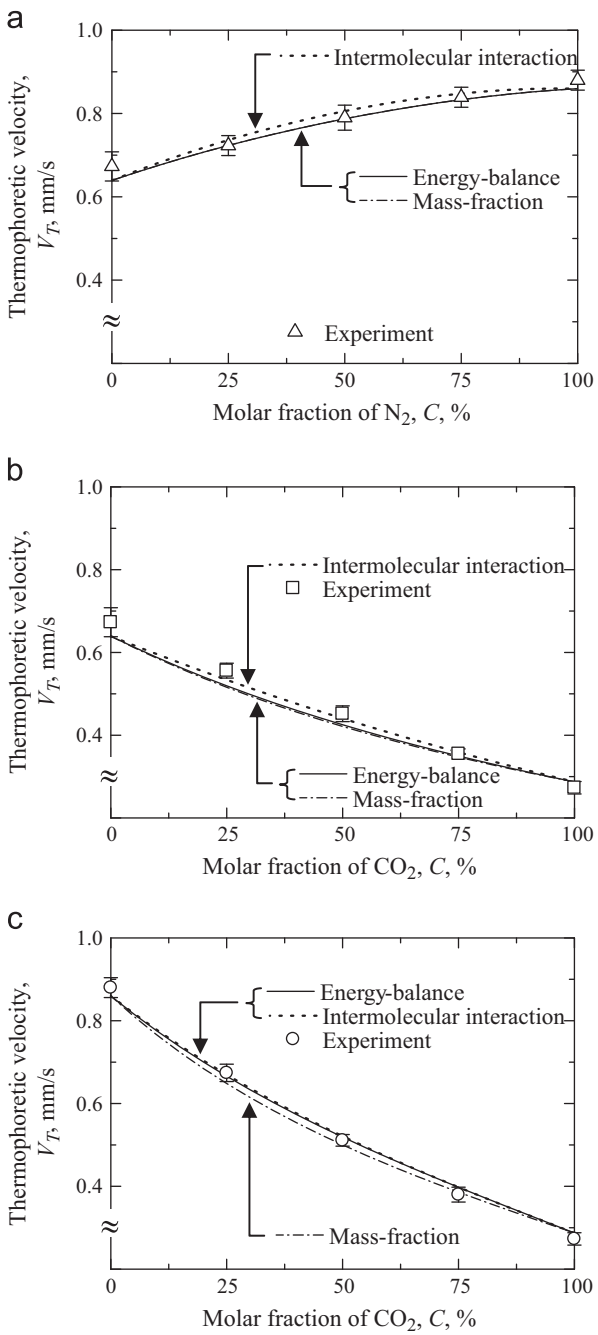

Fig. 1. Thermophoretic velocity for each gas mixture. Error bars represent the confidence interval (95%) for the mean. (a) Ar-N_2, (a) Ar-CO_2 and (c) N_2-CO_2.

mass-fraction methods are almost identical. On the other hand, in the case of nitrogen–carbon dioxide, predictions by the energy-balance and the intermolecular-interaction methods give close results while the mass-fraction method is distinguishable from others. Although there is slightly difference between methods, all predictions agree satisfactorily with the experimental result for argon–nitrogen. For argon–carbon dioxide, disagreements are seen between the experimental result and predictions by the energy-balance and the mass-fraction methods. For nitrogen–carbon dioxide, slightly disagreement is noticeable between the mass-fraction method and the experimental result at 25% carbon dioxide. The intermolecular-interaction method seems to be the best for all those mixture conditions.

Comparisons of thermophoretic velocities between predictions and experiments for gas mixtures are shown in Fig. 1. Although the difference is not so remarkable, the intermolecular-interaction method seems to be the best among compared three methods; the energy-balance and the mass-fraction methods underestimate the velocity for argon-carbon dioxide.

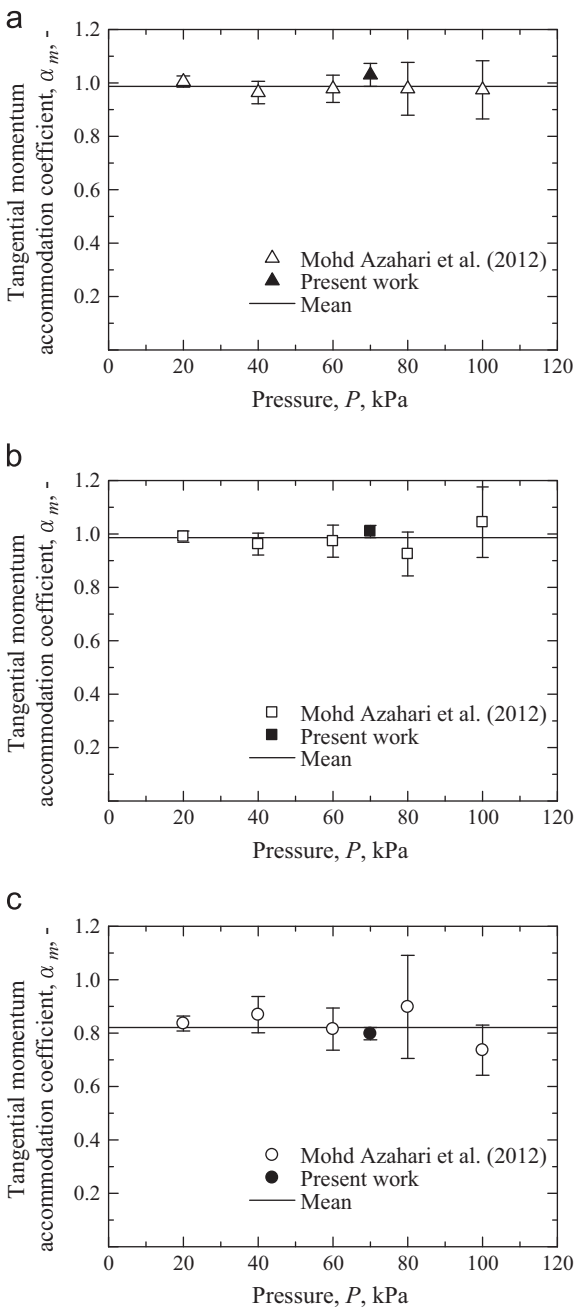

Fig. 2. Tangential momentum accommodation coefficient for each pure gas. Error bars represent the confidence interval (95%) for the mean. (a) Argon, (b) Nitrogen and (c) Carbon dioxide.

Table 2
Tangential momentum accommodation coefficient α_m for each pure gas.

Gas	α_m
Argon	0.987
Nitrogen	0.986
Carbon dioxide	0.821

Table 3
Estimated tangential momentum accommodation coefficient α_m for each gas mixture.

Ratio	Ar:N_2	Ar:CO_2	N_2:CO_2
1.00:0.00	0.987 ± 0.028	0.987 ± 0.028	0.986 ± 0.026
0.75:0.25	0.989 ± 0.027	0.991 ± 0.025	0.965 ± 0.028
0.50:0.50	0.993 ± 0.031	0.949 ± 0.029	0.905 ± 0.022
0.25:0.75	0.992 ± 0.026	0.877 ± 0.022	0.846 ± 0.033
0.00:1.00	0.986 ± 0.026	0.821 ± 0.031	0.821 ± 0.031

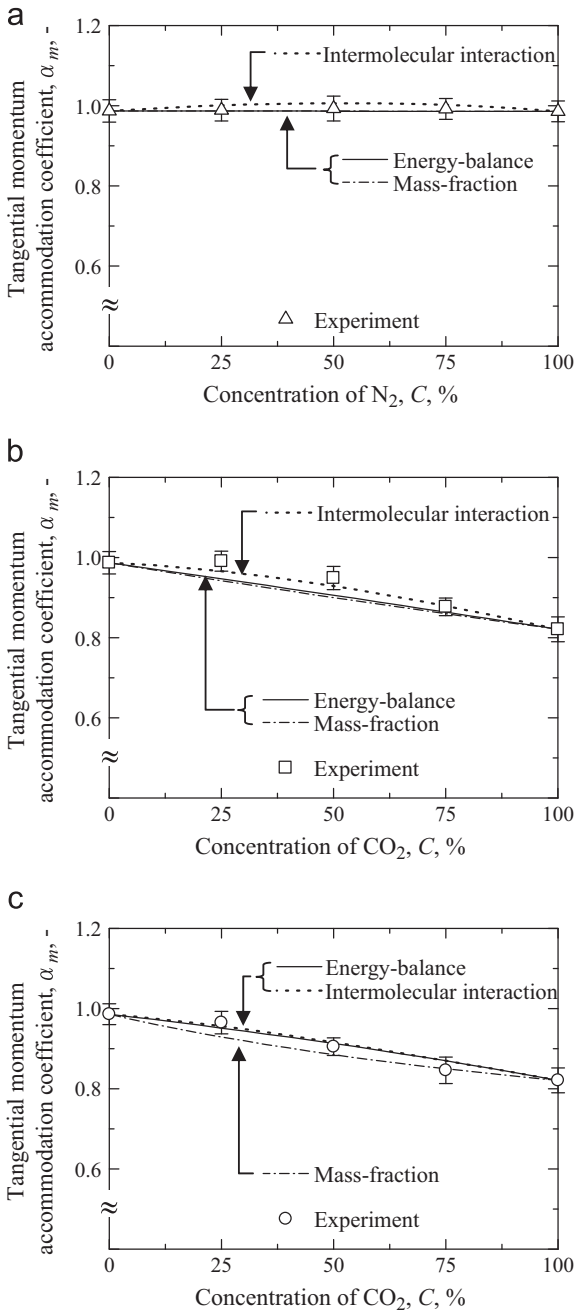

Fig. 3. Comparison of tangential momentum accommodation coefficient for each gas mixture. Error bars represent the confidence interval (95%) for the mean. (a) Ar-N_2, (b) Ar-CO_2 and (c) N_2-CO_2.

Table 4
Comparison of coefficients for pure gases.

Tested gas	α_m	α_t	Solid material	Reference
Argon	0.931	1.102	Steel spheres (polished surface)	Thomas and Lord (1974)
	1.049	1.161	Steel spheres (rough surface)	Thomas and Lord (1974)
	0.916	1.000	Glass	Sharipov (2004)
	1.000	0.900	Paraffin	Prodi et al. (2007)
	0.987	1.000	PMMA	This work
Nitrogen	1.000	0.680	Tungsten	Douglas (1982)
	0.911	1.000	Glass	Sharipov (2004)
	1.000	0.900	Paraffin	Prodi et al. (2007)
	0.986	1.000	PMMA	This work
Carbon dioxide	1.000	0.720	Tungsten	Douglas (1982)
	1.000	0.450	Glass	Li and Davis (1995b)
	1.000	0.450	Polystyrene latex (PSL) sphere	Li and Davis (1995b)
	0.993	1.000	Glass	Sharipov (2004)
	0.821	1.000	PMMA	This work

5. Discussion

A problem in the determination of coefficients of a gas mixture is the uncertainty of those values of composing pure gases. Different researchers have proposed different values for a same pure gas. Table 4 shows comparisons of coefficients between several references for the concerned pure gases; the values obtained in this work are also shown. These differences in the table infer the possibility that the accommodation coefficient is dependent on the adopted method and/or the material of the solid. The surface condition of the solid wall may also have some influence: Thomas and Lord (1974) have measured accommodation coefficients for polished and rough surfaces of steel spheres to find some difference as shown in the table.

This problem should be considered when making quantitative comparison between values from different research works. With regard to the current and its preceding works, all experimental data are obtained from the same method and the same kind of particles. Thus, the comparison given in this work will not be concerned directly by the problem.

Another problem is the assumption that the thermal accommodation coefficient is always at unity regardless of the mixing condition. This does not concern when applying energy-balance and mass-fraction based methods, since both these methods do not alter the coefficient of the mixture when both the pure gases have the same value at unity. The intermolecular-interaction-based method, on the other hand, may change the value of the thermal accommodation coefficient depending on the concentration as is the case of the tangential momentum accommodation coefficient. Authors did not find so far any reference that shows the way to calculate the thermal accommodation coefficient on the intermolecular interaction basis. Although there are such vulnerable points in the treatment of coefficients, the current work would be informative for a practical use in predicting the thermophoretic velocity for gas mixtures. Experimental results are satisfactorily predicted when the thermal accommodation coefficient is assumed to be unity and the other coefficient is calculated from pure gas values by means of the intermolecular-interaction-based method.

6. Conclusions

In this study, the thermophoretic velocity of gas mixtures are experimentally measured, and following results are obtained:

1. The thermophoretic velocity depends on the concentration of the gas mixture. For an argon–nitrogen mixture, the velocity increases as the concentration of nitrogen increases; for argon–carbon dioxide and nitrogen–carbon dioxide mixtures, the velocity decreases as the concentration of carbon dioxide increases.
2. The tangential momentum accommodation coefficient of a gas mixture is estimated from experimental results to clarify its dependence on the concentration by assuming the thermal accommodation coefficient at unity. The estimated coefficient is compared with predictions from three methods; it is found that the intermolecular-interaction-based method gives the best prediction among those three methods for all mixture conditions.
3. It is shown that the thermophoretic velocity under a binary gas mixture condition is practically predicted from the intermolecular-interaction-based method.

Acknowledgment

A part of this work was supported by JSPS KAKENHI 24560225.

References

ANSYS Fluent 12.0 theory guide. ANSYS, Inc.,United States, 2009.

Bentz, J.A., Tompson, R.V., & Loyalka, S.K. (1999). Viscosity and velocity slip coefficients for gas mixtures: measurements with a spinning rotor gauge. *Journal of Vacuum Science and Technology A*, *17*, 235–241.

Chang, Y.C., & Keh, H.J. (2012). Effects of thermal stress slip on thermophoresis and photophoresis. *Journal of Aerosol Science*, *50*, 1–10.

Dobashi, R., Kong, Z.W., Toda, A., Takahashi, N., Suzuki, M., & Hirano, T. (2000). Mechanism of smoke generation in a flickering pool flame. Proceeding of the 6th International Symposium on Fire Safety Science, 255–264.

Douglas, F.S. (1982). Energy and tangential momentum accommodation coefficients on gas covered tungsten. *Journal of Chemical Physics*, *76*, 3814–3818.

Hoshino, A., Suzuki, M., & Masuda, W. (2010a). Numerical analysis on thermophoretic phenomenon in slip flow regime considering thermal stress efeect. In: Proceedings of the 21st International Symposium on Transport Phenomena.

Hoshino, A., Suzuki, M., & Masuda, W. (2010b). Influence of particle size distribution on measurement accuracy of thermophoretic velocity. Proceeding of the 48th Symposium (Japanese) on Combustion, 464–465.

Ivchenko, I.N., Loyalka, S.K., & Tompson, R.V., Jr. (1997). Slip coefficients for binary gas mixtures. *Journal of Vacuum Science and Technology A*, *15*, 2375–2381.

Ivchenko, I.N., Loyalka, S.K., & Tompson, R.V., Jr. (2007). *Analytical Methods for Problems of Molecular Transport*. Springer: The Netherlands.

Kihara, T. (1975). The Chapman-Enskog and Kihara approximations for isotopic thermal diffusion in gases. *Journal of Statistical Physics*, *13*, 137–143.

Li, W., & Davis, E.J. (1995a). Measurement of the thermophoretic force by electrodynamic levitation: microspheres in air. *Journal of Aerosol Science*, *26*, 1063–1083.

Li, W., & Davis, E.J. (1995b). The effects of gas and particle properties on thermophoresis. *Journal of Aerosol Science*, *26*, 1085–1099.

Mikami, H., Endo, Y., & Takashima, Y. (1966). Heat transfer from a sphere to rarefied gas mixtures. *International Journal of Heat and Mass Transfer*, *9*, 1435–1448.

Mohd Azahari, B.R., Mori, M., Suzuki, M., & Masuda, W. (2012). Effects of gas species on pressure dependence of thermophoretic velocity. *Journal of Aerosol Science*, *54*, 77–87.

Morse, T.F., Wang, C.Y., & Cipolla, J.W., Jr. (1985). Laser-induced thermophoresis and particle deposition efficiency. *International Journal of Heat and Mass Transfer*, *107*, 155–160.

Prodi, F., Santachiara, G., Di Matteo, L., Vedernikov, A., Beresnev, S.A., & Chernyak, V.G. (2007). Measurements of thermophoretic velocities of aerosol particles in microgravity conditions in different carrier gases. *Journal of Aerosol Science*, *38*, 645–655.

Richard, S.B. (1964). Approximate formulas for viscosity and thermal conductivity of gas mixtures. NASA Technical Note, TN D-2502.

Sharipov, F. (2004). Data on the velocity slip and temperature jump coefficients. *Proceeding of Euro SimE*, 243–249.

Suzuki, M., Maruko, K., Iwahara, K., & Masuda, W. (2009a). Accurate measurement of thermophoretic velocity under high temperature gradient. In: Proceedings of the 6th International Symposium on Scale Modelling (ISSM6), 1.12.1–1.12.8.

Suzuki, T., Suzuki, M., & Masuda, W. (2009b). Effect of water vapor to thermophoresis phenomenon. In: Proceeding of the 47th Symposium (Japanese) on Combustion, 448–449.

Thomas, L.B., & Lord, R.G. (1974). Comparative measurements of tangential momentum and thermal accommodations on polished and on roughened steel spheres. International Symposium on Rarefied Gas Dynamics, 8, 405–412.

Toda, A., Ohi, Y., Dobashi, R., Hirano, T., & Sakuraya, T. (1996). Accurate measurement of thermophoretic effect in microgravity. *Journal of Chemical Physics*, *105*, 7083–7087.

Toda, A., Ohnishi, H., Dobashi, R., Hirano, T., & Sakuraya, T. (1998). Experimental study on the relation between thermophoresis and size of aerosol particles. *International Journal of Heat and Mass Transfer*, *41*, 2710–2713.

Waldmann, L. (1959). Uber die kraft eines inhomogenen gases auf kleine suspendierte kugeln. *Zeitschrift Naturforschung Teil A*, *14*, 589–599.

Wise, H., Wood, B.J., & Rajapakse, Y. (1966). Heat transfer in reacting gases: thermal conductivity and accommodation coefficient measurements in gas mixture O andO_2. *The Physics of Fluids*, *9*, 1321–1327.